An ***IPRF*** Research Report

Innovative Pavement Research Foundation

Airport Concrete Pavement Technology Program

Report IPRF-01-G-002-03-3

Design and Construction of Concrete Pavement for Aircraft De-icing Facilities

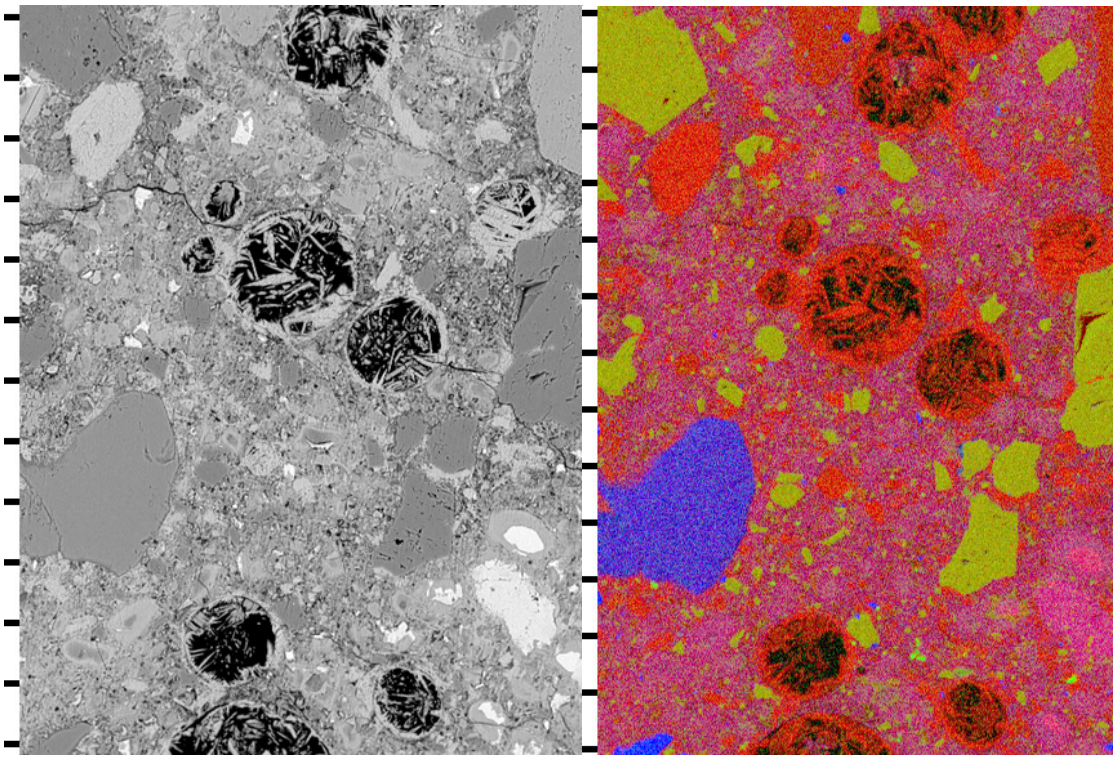

Programs Management Office
5420 Old Orchard Road
Skokie, IL 60077

April 2006

An ***IPRF*** Research Report

Innovative Pavement Research Foundation

Airport Concrete Pavement Technology Program

Report IPRF-01-G-002-03-3

Design and Construction of Concrete Pavement for Aircraft De-icing Facilities

Principal Investigator

Dr. Thomas J. Van Dam, P.E.

Contributing Authors

Karl R. Peterson, Michigan Technological University

Kurt D. Smith, P.E., Applied Pavement Technology

Dr. Lawrence L. Sutter, Michigan Technological University

David G. Peshkin, P.E., Applied Pavement Technology

Russell G. Alger, Michigan Technological University

Programs Management Office

5420 Old Orchard Road

Skokie, IL 60077

This report has been prepared by the Innovative Pavement Research Foundation under the Airport Concrete Pavement Technology Program. Funding is provided by the Federal Aviation Administration under Cooperative Agreement Number 01-G-002. Dr. Satish Agrawal is the Manager of the FAA Airport Technology R&D Branch and the Technical Manager of the Cooperative Agreement. Mr. Jim Lafrenz, P.E., is the Program Director for the IPRF.

The Innovative Pavement Research Foundation and the Federal Aviation Administration thank the Technical Panel that willingly gave of their expertise and time for the development of this report. They provided oversight and technical direction to the research team. Members of the Technical Panel for this project include:

Mr. E.C. Hunnicutt, P.E.	Federal Aviation Administration
Mr. Jay Malo, P.E.	Carter and Burgess, Inc.
Mr. William (Bill) Verfuss, P.E.	McFarland-Johnson, Inc.
Dr. Paul D. Tennis	Portland Cement Association
Mr. Tom McGonigle	Sjostrom & Sons, Inc.
Mr. Steve Waalkes, P.E.	American Concrete Pavement Association

The members of the research team would also like to express appreciation to the various airport authorities who participated in the study and granted access to their facilities for the field evaluation and testing.

TABLE OF CONTENTS

Executive Summary viii
1. Introduction 1
2. literature review 3
2.1. Aircraft Deicing Practices 3
2.2. Potential Concrete Distress Mechanisms 3
2.2.1. Enhanced Freeze-Thaw Damage 4
2.2.2. Chemical and Bacteriological Deterioration 6
2.3. Summary of Literature Review 7
3. Summary of Initial Field Visits 8
3.1. Introduction 8
3.2. Field Evaluation Approach 8
3.3. Summary of Airport Inspections 11
3.3.1. Airport Alpha 11
3.3.2. Airport Beta 15
3.3.3. Airport Charlie 17
3.3.4. Airport Delta 18
3.3.5. Airport Echo 21
3.3.6. Airport Foxtrot 23
3.3.7. Airport Golf 25
3.3.8. Airport Hotel 29
3.4. Overall Summary and Recommendations from Initial Field Visits 30
4. Forensic Evaluation 33
4.1. Forensic Field Evaluation 33
4.2. Strength Testing 33
4.3. Petrographic Analysis 35
4.3.1. Airport Alpha 36
4.3.2. Airport Delta 47
4.3.3. Airport Echo 49
4.3.4. Airport Foxtrot 57
4.3.5. Airport Golf 65
4.3.6. Summary of Petrographic Data 72
5. Data Analysis 75
5.1. Airport Alpha 75
5.2. Airport Delta 76
5.3. Airport Echo 76
5.4. Airport Foxtrot 77
5.5. Airport Golf 77
5.6. Summary 78
6. Recommendations for Mitigation and Prevention of Future Deterioration 80
6.1. Mixture Design, Proportioning/Batching, and/or Placement 80
6.2. Air-Void Systems 81
6.3. Curing Practices 82
7. Conclusions And Recommendations 84

7.1. Conclusions 84
7.2. Recommendations for Future Work 85
8. References 87

LIST OF FIGURES

Figure 1. FAA Regions 9
Figure 2. Overview of deicing pad inspected at Airport Alpha 13
Figure 3. Low-severity spalling (left) and low-severity patch (right) on sample unit 1 at Airport Alpha 14
Figure 4. Fine hairline cracking observed in sample unit 1 at Airport Alpha 14
Figure 5. Fine hairline cracks near a joint in sample unit 2 at Airport Alpha 15
Figure 6. Overview of deicing facility at Airport Beta 16
Figure 7. Trench drains around deicing facility at Airport Beta 16
Figure 8. Low-severity spalling (left) and hairline crack (right) in sample unit 1 at Airport Beta 17
Figure 9. Overview of deicing facility at Airport Charlie 18
Figure 10. Hairline cracking observed in sample unit 1 at Airport Charlie 18
Figure 11. Joint spalling in sample unit 1 at Airport Charlie 19
Figure 12. Overview of deicing facility at Airport Delta 20
Figure 13. Sealant adhesive failure on sample unit 1 at Airport Delta 20
Figure 14. Snowplow damage on sample unit 2 at Airport Delta 21
Figure 15. Overview of deicing facility at Airport Echo 22
Figure 16. Hairline cracking observed in sample unit 1 at Airport Echo 22
Figure 17. Overview of deicing facility at Airport Foxtrot 23
Figure 18. Map and hairline cracking observed on sample unit 1 at Airport Foxtrot 24
Figure 19. Map and hairline cracking observed on sample unit 2 at Airport Foxtrot 24
Figure 20. Surface scaling observed on sample unit 2 at Airport Foxtrot 24
Figure 21. Overview of Deicing Pad E (left) and Deicing Pad C (right) at Airport Golf 25
Figure 22. Cracking, patching, and spalling observed on sample unit 1 of Deicing Pad E at Airport Golf 26
Figure 23. Map cracking observed on sample unit 1 of Deicing Pad E at Airport Golf 26
Figure 24. Cracking, popouts, and map cracking observed on sample unit 2 of Deicing Pad E at Airport Golf 27
Figure 25. Cracking (left) and overbanded sealant (right) on sample unit 1 of Deicing Pad C at Airport Golf 27
Figure 26. Hairline cracking observed on sample unit 1 of Deicing Pad C at Airport Golf 28
Figure 27. Hairline cracking observed on sample unit 2 of Deicing Pad C at Airport Golf 28
Figure 28. Overview of deicing facility at Airport Hotel 29
Figure 29. Joint sealant (upper left, sample unit 1), popout (upper right, sample unit 2), and overall slab condition (bottom, sample unit 2) at Airport Hotel 30
Figure 30. Flowchart for assessing likelihood of MRD (Van Dam et al. 2002) 31
Figure 31. Fundamental process for analyzing a deteriorated concrete sample (Van Dam et al. 2002) 36
Figure 32. Close-up of irregular voids from Core C, (left) and core G, (right) Airport Alpha 37
Figure 33. Polished slabs from Airport Alpha. Slabs oriented to show cross-section through pavement, pavement surface at right-hand side, ticK marks every 2 cm 38
Figure 34. Polished slabs from Airport Alpha site after treatment to enhance visibility of air voids and cracks. Slabs oriented to show cross-section through pavement, pavement surface at right-hand side, ticK marks every 2 cm 39

Figure 35. Close-up of polished slab prepared from top third of core C, Airport Alpha after treatment to emphasize locations of air voids and cracks. Tick marks every cm 40
Figure 36. Stereo-microscope images of aggregates and cracks that picked up yellow coloration from sodium cobaltinitrite stain. Image on left from polished slab from bottom third of core A; image on right from pavement surface on the top third of core F, Airport Alpha 40
Figure 37. Petrographic microscope images to show cross-section at pavement surface from core F, Airport Alpha. From left to right: plane polarized light, crossed polars, and epifluorescent mode. Tick marks every mm 42
Figure 38. BSE images of localized region in cement paste of extremely high porosity on polished thin section from core C, Airport Alpha. Tick marks every 250 micrometers 42
Figure 39. Petrographic microscope images of localized region in cement paste of extremely high porosity, polished thin section from core C, Airport Alpha. From left to right: plane polarized light, crossed polars, and epifluorescent mode. Tick marks every 250 micrometers 43
Figure 40. BSE image (left) and elemental map (right) of calcium hydroxide deposits in entrained air voids from polished thin section from core C, Airport Alpha. Dolomite powder filler is also clearly visible in the elemental map, Ca = red channel, Mg = green channel, and Si = blue channel. Tick marks every 50 micrometers 43
Figure 41. Petrographic microscope images of calcium hydroxide deposits in entrained air voids from polished thin section from core C, Airport Alpha. From left to right: plane polarized light, crossed polars, and epifluorescent mode. Tick marks every 100 micrometers 44
Figure 42. Close-up petrographic microscope images of calcium hydroxide deposits in entrained air voids from polished thin section from core C, Airport Alpha. From left to right: plane polarized light, crossed polars, and epifluorescent mode. Tick marks every 50 micrometers 44
Figure 43. BSE image (upper left hand corner) and elemental maps showing calcite and potassium-bearing clay minerals in pore space within dolomite coarse aggregate particle on polished thin section from core C, Airport Alpha. In elemental maps, darker colored regions correspond to higher x-ray counts 45
Figure 44. Petrographic microscope images to show cement paste fraction from Airport Alpha. Clockwise from upper left hand corner: plane polarized light, crossed polars, and epifluorescent mode 46
Figure 45. Close-up petrographic microscope images to show cement grains and dolomite powder filler in cement paste fraction from Airport Alpha. The dolomite particles are clearly visible in the crossed polars image. Clockwise from upper left hand corner: plane polarized light, crossed polars, and epifluorescent mode 47
Figure 46. Polished slabs from core 44, Airport Delta. Slabs oriented to show cross-section through pavement, pavement surface at right-hand side, tick marks every 2 cm 48
Figure 47. Polished slabs from core 44, Airport Delta after treatment to enhance visibility of air voids and cracks. Slabs oriented to show cross-section through pavement, pavement surface at right-hand side, tick marks every 2 cm 48
Figure 48. Stereo-microscope images to show air void structure on polished slab from top third of core 44 away from joint, Airport Delta 48
Figure 49. Petrographic microscope images to show cross section at pavement surface from core 44, Airport Delta. From left to right: plane polarized light, crossed polars, and epifluorescent mode. Tick marks every mm 50

Figure 50. Close-up of cement paste in thin section from Airport Delta to show cement grains and fly ash particles in cement paste. From left to right, plane polarized and crossed polars 50
Figure 51. Close-up of alkali-silica reactive aggregate (black arrow) exposed on exterior of core D, Airport Echo..... 51
Figure 52. Polished slabs from Airport Echo. pavement surface at right-hand side; tick marks every 2 cm. Only core B sampled the entire depth. Dark discoloration of due to reduction of iron in cement grains by sulfur in ground granulated blast furnace slag..... 51
Figure 53. Polished slabs from Airport Echo after treatment to enhance visibility of air voids and cracks. Slabs oriented to show cross-section through pavement, pavement surface at right-hand side; tick marks every 2 cm. Only core B sampled the entire pavement depth 52
Figure 54. Close-up of polished slab prepared from top third of core B, Airport Echo, after staining with sodium cobaltinitrite solution. Tick marks every cm..... 53
Figure 55. Stereo-microscope images to show air void structure on polished slab from middle third of core A adjacent to joint, Airport Echo 54
Figure 56. Petrographic microscope images to show cross-section through plastic shrinkage crack at pavement surface from core C, Airport Echo. From left to right: plane polarized light, crossed polars, and epifluorescent mode. Tick marks every mm..... 55
Figure 57. Petrographic microscope images to show reactive fine aggregate particle in polished thin section from core C, Airport Echo. From left to right: plane polarized light, crossed polars, and epifluorescent mode 55
Figure 58. Close-up BSE image to show perimeter of reactive fine aggregate particle in polished thin section from core C, Airport Echo. Incorporation of other fine aggregate particles into gel reaction product suggests gel production occurred before the concrete had set..... 56
Figure 59. Close-up petrographic microscope images to show cement grains and GBFS fragments in cement paste fraction from Airport Echo site. Clockwise from upper left hand corner: plane polarized light, crossed polars, reflected light, and epifluorescent mode..... 57
Figure 60. Close-up images of irregular voids, core A on left, core G on right..... 58
Figure 61. Polished slabs from Airport Foxtrot. Slabs oriented to show cross-section through pavement, pavement surface at right hand side, tick marks every 2 cm..... 59
Figure 62. Polished slabs from Airport Foxtrot after treatment to enhance visibility of air voids and cracks. Slabs oriented to show cross-section through pavement, pavement surface at right-hand side, tick marks every 2 cm..... 60
Figure 63. Close-up of polished slab prepared from top third of core C, Airport Foxtrot, after staining with sodium cobaltinitrite solution. Tic marks every cm..... 61
Figure 64. Stereo-microscope images to crack that picked up yellow coloration from sodium cobaltinitrite stain on the top third of core C away from joint, Airport Foxtrot..... 61
Figure 65. Petrographic microscope images of polished thin section from core C, Airport Foxtrot, showing cross section through pavement surface and carbonation along crack. From left to right: plane polarized, crossed polars, and epifluorescent mode. Tick marks every mm.... 62
Figure 66. Epifluorescent mode petrographic microscope images from polished thin section from core B, Airport Foxtrot. Note fairly uniform cement paste, and round entrained air voids..... 63
Figure 67. Epifluorescent mode petrographic microscope images from polished thin section from core A, Airport Foxtrot. Note slightly more irregularly shaped entrained air voids, and sub-entrained air sized gaps in the cement paste 63

Figure 68. BSE image (left) and elemental map (right) of crack lined with alkali silica reaction product and entrained air voids filled with secondary ettringite deposits in polished thin section prepared from core C, Airport Foxtrot. In elemental map, Ca = red channel, K = green channel, and Si = blue channel. Tick marks every 100 micrometers..... 64
Figure 69. Petrographic microscope images of crack lined with alkali silica reaction product, and entrained air voids filled with secondary ettringite deposits in polished thin section prepared from core C, Airport Foxtrot. From left to right: plane polarized, crossed polars, and epifluorescent mode. Tick marks every 100 micrometers 64
Figure 70. Close-up petrographic microscope images to show cement grains and fly ash in cement paste fraction from Airport Foxtrot. Clockwise from upper left hand corner: plane polarized light, crossed polars, and epifluorescent mode 65
Figure 71. Polished slabs from Airport Golf. Slabs oriented to show cross-section through pavement, pavement surface at right-hand side, tick marks every 2 cm. Dark discoloration of cement paste due to reduction of iron in cement grains by sulfur present in air-cooled blast furnace slag coarse aggregate..... 66
Figure 72. Polished slabs from Airport Golf after treatment to enhance visibility of air voids and cracks. Slabs oriented to show cross-section through pavement, pavement surface at right-hand side, tick marks every 2 cm..... 67
Figure 73. Close-up of polished slab prepared from bottom third of core D, Airport Golf after staining with sodium cobaltinitrite solution. Tick marks every cm..... 68
Figure 74. Stereo-microscope images of polished slab from middle third of core C showing ettringite filled entrained air voids both before (left) and after (right) staining with barium chloride and potassium permanganate solution 69
Figure 75. Stereo-microscope images to show air-void structure on polished slab from top third of core C away from joint, Airport Golf 69
Figure 76. Petrographic microscope images of polished thin section from core C, Airport Golf, showing cross section through pavement surface and carbonation along crack. From left to right: plane polarized, crossed polars, and epifluorescent mode. Tick marks every mm 70
Figure 77. BSE image (left) and elemental map (right) of crack lined with ettringite deposits in polished thin section prepared from core C, Airport Golf. In elemental map, Ca = red channel, S = green channel, and Al = blue channel. Tick marks every 100 micrometers ... 71
Figure 78. Petrographic microscope images of crack lined with ettringite deposit in polished thin section prepared from core C, Airport Golf. From left to right: plane polarized, crossed polars, and epifluorescent mode. Tick marks every 100 micrometers 71
Figure 79. Close-up of cement paste in thin section from Airport Golf to show cement grains and fly ash particles in cement paste. From left to right, plane polarized and crossed polars 72
Figure 80. Total original air content versus original spacing factor for all concrete tested using ASTM C 457..... 82

LIST OF TABLES

Table 1. Airports included in initial field visits 8
Table 2. PCI distress types for concrete airfields (ASTM 1998) 10
Table 4. Concrete mix proportions used at Airport Alpha 11
Table 3. Summary of selected airport deicing pad design, construction, and performance data. 12
Table 6. Coring pattern and core disposition for the Six Cores at Each location 34
Table 7. Compressive and split tensile strength data. 34
Table 8. Summary of air-void statistics from all of the airport sites 73
Table 9. Cementitious constituents present in airport deicer pads 73
Table 10. Results of capillary fluorescence measurements from thin sections prepared from field sites and compared to measurements from thin sections prepared from 28-day moist cured mortar cylinders of known *w/c*. 74
Table 11. Level of significance of distresses observed at each site 79

EXECUTIVE SUMMARY

Premature distress, in the form of scaling, joint spalling, crazing, and map cracking of the slab surface, has been observed on some concrete airfield pavement dedicated deicing facilities (DDFs) in North America, occurring as soon as 2 to 3 years after construction. Because the DDFs are specialized facilities that are used strictly for deicing aircraft, there was a concern that the heavy applications of glycol-based deicing fluids might somehow be contributing to the development of the premature distress through interactions with the concrete constituent materials, the construction techniques, and the environment.

This project was sponsored by the IPRF in order to determine if there was a relationship between the application of the aircraft deicing fluids and the observed distress. Members of the research team conducted an initial visit of nine airports with concrete pavement DDFs, and then conducted more detailed follow-up investigations at four of those airports. During these visits, a detailed visual assessment of the concrete pavement was conducted, and cores were obtained from various locations within each DDF for later laboratory analysis and petrographic evaluation. Available materials, pavement design, and construction information was also collected. Concrete from a fifth airport considered in good condition (without any deicing-related deterioration) was also evaluated for comparison. Based on the information gathered, the following conclusions are drawn from this study:

- No common cause of distress could be assigned to the concrete at the DDFs included in this study. Furthermore, there is no evidence to suggest that the use of glycol-based aircraft deicers is directly implicated in the chemical or microbial degradation of concrete. Indirectly, at one site the extensive use of glycol-based deicers may be contributing to the infilling of the air-void system with calcium hydroxide.

- The most common problems associated with the evaluated concrete can be broadly categorized as poor placement and consolidation and poor finishing and curing. In general, the concrete lacked uniformity not only from location to location, but from the top of the core to the bottom. Entrapped air, at times resulting in an interconnected void network, was prevalent in concrete at three of the five airports studied. Mixture proportioning has a direct impact on workability, and thus may be contributing to the consolidation problems. Plastic shrinkage and poor consolidation were often associated with observed surface cracking.

- The concrete air-void systems were marginal in many cases, with spacing factors being at or above the 0.200 mm maximum limit specified in ASTM C 457. Often, the spacing factor was found to be adequate in a portion of the core and inadequate in another. At this time, a poor air-void system is thought to be contributing to the observed distress at only a single site, yet over time, distress may develop at other sites due to the poor air-void systems observed. The environmental conditions present on a DDF are fairly severe due to the presence of moisture under freezing conditions and induced freeze-thaw cycles. It seems plausible that the intensive usage of glycol-based deicers characteristic of DDF operations may contribute to physical paste freeze-thaw (F-T) damage due to increased osmotic pressures, thermal shock, and increased saturation of the concrete, and therefore a good air-void system is critical to good performance.

- Alkali-silica reactive (ASR) aggregate particles were observed in samples from three of the sites, but in no case was the occurrence of reactive aggregates linked to the observed distress. At two sites, reactive fine aggregate particles were observed but without any apparent deleterious effect. At another site, ASR was localized in the vicinity of a macrocrack likely caused by drying shrinkage. Future damage due to ASR cannot be ruled out.

- In general, current construction practices appear adequate to prevent the construction-related problems observed. Although the extremely stiff mixtures associated with slip-form paving of airport pavements can pose difficulties during placement, it is clear from the example set at the good performing site that such mixtures can be placed with little entrapped air and sufficient entrained air. Better mixture design and proportioning, improved consolidation, and the timely and thorough application of an effective membrane-forming curing compound would prevent much of the distress observed.

As is true with most research projects, the findings of this study raise questions that should be addressed in the future. The following recommendations are made for future work:

- Ensuring that a proper air-void system is entrained in the concrete is difficult problem, as common test methods only measure the total air content of the fresh concrete and not the adequacy of the air-void system (e.g., spacing factor, specific surface). Until a proven method is available to measure the air-void system characteristics in fresh concrete, ASTM C 457 should be used during the mixture design process to verify that a suitable air-void system can be created with the specific materials to be used on the project, particularly for concrete for construction of DDFs.

- Poor consolidation was implicated in much of the deterioration observed on the DDFs studied. Work should be conducted to develop a simple test method and specification to verify that the as-placed concrete has been adequately consolidated. Such a test method and specification could be based on a test method similar to ASTM C 642, *Standard Test Method for Specific Gravity, Absorption, and Voids in Hardened Concrete*. A workable approach might be to use concrete cores randomly extracted to verify pavement thickness after construction, which are then subdivided into smaller sections and individually tested to determine the volume of permeable pore space (voids) in the top, middle, and bottom of the core. An acceptance criterion could be established, such as maximum allowable percent permeable voids or the ratio of percent permeable voids from field concrete compared to well-consolidated concrete made during the mixture design process. This would form a practical basis for judging whether adequate consolidation had been achieved.

- All but one of the pavements studied was constructed in 1998 or 1999, meaning that the specimens evaluated had only been subjected to six or seven winters prior to extraction and testing. Although there is currently little evidence that paste freeze-thaw damage is causing distress, there is sufficient evidence to support some level of concern regarding future performance. There are on-going discussions regarding the appropriateness of the limit on the spacing factor set in the ASTM C 457 procedure. Some have suggested that it can be raised given the higher strength common in modern pavement concrete. Alternatively, the

environment present on DDFs is unique and potentially harsh, and thus the limit may actually be too high. Clearly, more research is needed to determine what limits on the entrained air-void system need to be set for airport concrete in general, and for concrete used for DDFs specifically. In addition, better test methods for assessing the air-void system parameters in fresh and hardened concrete need to be developed.

- The proper use of supplementary cementitious materials (e.g., fly ash, ground granulated blast furnace slag) will enhance workability, decrease the amount of calcium hydroxide in the hydrated paste, and decrease concrete permeability. Only one of the sites studied did not incorporate supplementary cementitious materials in the mix design, and it was the site with the highest measured capillary porosity and the only site with significant infilling of secondary calcium hydroxide in the air voids. Additional work should be conducted to evaluate what, if any, benefit supplementary cementitious materials might have in improving the durability of concrete used for DDFs.

1. INTRODUCTION

Portland cement concrete is often used in the construction of pavement facilities at airports around the world. Observations of the performance of some concrete airfield pavement dedicated deicing facilities (DDFs) suggest that premature pavement distress of unknown origin and extent may be occurring, in some cases as soon as 2 to 3 years after construction. Such distress is reportedly characterized by scaling, joint spalling, crazing, and/or map cracking of the slab surface.

Because DDFs are specialized facilities that are used strictly for deicing aircraft, they are largely unused during most of the year and only see traffic during the winter months when aircraft are diverted onto the facilities and deiced and/or anti-iced. During these times, aircraft traffic is channelized and the concrete immediately in the vicinity of the aircraft deicing area is heavily inundated with glycol-based deicing fluids.

The extent to which the deicing chemicals are contributing to this deterioration is not known; neither are the possible interactions between these chemicals and the concrete constituent materials, the construction techniques, and the environment. To help quantify the nature and extent of the deterioration, this research was conducted with the following objectives:

- Determine the extent of concrete pavement distresses at selected dedicated deicing facilities in North America through site visits and meetings with airport operations personnel.

- Perform a forensic analysis to determine the extent and nature of distressed concrete obtained from such facilities.

- Determine the cause(s) of concrete distress at the facilities and what link, if any, there is to the use of aircraft deicing chemicals.

- Provide an overview of the challenges, potential solutions, and information (including future research) needed to prevent deterioration of future deicing facilities.

Thus, the primary purpose of this research was to investigate the possible role that aircraft deicing chemicals played in deterioration of concrete at dedicated deicing facilities and to develop recommendations for mitigating such deterioration in future construction projects. This research was intended to focus on the physical and/or chemical effect(s) that aircraft deicing chemicals have on concrete used in DDFs, where the concentrations of such solutions are much higher than in non-dedicated, apron-based deicing operations.

The objectives of this study were met through the execution of a research plan consisting of the following ten work tasks:

Task 1: Research Plan and Review of Literature: This task reviewed and synthesized available literature on the potential for glycol-based deicing chemicals to affect concrete durability.

Task 2: Devise and Populate Database of Deicing Facilities: This task included the site evaluation of nine North American airports that have dedicated deicing facilities and the

creation of a database that includes construction, maintenance, and climatic data. This information was used to select airports for further evaluation in Task 4.

Task 3: Interim Report and Data Review: An *Interim Report* was prepared and submitted to IPRF describing the work conducted in Tasks 1 and 2 and a proposed revised work plan for the detailed forensic study of four airports that was conducted in the remaining tasks in the study. This report was submitted to IPRF in a meeting with the Technical Panel on May 12, 2005 to discuss the findings.

Task 4: Forensic Field Study: Four of the airports that were previously visited were revisited and inspected. Core samples were obtained for forensic analysis.

Task 5: Laboratory Analysis: A detailed petrographic analysis was conducted on the specimens obtained in Task 4 to determine the distress mechanisms at work.

Task 6: Data Analysis: The data collected in Tasks 2, 4, and 5 were used to determine the cause(s) of deterioration and whether the use of glycol-based aircraft deicers is potentially contributing to the observed distress.

Task 7: Draft Final Report Preparation and 75% Review Meeting: A draft of the final report that details the work conducted in tasks 1 through 6 was prepared.

Task 8: Advanced Final Report Preparation and Submittal: The panel and IPRF determined that this task was note considered necessary.

Task 9: Advance Final Report Revisions: The panel and IPRF determined that this task was note considered necessary.

Task 10: Final Report: The Final Report and Executive Report are submitted in final format.

This *Final Report* includes the following:

- The findings of the literature review regarding the effects of glycol deicing agents on concrete airfield pavements.
- The results of the initial and follow-up visual assessment of the selected airport concrete pavement deicing pads.
- A description of the forensic petrographic analysis of the obtained specimens.
- An analysis of the data to determine the most likely cause(s) of deterioration.
- A description of potential preventive and mitigative strategies to address observed distress.
- Recommendations for future work to better understand the problems observed.

2. LITERATURE REVIEW

The focus of the study was on the potential physical and chemical impact(s) that aircraft deicing chemicals have on concrete used in dedicated facilities. The review of the literature focuses on current aircraft deicing practices and the potential impact such practices have on concrete deterioration. A summary of the literature review is provided in the next sections.

2.1. AIRCRAFT DEICING PRACTICES

The chemicals used for aircraft deicing are distinctly different than those commonly used for pavement deicing. For roadways, it is the chloride salts of calcium, magnesium, and sodium (along with other chemicals containing calcium and magnesium) that are primarily used. For airside pavements at airports, only non-chloride deicing agents are used, including urea, potassium acetate, sodium acetate, sodium formate, calcium magnesium acetate, and propylene and ethylene glycols (Mericas and Wagoner 2003). The latter two deicers are typically not used for deicing pavement, but are commonly used for aircraft deicing, making up 30 to 70 percent of the as-applied solution, with propylene glycol increasingly being used because of toxicity concerns with ethylene glycol (Ritter 2001).

In a survey conducted in the initial phases of this study, 40 North American airports were contacted regarding their aircraft deicing operations. Of those, 30 reported having dedicated pavement facilities for aircraft deicing, 21 of which were constructed of concrete. Of all airports surveyed, 40 percent reported using propylene glycol, 20 percent ethylene glycol, 10 percent used both, and 30 percent did not specify which deicing chemical they used.

In aircraft deicing, a Type I deicing agent is typically about 90 percent glycol and 8 percent water, but it may be further diluted with additional water depending on ambient temperatures. Proprietary additives, such as surfactants, thickening agents, pH buffers, corrosion inhibitors, flame retardants, and dyes may also be present. The solution is heated to 150 to 180 ^{o}F and applied under pressure to remove ice, snow, and frost (Ritter 2001).

However, Type I agents provide a holdover time of only 5 to 15 minutes. For longer holdover times, either Type II or Type IV anti-icing solutions are applied, effectively extending holdover times to about 30 minutes and 80 minutes, respectively. Anti-icing fluids, which are not diluted, are applied unheated and are about 65 percent glycol. They contain a polymer thickener to enhance adherence to the aircraft surfaces (Ritter 2001).

2.2. POTENTIAL CONCRETE DISTRESS MECHANISMS

As previously noted, aircraft deicing (and anti-icing) fluids are substantially different from roadway deicers and most airside pavement deicers. Being organic in nature (propylene glycol: $C_3H_8O_2$, ethylene glycol: $C_2H_6O_2$) and free of chlorides, some of the physical and chemical mechanisms responsible for the adverse effects of deicers on highway transportation structures (e.g. corrosion of embedded steel and salt crystallization pressures) are not relevant. These deicing agents also have little potential to accelerate alkali-silica reactivity as would alkaline halide, salt-based pavement deicers or those containing potassium, such as potassium acetate. Yet, based on the available literature, the use of glycol-based aircraft deicers could, in theory, contribute to concrete deterioration through enhanced paste freeze-thaw damage and/or chemical/bacteriological deterioration.

2.2.1. Enhanced Freeze-Thaw Damage

When saturated concrete is exposed to alternating cycles of freezing and thawing, the hydrated cement paste that binds the concrete can be damaged. As this damage accumulates and triggers the development of visible distress, it is referred to as paste freeze-thaw (F-T) damage. It has long been recognized that F-T damage to the cement paste phase can occur at the pavement surface or internally (Powers 1945). Surface scaling or crazing most often occurs in the presence of deicers, which amplify the pressures generated through freezing and thawing. Although the exact causes of deicer scaling/crazing are not known, it is commonly thought to be primarily a form of physical attack, possibly resulting from a combination of factors similar to those that cause paste F-T damage (Mindess, Young, and Darwin 2003; ACI 1992; Marchand, Sellevold, and Pigeon 1994; Pigeon 1994; Pigeon and Plateau 1995).

The most widely accepted theories consider either hydraulic or osmotic pressures (or a combination of the two) to be the primary causes. It is generally agreed that the magnitude of these internal pressures is dependent on the concrete pore structure, moisture content, pore water chemistry, rate of freezing and/or length of the freezing cycle. The temperature at which water will freeze is a function of the size of the pore in which it is contained and the concentration of dissolved ions in the water. In general, the smaller the pore and the higher the concentration of dissolved ions, the lower the temperature at which the water will freeze. An excellent review of the literature related to these phenomena is provided by Marchand, Sellevold, and Pigeon (1994).

Powers (1945) first attributed F-T damage to excessive hydraulic pressures resulting from the expansion of ice. He proposed that as ice gradually forms at discrete sites in a saturated capillary pore system, the resulting 9 percent volume expansion causes the surrounding unfrozen water to be expelled under pressure away from the freezing sites. Depending on the nature of the pore system, excessive internal stresses can be generated by hydraulic pressures resulting from resistance to this flow. The pressurized water moving away from the freezing sites would find relief at the purposefully entrained air voids, where it could then presumably freeze without causing damage.

Based on experimental results, Powers (1945) recognized that the spacing between these spherical, microscopic air voids, rather than the total volume of air in the concrete, was the better measure of resistance to F-T damage. Building on this, he developed equations that provided an average measure of the distance that water within the paste must travel to reach the surface of an air void (Powers 1949). He proposed the adoption of a void-spacing factor, now known as the Powers spacing factor, as the basis of protecting the paste from F-T damage. It is interesting to note that this pioneering work based on the hydraulic pressure theory still forms the primary basis of specifying F-T resistant concrete (see ASTM C-457).

More recent theories (Powers 1975) consider osmotic potential to be the primary cause of excess internal stress. As previously mentioned, the temperature at which water will freeze in concrete is a function of the concentration of dissolved ions as well as the pore size in which it is contained. Because of physical and chemical surface interactions between water and the surfaces of hydrated cement, the smaller the pore size, the lower the temperature required to cause freezing (Setzer 1990). Because of their relatively large size, the partially saturated, entrained air voids are likely initial freezing sites. They are only partially saturated, or possibly only damp, since the menisci that form in the smaller capillary pores generate higher surface tension and are thus more completely saturated. As the pore water solution freezes, only pure water forms ice.

Thus, the remaining unfrozen liquid at the freezing sites becomes more highly concentrated with dissolved ions. The less concentrated solution in the surrounding paste is then drawn to the freezing sites to maintain thermodynamic equilibrium. The driving force for the movement of this solution is a function of the concentration gradient. As the unfrozen solution at the freezing sites is diluted by the infusion of surrounding water, additional ice growth occurs. This progressive ice formation can occur at any solute concentration, including zero, and is referred to as ice-accretion (Powers 1949, Powers 1975).

This process of pore water moving from the capillary system to air voids will continue until one of two possible conditions prevail. If adequate air-void space exists, sufficiently distributed throughout the paste, all of the freezable water will eventually diffuse to the freezing sites inside the air voids, eliminating further fluid flow. This drains the surrounding capillary pore system, eliminating the possibility of paste F-T damage.

The other possible outcome is that the air-void system is inadequate to accommodate all of the surrounding unfrozen water. If this occurs, osmotic pressures will increase due to the remaining differences in dissolved ions concentrations between the liquid in the air voids and the bulk solution within the capillary pores. Pressures of any kind, whether caused by loading, hydraulic forces, or osmotic forces, that approach or exceed the tensile strength of the hardened cement paste will naturally cause damage. The rate of temperature drop also has an impact, with a rapid drop in temperature being more severe as it will not allow the water time to diffuse to the air voids before damage occurs.

Another key point is that the pore water solution in a hydrated cement paste contains varying levels of dissolved ions, including sodium and potassium alkalis and dissociated forms of deicer chemicals. Because of this, the water in the capillary pores can become supercooled, where it remains in a liquid state at temperatures well below 32° F. Rapid ice formation may result if the solution becomes more dilute and/or the temperature continues to drop. This leads to a rapid development of pressure in the remaining liquid that is difficult to dissipate without damage.

Little information is available in the literature regarding the direct effects of glycol-based deicers on the durability of concrete. But in light of the discussion above, it seems plausible that increased osmotic pressure due to alteration of the pore solution chemistry, increased concrete saturation, thermal shock from the heat generated due to melting ice with heated aircraft deicers, and the rapid formation of ice are all possible contributors to deterioration of concrete DDFs. Deicing aircraft on DDFs results in relatively long periods of wetting that occur during periods of freezing climatic conditions. During these periods, the concrete will become saturated and the pore solution chemistry unbalanced. Often, the approach of cold fronts creates weather that merits aircraft deicing, thus the ambient temperatures may drop rapidly over the period of aircraft deicing operations. Although the high glycol concentration may prevent freezing at or just below the surface of the concrete, at some depth the glycol will not penetrate, increasing osmotic pressures. In addition, the thermal shock at this surface layer will increase as the often-heated deicing solution contacts the frozen concrete surface. And finally, the rapid formation of ice in supercooled pore solution may also contribute to increased stress development. In combination, the physical stresses generated due to freezing and thawing in the concrete during aircraft deicing operations and immediately afterwards could be considerable.

Another factor that was considered as potentially playing a role in enhancing the physical F-T damage to the cement paste is the reduction of the pore solution surface tension in the capillary

pores due to the presence of glycol-based deicers. Work conducted on a glycol-based shrinkage reducing admixture (SRA) consisting of glycol and ether isomeric compounds found that the SRA functions by reducing the surface tension of the pore water solution, lowering capillary tension forces (Jeknavorian and Barry 1999).

Another study of a propylene glycol-derived SRA also stated that the effectiveness of the admixture was due to the reduction of capillary pore surface tension (Shah et al. 1996). Although the focus of these papers was not concrete deterioration, the fact that glycol-based SRAs reduce the surface tension of the capillary pore solution was considered potentially relevant to this study. As discussed, the surface tension in the capillary pore solution prevents the larger entrained air voids from saturating, making them available to protect the paste against F-T damage. If the presence of glycol-based aircraft deicers reduces the surface tension of the capillary pore solution in concrete, it is reasonable to assume that this might result in an increase in saturation of the entrained air voids, contributing to F-T damage.

2.2.2. Chemical and Bacteriological Deterioration

In addition to physical attack due to freezing and thawing, chemical and microbial activity were also considered to potentially contribute to the deterioration of concrete subject to glycol-based aircraft deicers. It is known that the solubility of calcium hydroxide, which is an important component in hydrated cement paste, is significantly increased as temperatures decrease. In the presence of glycols, the freezing temperature of the pore solution will be depressed, thus increasing the solubility of the calcium hydroxide. Potentially amplifying this effect is the possibility that the presence of glycol in solution may also increase calcium hydroxide solubility. At a solution temperature of 77 ^{o}F, the solubility of calcium hydroxide increases from 0.159 to 13.332 grams per 100 grams of saturated solution with the addition of 35 grams of sugar (Cheney 2004). This effect was substantiated in a study of deteriorated concrete specimens soaked in a glucose solution (Housewright et al. 2004). The calcium hydroxide depletion significantly increased the porosity of the hydrated cement paste, weakening it while making it more permeable. Although glycols are technically not “sugars,” the potential for calcium hydroxide depletion exists, especially for a deicing solution that is applied near or below freezing.

In addition, ethylene and propylene glycol aircraft deicers are known to provide a nutrient source to bacteria, actinomycetes, and fungi (Cox 1978; Sabeh and Narasiah 1992). A large body of knowledge exists to study this biodegradation, primarily from the perspective of bioremediation of waste from aircraft deicing operations. Of direct interest to this study is that as biodegradation occurs, acids and carbon dioxide are produced at different stages of the process (Cox 1978; Veltman, Shoenberg, and Switzenbaum 1998; Willets 1981; Zitomer and Tonuk 2003). None of these studies investigated whether biodegradation was occurring in the concrete, yet it may be possible that the surface of the concrete could provide a suitable habitat for organisms that biodegrade glycol-based deicing solutions. As biodegradation occurs, the acids produced would contribute to the leaching of the calcium hydroxide discussed previously, increasing the porosity of the concrete and making it more susceptible to additional degradation.

2.3. SUMMARY OF LITERATURE REVIEW

There has been very little written on the effects of glycol on concrete and only a single, non-conclusive, paper was found that specifically examines the impact of glycol-based deicers on the F-T durability of concrete (Minsk 1977). The general assumption in the literature is that glycols are benign with respect to concrete deterioration and thus they have not been the focus of past research efforts. But the construction of DDFs, where concrete pavement is being subjected to high concentrations of glycol-based aircraft deicers over relatively long periods of time, has created a situation that has not previously existed. It therefore seemed plausible that potential physical and chemical mechanisms of distress exist and that a more thorough analysis is justified to ascertain whether such mechanisms are actually at work on concrete airfield pavement DDFs.

3. SUMMARY OF INITIAL FIELD VISITS

3.1. INTRODUCTION

A series of initial field visits to airports with dedicated deicing facilities was planned as the first step in determining whether aircraft deicing agents were contributing to the development of premature distress on these pavements. A comprehensive list of airports containing dedicated deicing facilities was obtained from the Federal Aviation Administration (FAA) and reviewed with regard to pavement age and geographic distribution to create a contact list of 25 airports. Telephone conversations with representatives from these airports pared down the list to a total of nine airports selected for initial inspections. A summary of the airports included in the initial field visits is provided in table 1.

TABLE 1. AIRPORTS INCLUDED IN INITIAL FIELD VISITS

Airport	FAA Region	Facility Type	Year Built	Slab Design	Avg. Ann Precip, in	Freezing Index[1]	Avg. Ann F-T Cycles[2]	Inspection Date	No. Pads Inspected
Alpha	AGL	Dedicated Deicing Pad	1998	15-in JPCP	30.1	3359	6-8	10/15/2004	1
Beta	ASO	Dedicated Deicing Pad	1995	14-in JPCP	48.1	91	1-2	10/29/2004	1
Charlie	AEA	Dedicated Deicing Pad	1998	16-in JPCP	34.0	695	5-7	11/11/2004	1
Delta	AGL	Dedicated Deicing Pad	1998	16-in JPCP	29.4	1711	3-5	11/12/2004	1
Echo	AEA	Dedicated Deicing Pad	1999	15-in JPCP	41.9	75	4-5	12/6/2004	1
Foxtrot	ANM	Dedicated Deicing Pad	1999	17-in JPCP	15.8	285	8-10	12/10/2004	1
Golf	AEA	Dedicated Deicing Pad	1990 2000	15-in JPCP 17-in JPCP	37.9	412	6-8	12/20/2004	2
Hotel	AGL	Dedicated Deicing Pad	1996	15-in JPCP	39.6	433	6-8	12/21/2004	1
India[3]	ANM	Gate Deicing Pad	1990s	JPCP	37.1	33	1-3	1/7/2005	1

[1]30-Year Average
[2]Near Surface
[3]This airport was dropped from the study once the inspection revealed that no dedicated deicing facilities were present.

3.2. FIELD EVALUATION APPROACH

Between October 2004 and January 2005, visits to each of the nine airports listed in table 1 were conducted. In the course of these visits, team members conducted a detailed visual assessment of the concrete pavement deicing facility to determine the nature and extent of deterioration. In general, the survey guidelines developed under a recent Federal Highway Administration (FHWA) project were followed (Van Dam et al. 2002). These guidelines provide a standardized approach for the field evaluation of concrete pavements exhibiting materials-related distress (MRD), such as the fine cracking, scaling, and perhaps spalling that might be exhibited by concrete pavements exposed to aircraft deicing agents. However, these guidelines were modified slightly for use on airfield pavements and to incorporate the Pavement Condition Index (PCI) survey method as documented in ASTM D 5340 (ASTM 1998).

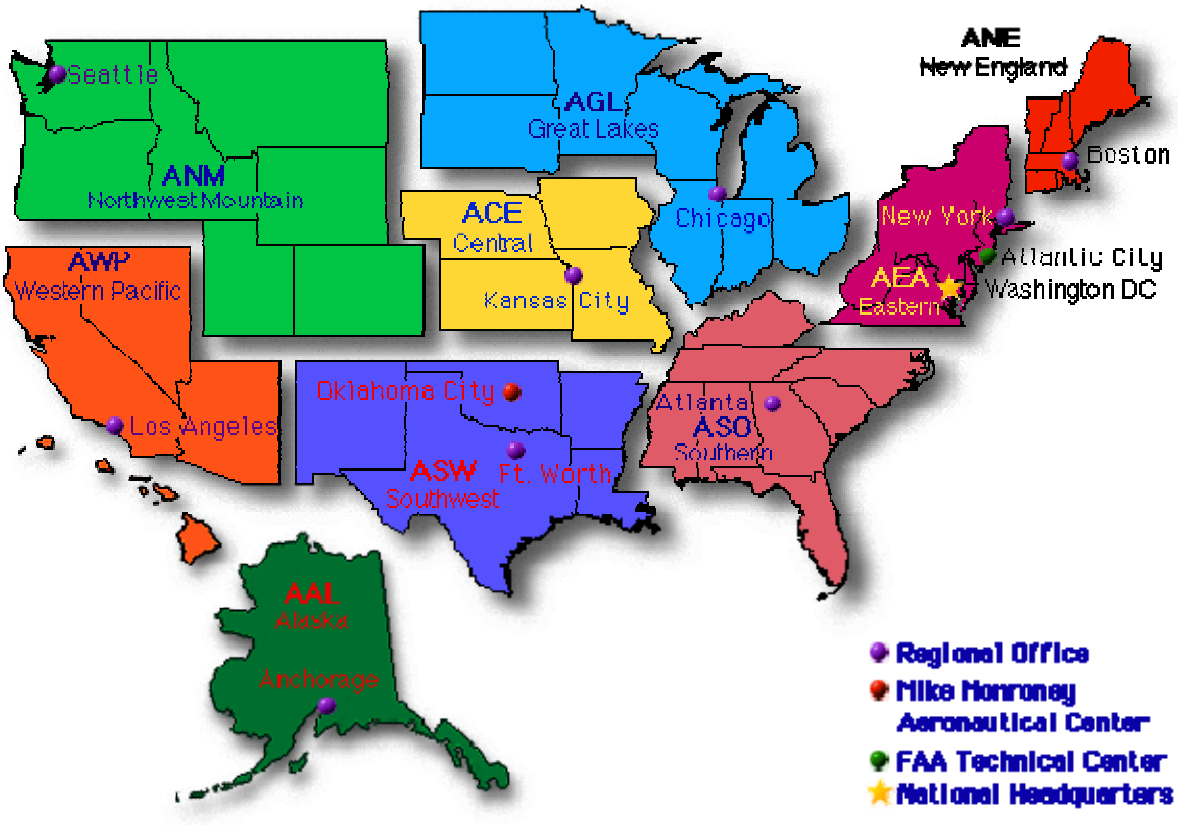

FIGURE 1. FAA REGIONS

Most of the airports had multiple DDFs, all of which were briefly inspected before selecting one for detailed inspection. Two DDFs were ultimately inspected for Airport Golf, and in the case of Airport India it was discovered at the time of inspection that it did not have a DDF. In this case, drive-by inspections were completed of the gates where deicing was conducted, but detailed inspections were not deemed warranted. Airport India was thus dropped from further study.

Initially, the inspection team walked over each deicing pad looking for any particular signs of MRD, such as map cracking, scaling, or spalling. Next, to provide more detailed information about the overall performance of the pavement, two separate sample units (defined as an area of approximately 20 contiguous slabs) were selected from each deicing pad: one from the central portion of the deicing pad where the channelized flow of the aircraft and the position of the deicing boom would lead to high concentrations of deicer and one from the outer portion of the deicing pad away from the aircraft deicing area where deicer concentrations are expected to be lowest. For the purposes of this work, these two sample units per deicing facility were deemed adequate to identify the presence and extent of general pavement distress.

Within each sample unit, a PCI survey was conducted in accordance with ASTM D 5340 (ASTM 1998). The PCI procedure was developed by the Army Corps of Engineers as a means of determining the current condition of a pavement network (Shahin and Walther 1990). Extensive work went into the development of a numerical index value that is used to represent the pavement's structural integrity and its surface operational condition based on the observed distress. The resulting PCI value ranges from 0 (indicating a "failed" pavement) to 100 (indicating a "perfect" pavement) and accounts for the types of distress, the severity of the distresses, and the amount or extent of the distresses. The associated effects of these factors are

combined into a composite PCI value through established "weighting factors" so that it more accurately reflects the overall performance of the pavement (Shahin and Walther 1990).

The specific distress types recognized by the PCI procedure are listed in table 2. Although the procedure only requires the recording of the presence of distresses, team members also recorded actual distress quantities and locations within the slabs. Furthermore, as discussed later, team members tried to capture associated distress manifestations (crack patterns, staining, material depositions) that may be useful in identifying MRD. This is because the PCI method is generally insensitive to some of the subtle features characteristic of MRD, including fine cracking, staining, exudate, and so on. As a result, a pavement in the early stages of a serious MRD problem may rate as being in excellent condition according to the PCI method but may ultimately pose a significant foreign object damage (FOD) potential once the MRD progresses; something that can happen in a fairly short amount of time.

TABLE 2. PCI DISTRESS TYPES FOR CONCRETE AIRFIELDS (ASTM 1998)

Distress Type	Severity Levels	How Rated/ Recorded
Blowup	L, M, H	Per slab basis/Highest severity recorded
Corner Break	L, M, H	Per slab basis/Highest severity recorded
Cracks: Longitudinal, Transverse, Diagonal	L, M, H	Per slab basis/Highest severity recorded
Durability (D-) Cracking	L, M, H	Per slab basis/Highest severity recorded
Joint Seal Damage	L, M, H	Per sample unit/Average condition recorded
Patching, Small	L, M, H	Per slab basis/Highest severity recorded
Patching, Large and Utility Cuts	L, M, H	Per slab basis/Highest severity recorded
Popouts	None	Per slab basis
Pumping	None	Per slab basis
Scaling/Map Cracking/Crazing	L, M, H	Per slab basis
Settlement or Faulting	L, M, H	Per slab basis
Shattered Slab/Intersecting Cracks	L, M, H	Per slab basis/Highest severity recorded
Shrinkage Cracks	None	Per slab basis
Spalling (Longitudinal and Transverse Joint)	L, M, H	Per slab basis/Highest severity recorded
Spalling (Corner)	L, M, H	Per slab basis/Highest severity recorded

Upon completion of the PCI surveys of each sample unit, a more detailed MRD survey was conducted. This involved the selection of a single slab within each sample unit that had been previously noted to be exhibiting MRD (if no such distress was noted, this detailed inspection was not conducted). This single slab was then inspected in detail, noting specific distress characteristics such as the following:

- Typical cracking pattern (location, orientation, extent, crack size).
- Staining (location, color).
- Exudate (presence, color, extent).
- Scaling (location, area, depth).
- Any other unusual surface characteristics.

During the inspections, a photo summary of the general DDF layout, conditions, and specific distresses was compiled.

Finally, if available, plans and specifications from the construction of the deicing facilities were obtained to provide design and construction information. Unfortunately, in many cases, detailed design and construction documentation was not available.

3.3. SUMMARY OF AIRPORT INSPECTIONS

A summary of the pavement design, construction, and performance data collected for the various airport pavements as part of the initial site visits is provided in table 3. More detailed performance information for each individual airport is provided in the following sections.

3.3.1. Airport Alpha

The pavement deicing pads at Airport Alpha were built in 1998 as part of the construction of a new central deicing facility intended to minimize the release of glycol to the environment. Five deicing pads, each nominally 340 ft by 780 ft, were constructed adjacent to one another sharing a comprehensive glycol collection system.

The pavement structure is a 15-in thick jointed plain concrete pavement (JPCP) design, with 20 ft by 20 ft slabs and a polyurethane joint sealant. Ethylene glycol is used as the aircraft deicing fluid. The concrete mix proportions used for the construction of the deicing pads is provided in table 4.

TABLE 4. CONCRETE MIX PROPORTIONS USED AT AIRPORT ALPHA

Component	**Quantity**
Stone (0.75 in)	826 lb/yd^3
Stone (1.5 in)	1,247 lb/yd^3
Sand	1,205 lb/yd^3
Cement (type 10)	522 lb/yd^3
Water	228 lb/yd^3
Air	5.0 percent
Total	4,035 lb/yd^3
w/c	0.44

TABLE 3. SUMMARY OF SELECTED AIRPORT DEICING PAD DESIGN, CONSTRUCTION, AND PERFORMANCE DATA

Airport	Facility Type	Sample Unit	Year Built	Type of Deicer	Slab Design	Slab Size (ft)	Sealant Type	PCI 2004	PCI 2005	Observed Distresses and Conditions
Alpha	Dedicated	1 (heavy)	1998	Ethylene Glycol	15-in	20 x 20	Poly-urethane	97	92	Low-severity spalling, low-severity patching, hairline cracking, gray exudate.
	Dedicated	2 (low)	1998	Ethylene Glycol	15-in	20 x 20	Poly-urethane	100	95	MRD hairline cracking.
Beta	Dedicated	1 (heavy)	1995	Propylene Glycol	14-in	25 x 25	Silicone	95		Low-severity joint spalling, hairline cracking, rust-colored staining at joints and slabs.
	Dedicated	2 (low)	1995	Propylene Glycol	14-in	25 x 25	Silicone	91		Low- and medium-severity joint spalling.
Charlie	Dedicated	1 (heavy)	1998	Propylene Glycol	16-in	25 x 25	Poly-urethane	89		Low-severity joint seal damage, low- and medium-severity joint spalling, hairline cracking.
	Dedicated	2 (low)	1998	Propylene Glycol	16-in	25 x 25	Poly-urethane	91		Low-severity joint seal damage, low-severity corner spalling, popouts.
Delta	Dedicated	1 (heavy)	1998	Propylene Glycol	16-in	25 x 25	Silicone	97		Low-severity patching.
	Dedicated d	2 (low)	1998	Propylene Glycol	16-in	25 x 25	Silicone	98		Low-severity corner spalling, few sliver spalls.
Echo	Dedicated	1 (heavy)	1999	Propylene Glycol	15-in	20 x 20	Silicone	91	87	Low-severity joint spalling, hairline cracking.
	Dedicated	2 (low)	1999	Propylene Glycol	15-in	20 x 20	Silicone	94	91	Low-severity joint spalling.
Foxtrot	Dedicated	1 (heavy)	1999	Propylene Glycol?	17-in	18.75 x 20	Silicone	73	86	Low-severity scaling, popouts, map cracking, some gray staining.
	Dedicated	2 (low)	1999	Propylene Glycol?	17-in	18.75 x 20	Silicone	87	84	Low-severity map cracking and scaling, popouts.
Golf	Dedicated Pad E	1 (heavy)	1990	Propylene & Ethylene Glycol	15-in	25 x 25	Hot-Poured	63		Medium-severity joint seal damage, low-severity patching, low-severity cracking, low-severity joint and corner spalling, hairline cracking.
	Dedicated Pad E	2 (low)	1990	Propylene & Ethylene Glycol	15-in	25 x 25	Hot-Poured	59		Medium-severity joint seal damage, popouts, low-severity patching, low-severity cracking, low-severity corner spalling, hairline cracking.
	Dedicated Pad C	1 (heavy)	1990	Propylene & Ethylene Glycol	15-in	25 x 25	Hot-Poured	57	53	Low-severity cracking, low-severity shattered slab, hairline cracking.
	Dedicated Pad C	2 (low)	1990	Propylene & Ethylene Glycol	15-in	25 x 25	Hot-Poured	62	61	Low- and medium-severity patching, low-severity cracking, low-severity shattered slab, hairline cracks.
Hotel	Dedicated	1 (heavy)	1996	Propylene Glycol	15-in	25 x 25	Hot-Poured	91		Low-severity crazing, few popouts, isolated hairline cracking.
	Dedicated	2 (low)	1996	Propylene Glycol	15-in	25 x 25	Hot-Poured	71		Low-severity crazing, heavy popouts.

Two sample units were selected from one of the pads for the detailed surveys: sample unit 1 (in the central portion of the DDF) and sample unit 2 (in an outer portion of the DDF). Overall, both sample units were in very good condition, exhibiting no signs of structural distress or widespread deterioration. Figure 2 shows an overview of the deicing pad that was inspected.

Sample unit 1, located in an area subjected to heavy applications of deicing fluids, had low-severity joint spalling and a low-severity small patch (see figure 3), as well as some hairline cracking at random locations within the slabs (see figure 4) on about five of the twenty slabs. A dark gray exudate was present in a few of the cracks. Poor consolidation was noted on the surface in four adjacent slabs.

The only distress in the second sample unit, located in an area subjected to lower applications of deicing fluids, was one slab exhibiting a very small amount of map cracking near a joint (see figure 5).

FIGURE 2. OVERVIEW OF DEICING PAD INSPECTED AT AIRPORT ALPHA

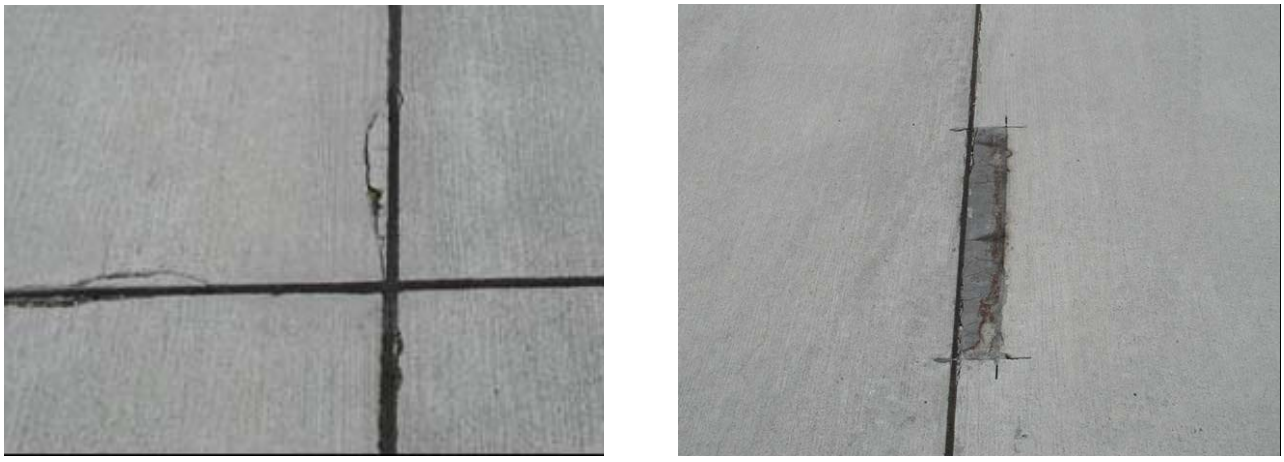

FIGURE 3. LOW-SEVERITY SPALLING (LEFT) AND LOW-SEVERITY PATCH (RIGHT) ON SAMPLE UNIT 1 AT AIRPORT ALPHA

FIGURE 4. FINE HAIRLINE CRACKING OBSERVED IN SAMPLE UNIT 1 AT AIRPORT ALPHA

FIGURE 5. FINE HAIRLINE CRACKS NEAR A JOINT IN SAMPLE UNIT 2 AT AIRPORT ALPHA

3.3.2. Airport Beta

In 1995, Airport Beta constructed a 300 ft by 300 ft DDF at the north end of the airport. The pavement is a 14-in JPCP design, with 25 ft by 25 ft slabs and silicone joint sealants. A trench drain collection system is constructed into the pavement around the outer perimeter of the facility to collect the propylene glycol deicing fluid. Figure 6 shows an overview of the deicing facility and figure 7 shows the trench drains located around the perimeter of the deicing facility.

Two sample units were selected from within the deicing facility for detailed evaluations. The first sample unit, located in an area where heavy concentration of deicing fluids are applied, had some low-severity joint spalling at a few of the joints (see figure 8). There was also some hairline cracking observed at a few of the joints and in a few of the slabs (see figure 8), with some of the cracks exhibiting a rust-colored staining. These cracks were typically less than 6 or 8 in long. The joint sealant was noted to be in good to excellent condition.

FIGURE 6. OVERVIEW OF DEICING FACILITY AT AIRPORT BETA

FIGURE 7. TRENCH DRAINS AROUND DEICING FACILITY AT AIRPORT BETA

FIGURE 8. LOW-SEVERITY SPALLING (LEFT) AND HAIRLINE CRACK (RIGHT) IN SAMPLE UNIT 1 AT AIRPORT BETA

The second sample unit, located in an area where lower levels of deicing fluids are applied, also had some low-severity joint spalling. Overall, the joint sealant was in good condition and no signs of MRD were observed.

3.3.3. Airport Charlie

Airport Charlie has dedicated deicing areas in proximity to departure runways. The Runway 22 Hold Pad has two marked deicing locations and a hold location identified as part of "De-Ice Pad C West;" within this area are three marked "positions" to channelize aircraft onto the pad for deicing operations. The two areas that were inspected under this project are close to positions 2 and 3 of that deicing pad. An overview of the facility is shown in figure 9.

This pavement was constructed in the late 1990s. The pavement structure consists of a 16-in thick JPCP, placed over a 4-in asphalt-treated base (ATB) constructed on a granular subbase. No positive drainage is provided beneath this pavement. Slabs are 25 ft by 25 ft, and all joints are sealed with a polyurethane fuel resistant sealant (Vulchem).

Sample unit 1, located in an area of higher deicing concentrations, is located almost entirely within deicing position 2. One slab exhibited map and hairline cracking over the entire surface (see figure 10), and another shows faint signs of similar cracking. Another slab had low-severity longitudinal and transverse joint spalling and one had medium-severity longitudinal and transverse joint spalling (see figure 11). The sealant was rated in fair to good condition.

The second sample unit was taken in an area away from heavy deicing concentrations, although two slabs from sample unit 2 are in the footprint of deicing position 3. However, those slabs did not exhibit any distress and the rest of the sample unit is outside of that deicing position. Two slabs within the sample unit exhibited low-severity corner spalling and one slab had some popouts.

FIGURE 9. OVERVIEW OF DEICING FACILITY AT AIRPORT CHARLIE

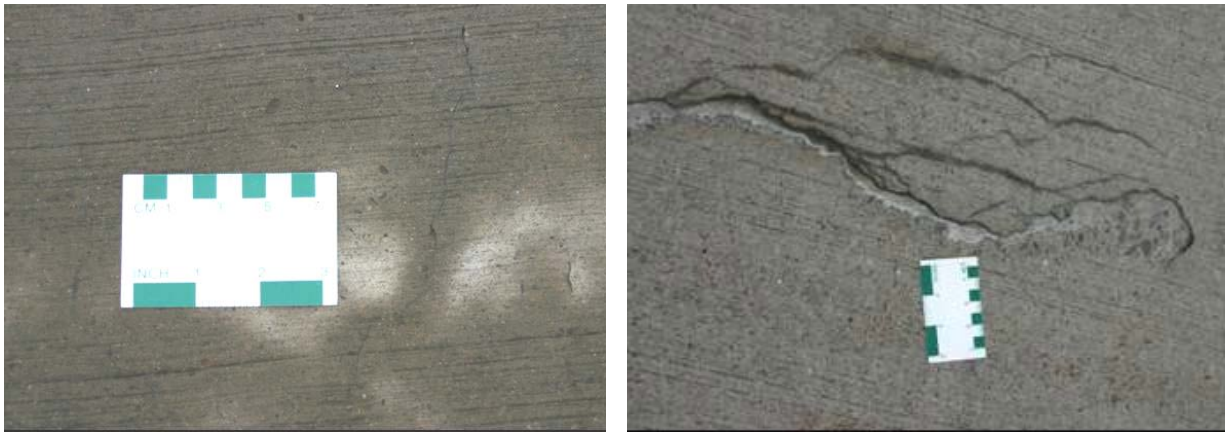

FIGURE 10. HAIRLINE CRACKING OBSERVED IN SAMPLE UNIT 1 AT AIRPORT CHARLIE

3.3.4. Airport Delta

The Runway 12L deicing pad is one of three deicing pads at Airport Delta. Each of the existing pads is located adjacent to a departing runway end and is available for aircraft that require deicing immediately prior to take off. This deicing pad, constructed in 1998, also doubles as the Runway 12L Hold Pad.

FIGURE 11. JOINT SPALLING IN SAMPLE UNIT 1 AT AIRPORT CHARLIE

The pavement structure consists of a 16-in thick JPCP design. Slabs are 25 ft by 25 ft and sealed with a silicone joint sealant material. The slabs are exposed to propylene glycol deicing fluids. Figure 12 shows an overview of the deicing facility.

The first sample unit, located in an area of higher deicing concentration, is situated in the middle of deicing position 6. There is one small patch noted within the sample unit; otherwise the pavement is in excellent condition. No cracking, staining, exudate, scaling, or other signs of surface deterioration are noted. The sealant was in fair to good condition, although some adhesive failures were noted (see figure 13).

The second sample unit is located in an area of the 12L Hold Pad that should receive little if any deicing application. One slab exhibited a low-severity corner spall and there were some sliver spalls, but it appears as if most damage is due to the scraping of snowplow blades rather than some type of pavement performance problem (see figure 14). The sealant was again noted in good condition.

FIGURE 12. OVERVIEW OF DEICING FACILITY AT AIRPORT DELTA

FIGURE 13. SEALANT ADHESIVE FAILURE ON SAMPLE UNIT 1 AT AIRPORT DELTA

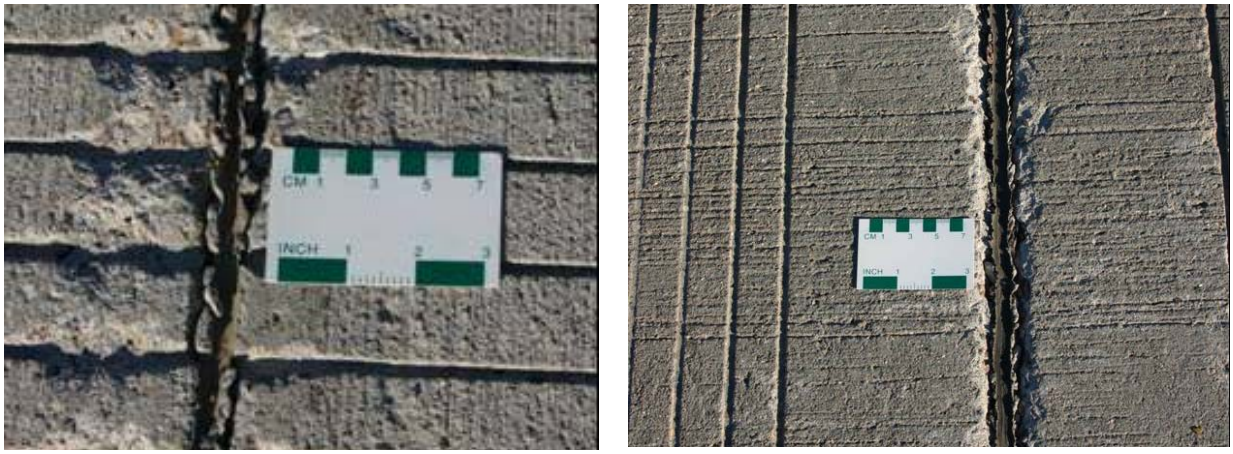

FIGURE 14. SNOWPLOW DAMAGE ON SAMPLE UNIT 2 AT AIRPORT DELTA

3.3.5. Airport Echo

In 1999, Airport Echo opened a dedicated deicing facility southeast of the main terminal and near the 28 end of Runway 10-28. The concrete area of the pad is about 28,900 yd^2, and contains trench collection drains at the perimeter and at fixed intervals within the pad itself. The pavement is a 15-in JPCP, with 20 ft by 20 ft slabs and a silicone joint sealant. Figure 15 gives an overview of the deicing pad.

Two separate sample units were surveyed at Airport Echo. The first sample unit was selected in an area of high deicer application, near the north end of the pad. This sample unit exhibited some joints with low-severity joint spalling; some fine hairline cracking was observed in the interior portions of the slab (at random locations and not part of any overall pattern), with no staining or exudate present (see figure 16). The overall condition of the joint sealant was good.

The second sample unit, taken in the south area of the pad in an area of lower deicer application, is performing similar to the first. It had some low-severity joint spalling at a few joints. No hairline cracking was observed, and the overall condition of the joint sealant was good.

In a final walk-over of the entire deicing pad, it was observed that the hairline cracking was more apt to be present at the north end of the pad. Furthermore, some structural cracking was observed at the south end of the pad, although not located within either sample unit.

FIGURE 15. OVERVIEW OF DEICING FACILITY AT AIRPORT ECHO

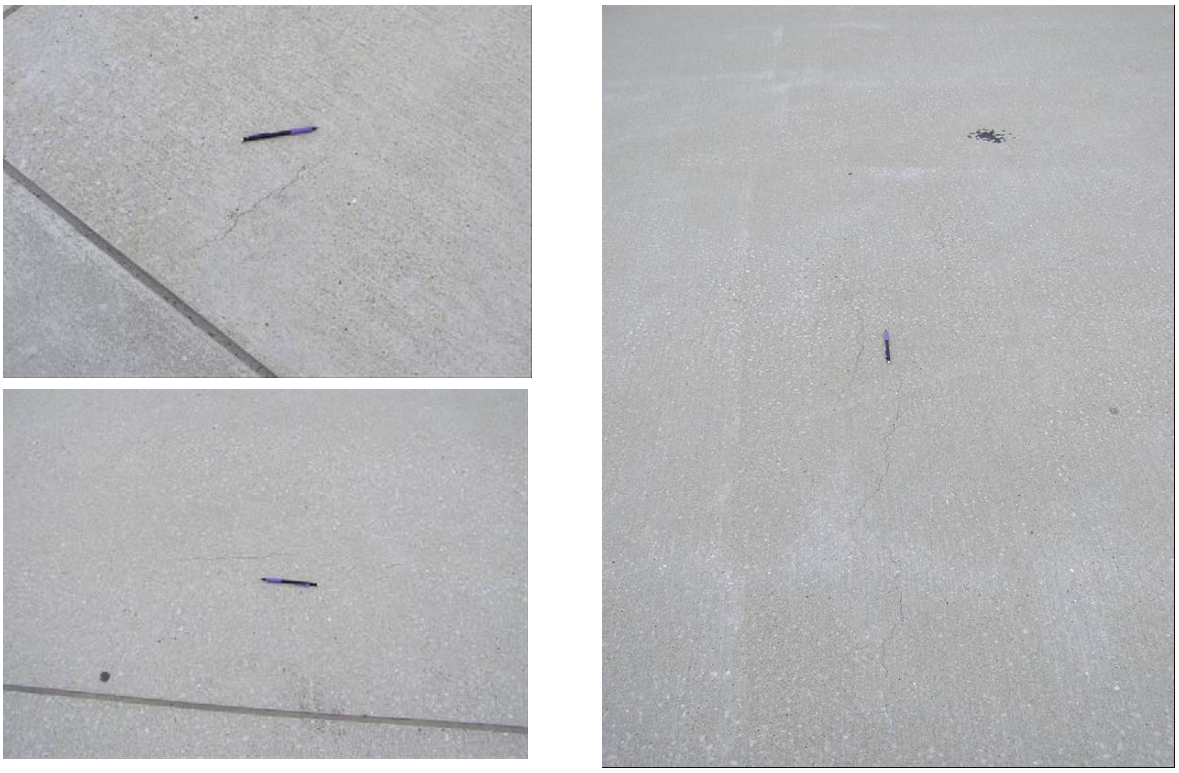

FIGURE 16. HAIRLINE CRACKING OBSERVED IN SAMPLE UNIT 1 AT AIRPORT ECHO

3.3.6. Airport Foxtrot

Deicing Pad B is one of three dedicated deicing areas at Airport Foxtrot. The pavement was constructed in 1999, and consists of a 17-in thick JPCP placed over a cement-treated base and a lime-treated subgrade. Load transfer is provided on all sides by 1.5-in diameter, 18-in long dowels. While there is no subsurface drainage, edge drainage is provided. The slabs are 18.75 ft by 20.25 ft, and all joints are sealed with silicone. Some of this is non-sag sealant, which was installed in 2004. All joints are also beveled. An overview of the deicing area is shown in figure 17.

FIGURE 17. OVERVIEW OF DEICING FACILITY AT AIRPORT FOXTROT

Sample unit 1 is located in an area of Deicing Pad B that is exposed to deicing fluids. All slabs exhibited popouts and seven of the slabs exhibited occasional hairline cracking identified as map cracking, shown in figure 18. The cracks were approximately 6 to 8 inches long, randomly located, and parallel to both longitudinal and transverse joints. There may also have been some fine map cracking. A dark gray staining was associated with a few of the cracks. There was also one panel that exhibited scaling in the center portion, less than 0.13 in deep.

Sample unit 2 is located directly to the east of the deicing pad, so it has much less exposure to deicing fluids. The slabs in this section exhibited occasional popouts, map cracking (on four slabs, see figure 19), and surface scaling (on one slab, see figure 20).

FIGURE 18. MAP AND HAIRLINE CRACKING OBSERVED ON SAMPLE UNIT 1 AT AIRPORT FOXTROT

FIGURE 19. MAP AND HAIRLINE CRACKING OBSERVED ON SAMPLE UNIT 2 AT AIRPORT FOXTROT

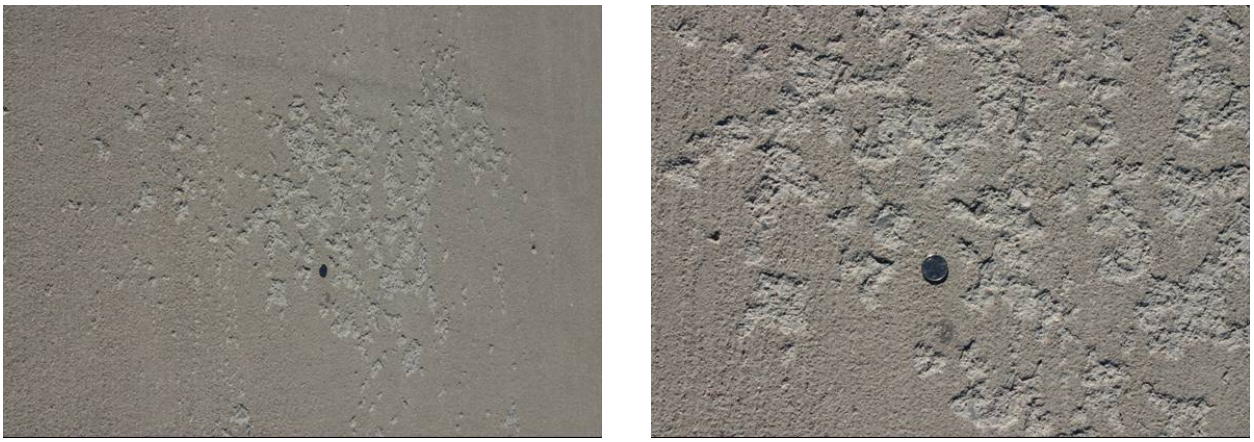

FIGURE 20. SURFACE SCALING OBSERVED ON SAMPLE UNIT 2 AT AIRPORT FOXTROT

3.3.7. Airport Golf

Airport Golf has a series of concrete pavement deicing pads constructed throughout the airport. For this project, two separate deicing pads were selected and inspected. One of the pads (Deicing Pad E) is centrally located within the airport and south of the control tower, and the other (Deicing Pad C) is located northeast of the tower near the 28 end of runway 10L-28R. Both deicing pads were built in 1990, have been exposed to propylene and ethylene glycol, and share similar design features: 15-in JPCP, 25-ft by 25-ft slabs, and a hot-poured asphaltic joint sealant. An overview of each deicing pad is shown in figure 21, with a summary of the performance of each deicing pad given below.

FIGURE 21. OVERVIEW OF DEICING PAD E (LEFT) AND DEICING PAD C (RIGHT) AT AIRPORT GOLF

Deicing Pad E

Two sample units were selected that reflect areas of the pavement subjected to heavy and light applications of deicing fluids. The first sample unit of this deicing pad (located in an area of heavy deicing application) is representative of a pavement in fair to good condition, but in need of structural rehabilitation. Major distresses observed were low-severity cracking, low-severity patching, and low-severity joint and corner spalling (see figure 22). Some very fine map cracking was observed on a few of the slabs, but without any staining or exudate present (see figure 23). The joint sealant was in fair to poor condition over the entire sample unit, due to hardening and oxidation of the material, and periodic signs of adhesive failures.

The second sample unit, located in an area of lower deicing concentration, was very similar in condition to that of the first sample unit, exhibiting low-severity cracking, low-severity patching, popouts, and low-severity joint and corner spalling. Again, some very fine map cracking was observed on a few of the slabs, and the joint sealant was noted to be in fair to poor condition. Some of the observed conditions are shown in figure 24.

FIGURE 22. CRACKING, PATCHING, AND SPALLING OBSERVED ON SAMPLE UNIT 1 OF DEICING PAD E AT AIRPORT GOLF

FIGURE 23. MAP CRACKING OBSERVED ON SAMPLE UNIT 1 OF DEICING PAD E AT AIRPORT GOLF


FIGURE 24. CRACKING, POPOUTS, AND MAP CRACKING OBSERVED ON SAMPLE UNIT 2 OF DEICING PAD E AT AIRPORT GOLF

Deicing Pad C

Two sample units were also inspected on the deicing pad C. The first sample unit was in an area of heavy deicer concentration and exhibited low-severity shattered slabs (a shattered slab is when cracking divides the slab into four or more pieces) and low-severity cracking. Some fine map cracking and a few short hairline cracks were observed on a few slabs. The joint sealant was in overall good condition, and had been placed in an overbanded configuration. Figures 25 and 26 illustrate some of the conditions on this sample unit.


FIGURE 25. CRACKING (LEFT) AND OVERBANDED SEALANT (RIGHT) ON SAMPLE UNIT 1 OF DEICING PAD C AT AIRPORT GOLF

FIGURE 26. HAIRLINE CRACKING OBSERVED ON SAMPLE UNIT 1 OF DEICING PAD C AT AIRPORT GOLF

The second sample unit was located in an area receiving lower deicing concentrations. This sample unit exhibited low-severity shattered slabs, low-severity cracking, and low- and medium-severity patching. A few short hairline cracks were observed at random locations over the sample unit (see figure 27) and the joint sealant (again placed in an overbanded configuration) was in good condition.

FIGURE 27. HAIRLINE CRACKING OBSERVED ON SAMPLE UNIT 2 OF DEICING PAD C AT AIRPORT GOLF

3.3.8. Airport Hotel

There are four dedicated deicing facilities located at Airport Hotel, of which two are associated with the passenger terminal. For this project, a portion of deicing apron 2, located just north of the terminal, was inspected. The pavement was built in 1996 and consists of a 15-in JPCP over a 6-in asphalt-treated permeable base. The slabs are 25 ft by 25 ft and the joints are sealed with a hot-poured material placed in an overbanded configuration. The deicing pads are exposed to propylene glycol deicing fluids. Figure 28 shows an overview of the deicing facility.

FIGURE 28. OVERVIEW OF DEICING FACILITY AT AIRPORT HOTEL

The first sample unit, located in an area of heavy deicer concentrations, was in good condition without any signs of cracking or spalling. The only observed distress was popouts on one slab (in order to be counted as a distress in the PCI procedure, popout density must exceed 3 popouts/yd^2). The joint sealant was in fair condition, corresponding to a medium-severity rating, and had been placed in an overbanded configuration. No signs of map cracking, crazing, or MRD were evident.

Although in an area of lower deicer concentration, virtually every slab in the second sample unit exhibited popouts; low-severity crazing was also observed on three slabs. The joint sealant was in fair to good condition and no cracking or spalling was present. Figure 29 shows some of the observed conditions on the deicing facility.

FIGURE 29. JOINT SEALANT (UPPER LEFT, SAMPLE UNIT 1), POPOUT (UPPER RIGHT, SAMPLE UNIT 2), AND OVERALL SLAB CONDITION (BOTTOM, SAMPLE UNIT 2) AT AIRPORT HOTEL

3.4. OVERALL SUMMARY AND RECOMMENDATIONS FROM INITIAL FIELD VISITS

The field visits conducted as part of this research project were performed to determine whether the observed deterioration could be identified as MRD that was somehow caused by the use of the aircraft deicing agents. At each facility included in this study, pavements both within a DDF (and therefore subjected to periodic applications of deicing fluids) and pavements outside of the DDF (and presumably not subjected to the same deicers, or subjected to far less deicer quantities) were examined. For a given DDF, little difference in condition was observed between the areas of heavy and light deicer application based on either PCI or the more detailed visual assessment. A flowchart for assessing the likelihood of an MRD (figure 30) was applied to each of the DDFs evaluated. As a result of this investigation, it was concluded that some sort of a materials-related distress might be present on the DDFs at Airports A, B, E, F, G (Pad C), and H.

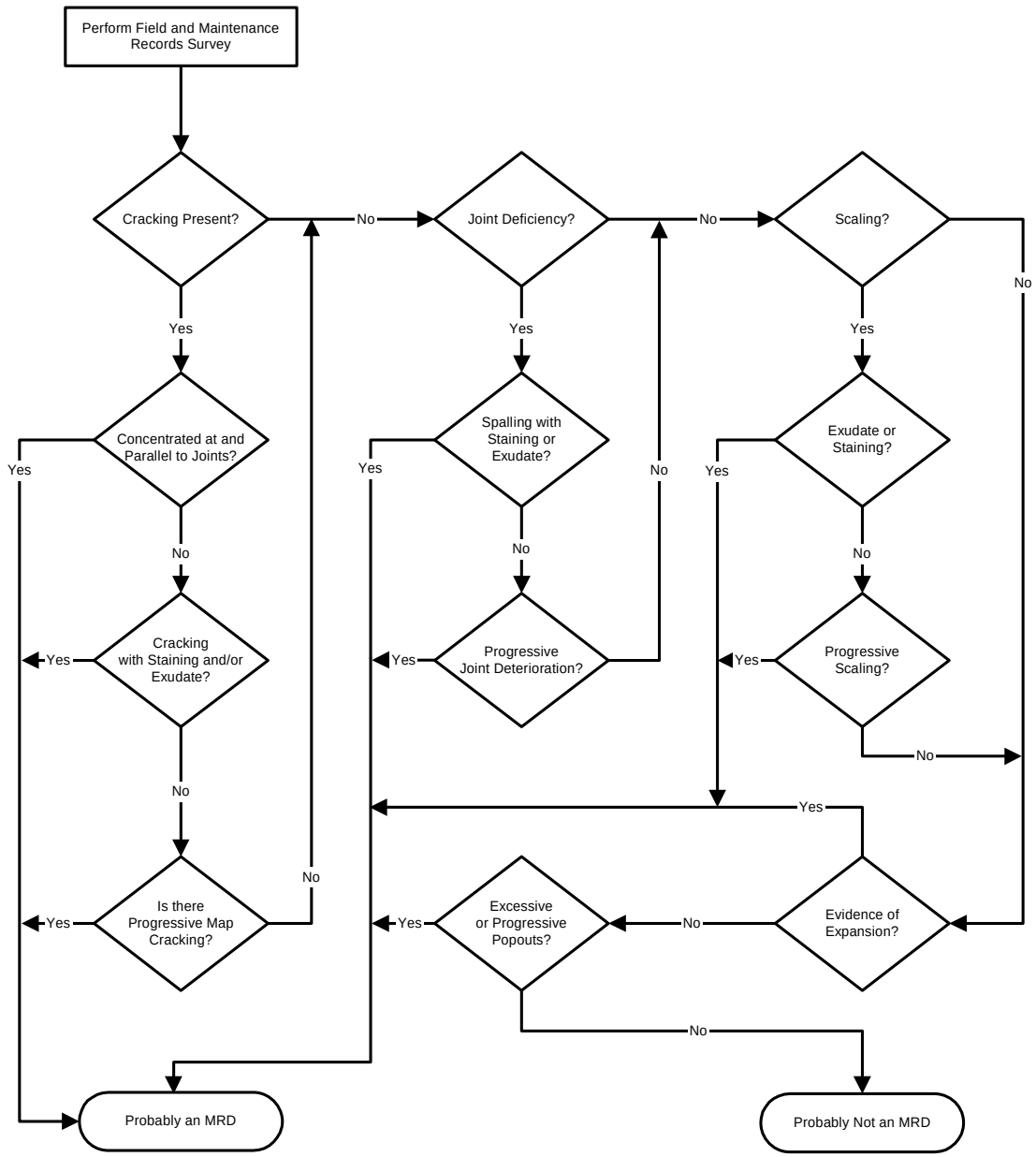

FIGURE 30. FLOWCHART FOR ASSESSING LIKELIHOOD OF MRD (VAN DAM ET AL. 2002)

From the visual condition surveys, the strongest evidence for MRD was at Airport Foxtrot, where a significant amount of cracking and spalling was observed with gray staining. The second most likely location was at Airport Alpha, where there were limited amounts of hairline cracking with exudate. Hairline cracking that appeared progressive in nature was observed at Airports E and G (Pad C), and Airport Beta had hairline cracking and rust colored staining at joints. At Airport Hotel, the main indicator for MRD was popouts. Based on these results, the four DDFs listed in table 5 were recommended for further evaluation. In addition, core samples were obtained from Airport Delta to evaluate factors contributing to its exceptional performance.

TABLE 5. AIRPORTS SELECTED FOR DETAILED FIELD INVESTIGATIONS

Airport	Year Built	Slab Design	Observed Distresses
A	1998	15-in JPCP 20 x 20 ft	Low-severity spalling, low-severity patching, hairline cracking, gray exudates.
E	1999	15-in JPCP 20 x 20 ft	Low-severity joint spalling, hairline cracking
F	1999	17-in JPCP 18.75 x 20 ft	Low-severity scaling, popouts, hairline cracking, some gray staining.
G, Pad C	1990	15-in JPCP 25 x 25 ft	Low-severity cracking, low-severity shattered slab, hairline cracking, map cracking.

4. FORENSIC EVALUATION

A forensic evaluation was conducted on the airports listed in table 5. This investigation included an additional visual assessment of the DDFs and also the collection of field core samples for strength testing and petrographic analysis. Two representative core specimens were also obtained from Airport Delta, although not from the actual DDF but instead from a nearby companion pavement with the same mix design.

4.1. FORENSIC FIELD EVALUATION

No forensic investigations were conducted at Airport Delta; two QC/QA cores from a nearby pavement using the same mixture design and materials as were used on the DDF were provided.

Because the pavement sections had undergone another winter of deicing operations at the time of coring, an additional visual inspection was conducted on the same sample units[1] initially examined to help provide insight into the progressive nature of the distress. Both a PCI survey and a detailed MRD inspection were once again conducted, but little perceivable differences were noted between the two inspections. Detailed information regarding the use of aircraft deicers at the selected airports was gathered and is tabulated in Appendix A. Airports D, E, F, and G are using propylene glycol-based deicer whereas Airport Alpha is using ethylene glycol-based deicer. Concentration varies from 30 to 55 percent depending on ambient temperatures.

The exact coring locations were established in the field based on the nature and extent of distress. The coring pattern and the disposition of each core are presented in table 6, where the core location refers to whether the core was obtained from an area receiving heavy or light deicer application and whether the core was located at a joint or interior (center) portion of the slab. Each core was immediately labeled, photographed, logged, and enclosed in plastic bubble wrap in preparation for shipping in accordance with previously developed procedures (Van Dam et al. 2002).

4.2. STRENGTH TESTING

Of the six cores obtained from each airport, two were used to assess strength. Michigan Tech conducted both the compressive (ASTM C 39) and split tensile (ASTM C 496) strength tests. In most cases, one 8-inch long compressive strength specimen and one or two 2-inch thick split tensile strength specimens were obtained from each core. The exceptions were at Airport Echo, where some of the cores fractured during the extraction process, and Airport Delta, where only two cores were available from the nearby pavement. The results of the strength testing are presented in table 7. Although more specimens would have to be tested to statistically assess the significance of the results, the relatively low tensile strengths recorded for Airports F and G are worth noting. It is possible that the concrete in these cores are showing signs of damage.

[1] Due to an error, it is likely that the same sample unit was not inspected in this case.

TABLE 6. CORING PATTERN AND CORE DISPOSITION FOR THE SIX CORES AT EACH LOCATION

Core ID	Deicer Application	Location	Condition	Type of Testing	
				Petrographic	Strength
A	Heavy	Joint	Distressed	X	
B	Heavy	Joint	No Distress	X	
C	Heavy	Center	Distressed	X	
D	Heavy	Center	No Distress		X
E	Light	Center	No Distress	X	X
F	Light	Center	No Distress		X

TABLE 7. COMPRESSIVE AND SPLIT TENSILE STRENGTH DATA.

Airport	Core	Compressive Strength (psi)	Split Tensile Strength (psi)
A	D	6469	781
	E	6082	713
D	33[1]	5894	414
			481
E	D	4617	528
	E	3373	
	F		461
F	D	7994	224
	E	7075	219
G	D	6363	161
	E	4189	179

[1] Cores from Airport Delta were provided by the airport and were identified differently than those obtained by the research team in the course of this study.

4.3. PETROGRAPHIC ANALYSIS

The petrographic analysis was performed following procedures developed in a previous research study conducted for the Federal Highway Administration (Van Dam et al. 2002). In addition to the optical and scanning microscopy techniques, high-resolution digital scanning was also used to assist in the forensic analysis.

A systematic approach was taken to examine the core specimens in an attempt to determine the cause of concrete pavement deterioration. The key to accurately identifying the deterioration mechanism(s) is to determine "what it is not" rather than "what it is." By using all available information without preconceived notions as to the cause of the problem, the analyst works through a process of elimination to determine the most likely cause(s) of deterioration. It is recognized that concrete is an inherently complex material and, particularly in the case of DDFs, can be subjected to very complex environmental conditions. Only through such a thorough, unbiased, and systematic evaluation can mechanisms of distress be identified and preventive strategies devised.

Although the strength testing provides a general measure of quality, it offers little direct information on the nature of the deterioration. To determine the nature deterioration, petrographic analysis was conducted on polished slabs and thin sections. The petrographic analysis used various instruments to examine the concrete microstructure, including visual assessment, staining techniques, stereo microscopy, petrographic microscopy, and scanning electron microscopy, as depicted in figure 31 (Van Dam et al. 2002). Optical stereo microscopy (stereo OM) was used to assess the overall condition of the microstructure and to determine relevant air-void system characteristics, including the spacing factor and specific surface, in accordance with ASTM C 457. Petrographic microscopy (petrographic OM) was conducted using the procedures described in ASTM C 856. The analysis also drew on information collected using a Philips XL-40 environmental scanning electron microscopy (ESEM) and a flatbed digital scanner.

The various samples were carefully and meticulously prepared to minimize altering the concrete microstructure. Various saws, laps, grinders, and polishers were used to create a mirror-like finish on polished slabs and concrete thin sections, which are ten times thinner than a human hair (20 to 30 microns). Polished slabs were viewed using the stereo OM to assess the air-void system and to direct future, more in-depth analysis. Areas of interest identified with the stereo OM were then prepared in thin section and viewed using the petrographic OM and the ESEM. In addition, crack mapping was conducted on polished slabs using the high-resolution digital scanner. The purpose of this evaluation was to observe "diagnostic features" such as bleeding, fractures, infilling of the air-void system, reaction products, and so on.

The following sections present a summary of the results of this analysis for each airport investigated. Detailed portfolios of the results from each airport are provided in Appendix B.

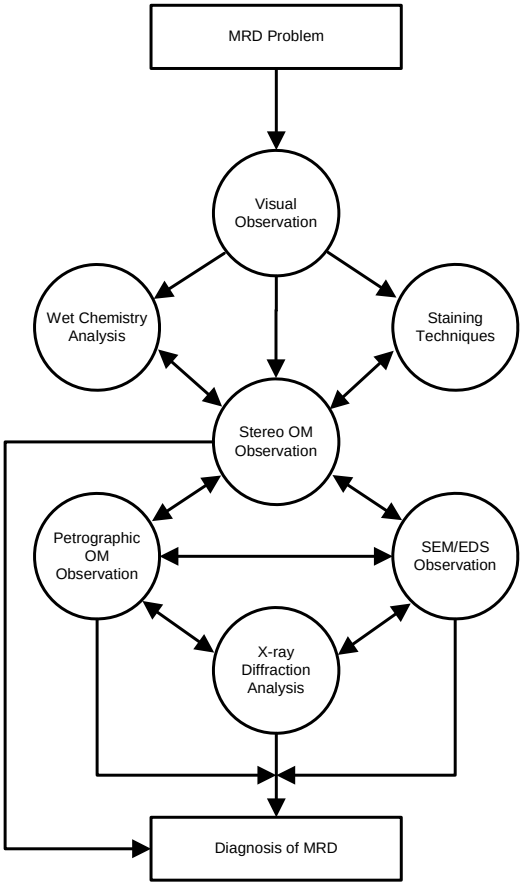

FIGURE 31. FUNDAMENTAL PROCESS FOR ANALYZING A DETERIORATED CONCRETE SAMPLE (VAN DAM ET AL. 2002)

4.3.1. Airport Alpha

Description of Cores as Received

A total of seven 4-in diameter cores were received. All of the cores fully represented the entire depth of the concrete with a thickness of approximately 14.5 in. Cores A and B were taken directly over pavement joints. Core A, split in half lengthwise by the joint, exhibited a break at a depth of about 7 in through one half of the core, and another break at a depth of about 8.5 in through the other half of the core. The fracture surfaces of the breaks in core A appeared fresh and clean. Core B did not exhibit any breaks other than the fracture plane from the joint. The remaining cores, all taken away from joints, did not exhibit any breaks, with the exception of core G. The break in core G occurred at a depth of approximately 4 in through a region of large interconnected air voids. Figure 32 shows close-up views of regions of large interconnected air voids observed in both cores C and G. Cores C and G also exhibited fine cracks at the pavement surface.

FIGURE 32. CLOSE-UP OF IRREGULAR VOIDS FROM CORE C, (LEFT) AND CORE G, (RIGHT) AIRPORT ALPHA

Stereo-Microscope and Flat-Bed Scanner Observations

Figures 33 and 34 present flat-bed scanner images of the polished slabs. All of the slabs from cores B and C were stained with phenolphthalein and a carbonation depth of 0.5 to 0.75 mm[2] was observed with minor additional carbonation along the joint in core B, and along the perimeters of the large interconnected air void network of core C. The large interconnected air void network of core C is best observed in figure 35. The remaining cores B, D, and F did not exhibit the same large interconnected air void networks. All of the slabs from cores A and F were stained with sodium cobaltinitrite. The coarse aggregate throughout the cores picked up the yellow stain, which is normally an indicator for alkali-silica reactivity. Figure 36 shows close-up stereo-microscope images of yellow stained regions on polished slabs from cores A and F. The coarse aggregate, a relatively pure dolomite, did not appear to be alkali-silica reactive in spite of picking up the yellow stain. The yellow stained cracks near the pavement surface on the polished slab prepared from core F may be due to locally increased alkali (potassium) concentrations. Enrichment in alkalies at the pavement surface has been associated by some researchers with the evaporation of soluble-alkali laden mix water (Dobie, 1986).

The air-void systems of the polished slabs for all airports were assessed according to ASTM C 457. Details for each core are presented in Appendix B. For Airport Alpha, the measured spacing factors were 0.197, 0.185, 0.197, and 0.399 mm for cores A, B, C, and F respectively. All but core F would be considered acceptable, being below the ASTM C 457 limit of 0.200 mm.

The coarse aggregate is composed of quarried carbonate rock (dolomite), and the fine aggregate is a carbonate rich (dolomite) sand.

[2] Note: It is standard convention to use metric units when presenting microcopy data.

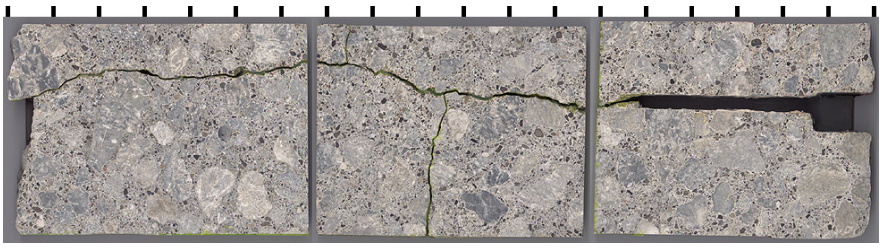

Core A, over joint, Airport Alpha

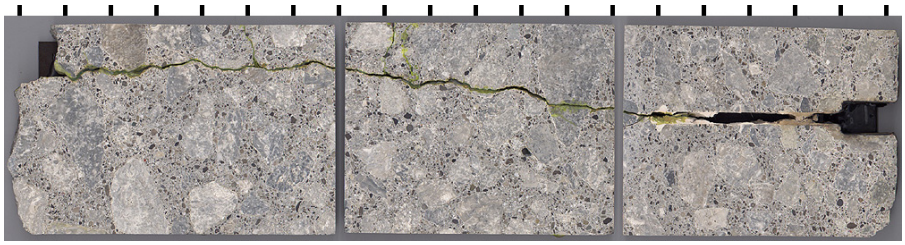

Core B, over joint, Airport Alpha

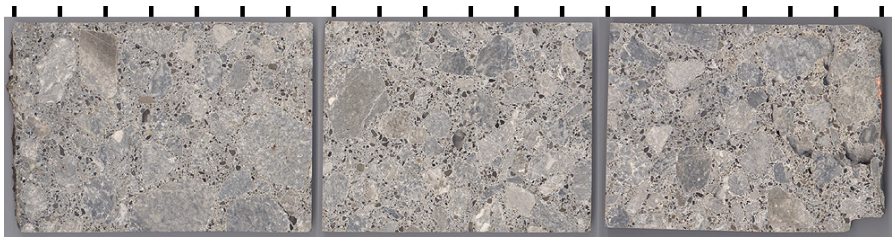

Core C, away from joint, Airport Alpha

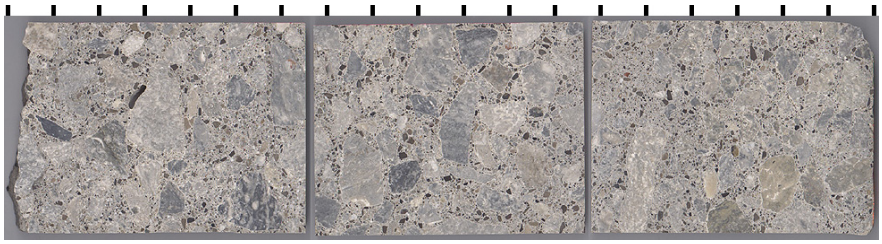

Core F, away from joint, Airport Alpha

FIGURE 33. POLISHED SLABS FROM AIRPORT ALPHA. SLABS ORIENTED TO SHOW CROSS-SECTION THROUGH PAVEMENT, PAVEMENT SURFACE AT RIGHT-HAND SIDE, TICK MARKS EVERY 2 CM

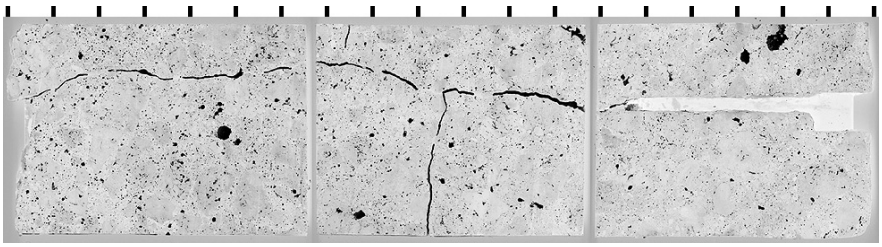

Core A, over joint, Airport Alpha

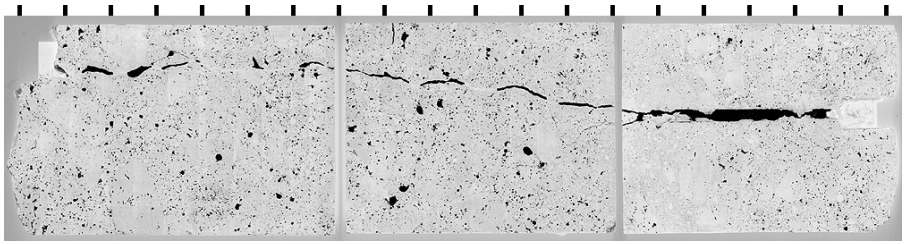

Core B, over joint, Airport Alpha

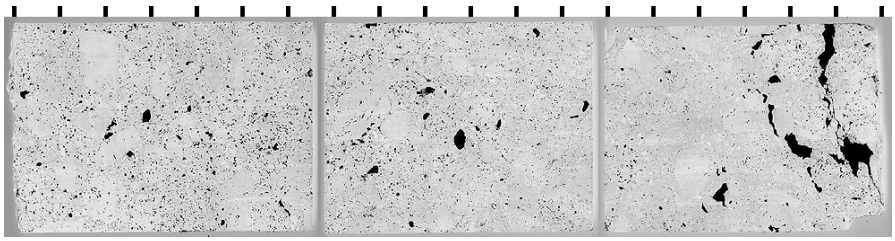

Core C, away from joint, Airport Alpha

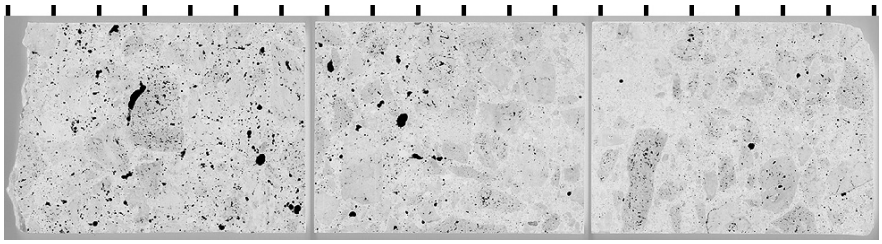

Core F, away from joint, Airport Alpha

FIGURE 34. POLISHED SLABS FROM AIRPORT ALPHA SITE AFTER TREATMENT TO ENHANCE VISIBILITY OF AIR VOIDS AND CRACKS. SLABS ORIENTED TO SHOW CROSS-SECTION THROUGH PAVEMENT, PAVEMENT SURFACE AT RIGHT-HAND SIDE, TICK MARKS EVERY 2 CM

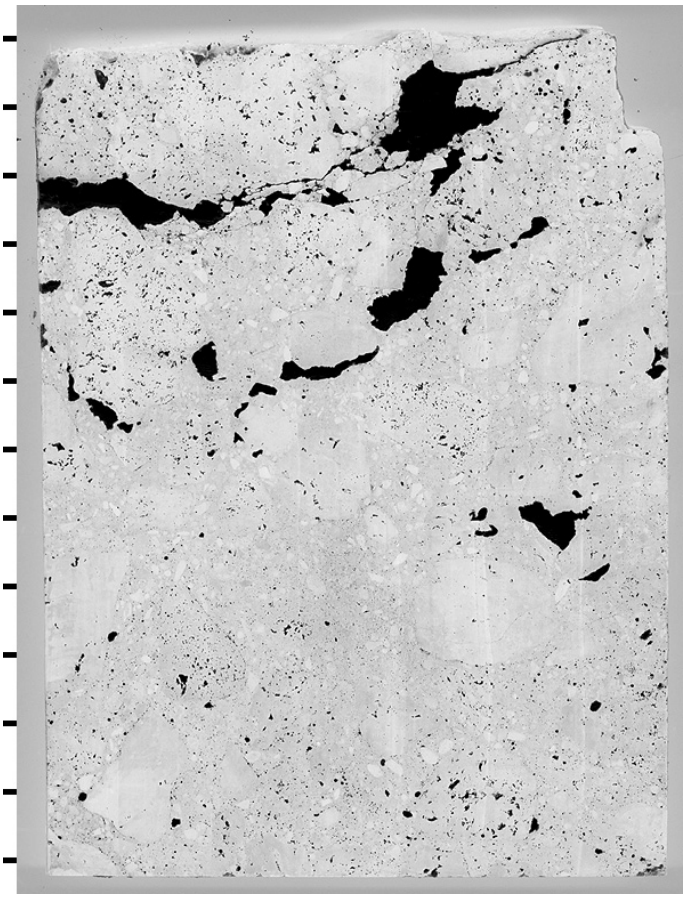

FIGURE 35. CLOSE-UP OF POLISHED SLAB PREPARED FROM TOP THIRD OF CORE C, AIRPORT ALPHA AFTER TREATMENT TO EMPHASIZE LOCATIONS OF AIR VOIDS AND CRACKS. TICK MARKS EVERY CM

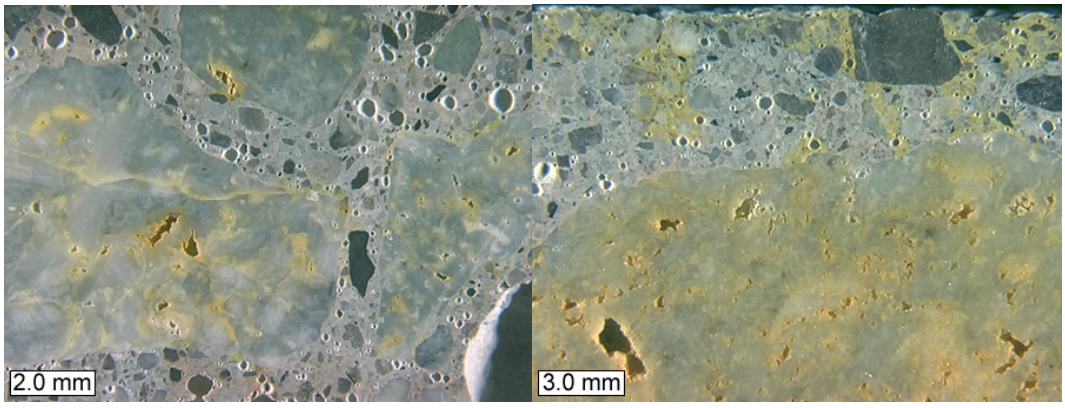

FIGURE 36. STEREO-MICROSCOPE IMAGES OF AGGREGATES AND CRACKS THAT PICKED UP YELLOW COLORATION FROM SODIUM COBALTINITRITE STAIN. IMAGE ON LEFT FROM POLISHED SLAB FROM BOTTOM THIRD OF CORE A; IMAGE ON RIGHT FROM PAVEMENT SURFACE ON THE TOP THIRD OF CORE F, AIRPORT ALPHA

Petrographic Microscope and SEM Observations

Two thin sections were prepared from the top third of each core. One of the thin sections from each slab, representing a depth of 40 to 80 mm, was used for measurements of the capillary fluorescence intensity of the cement paste. Through the procedure described in Appendix B, an equivalent water-to-cementitious (*w/c*) value of 0.41 +/- 0.04 was estimated for the Airport Alpha concrete. It is emphasized that the value of 0.41 is not an absolute measurement of *w/c*, but simply a comparison to the fluorescence intensity of the lab-produced mortar standards made with portland cement and cured for 28 days. It is useful for comparing the relative density of the hydrated cement paste and not as an absolute measure of the as-constructed *w/c*.

Figure 37 shows petrographic microscope images of a cross section at the pavement surface of core F. As can be seen in the crossed polar image of figure 37, carbonation extends to a depth of approximately 2 to 3 mm, in contrast with the 0.5 to 0.75 mm estimate from phenolphthalein staining. Figures 38 and 39 show back scattered electron (BSE) and petrographic microscope images of a localized region of extremely high *w/c* in polished thin section from core C. The high *w/c* region is adjacent to the large interconnected void network of core C, and together, suggests that the voids may have been due to excessive bleed water.

Figures 40 through 42 show BSE images, elemental maps, and petrographic microscope images of secondary calcium hydroxide crystals in the entrained air voids of a polished thin section from core C. Calcium hydroxide crystals were very common in the entrained air voids on all of the prepared thin sections from the Airport Alpha cores. In addition to the calcium hydroxide deposits, the elemental maps of figure 40 also show inert dolomite powder filler dispersed throughout the cement paste.

Figure 43 consists of a BSE image and elemental maps of a pore space in a dolomite coarse aggregate particle in polished thin section from core C. The pore space is lined by calcite and a potassium-bearing clay mineral. The potassium-bearing clay mineral is likely responsible for the strong uptake of the sodium cobaltinitrite indicator solution by the dolomite coarse aggregate. Figures 44 and 45 consist of petrographic microscope images to illustrate the constituents of the cementitious materials in the concrete. Dolomite powder filler can best be seen in the plane polarized image of figure 45.

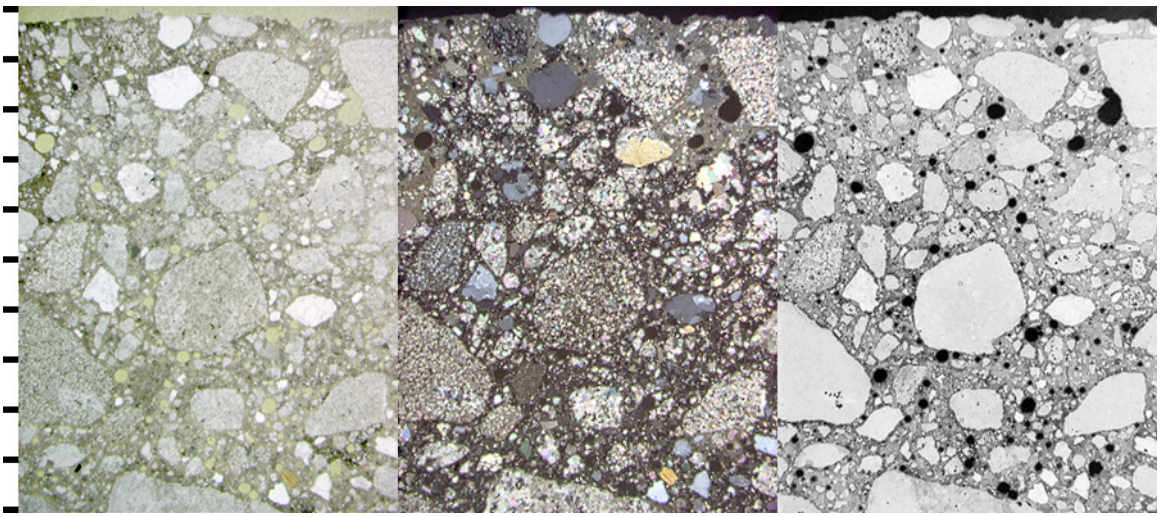

FIGURE 37. PETROGRAPHIC MICROSCOPE IMAGES TO SHOW CROSS-SECTION AT PAVEMENT SURFACE FROM CORE F, AIRPORT ALPHA. FROM LEFT TO RIGHT: PLANE POLARIZED LIGHT, CROSSED POLARS, AND EPIFLUORESCENT MODE. TICK MARKS EVERY MM

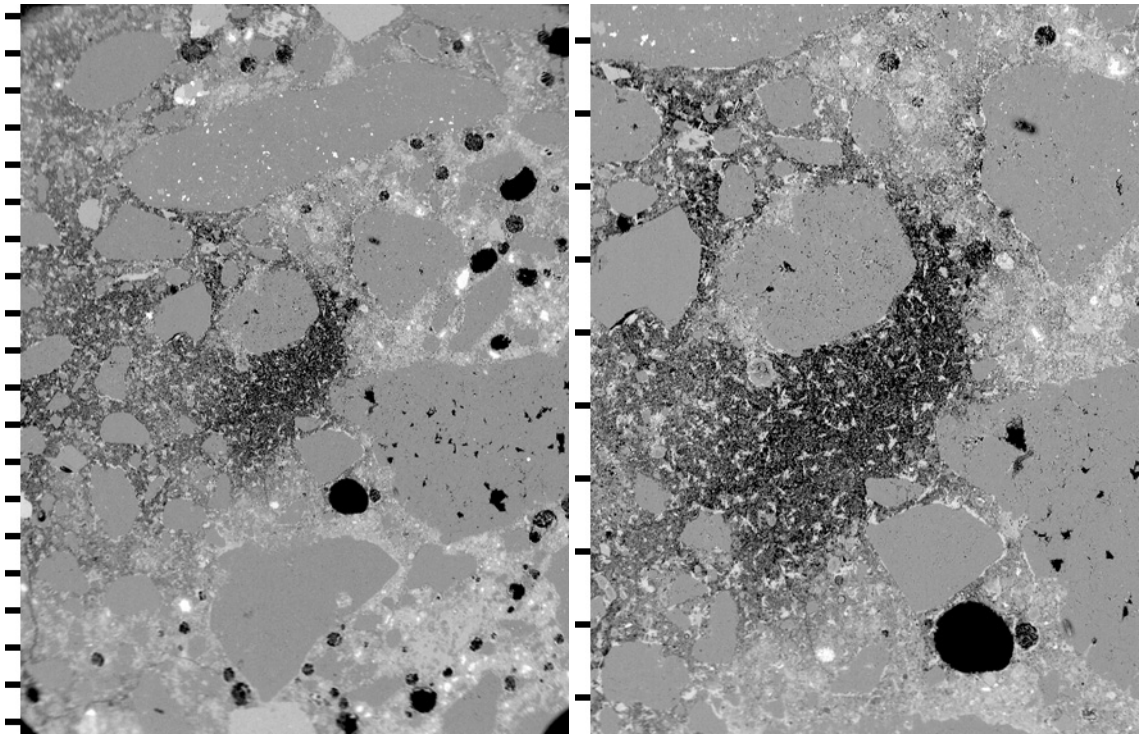

FIGURE 38. BSE IMAGES OF LOCALIZED REGION IN CEMENT PASTE OF EXTREMELY HIGH POROSITY ON POLISHED THIN SECTION FROM CORE C, AIRPORT ALPHA. TICK MARKS EVERY 250 MICROMETERS

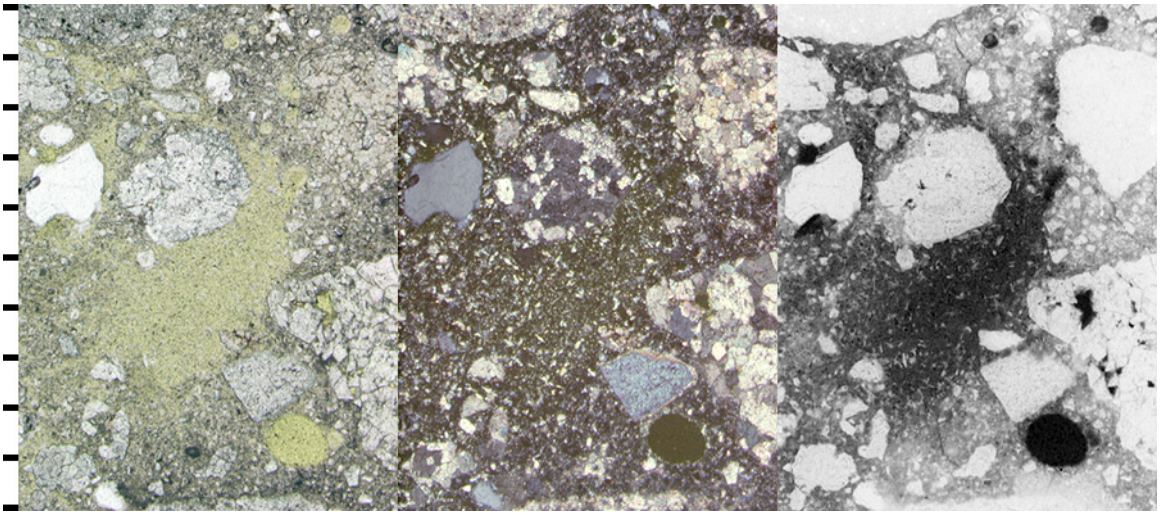

FIGURE 39. PETROGRAPHIC MICROSCOPE IMAGES OF LOCALIZED REGION IN CEMENT PASTE OF EXTREMELY HIGH POROSITY, POLISHED THIN SECTION FROM CORE C, AIRPORT ALPHA. FROM LEFT TO RIGHT: PLANE POLARIZED LIGHT, CROSSED POLARS, AND EPIFLUORESCENT MODE. TICK MARKS EVERY 250 MICROMETERS

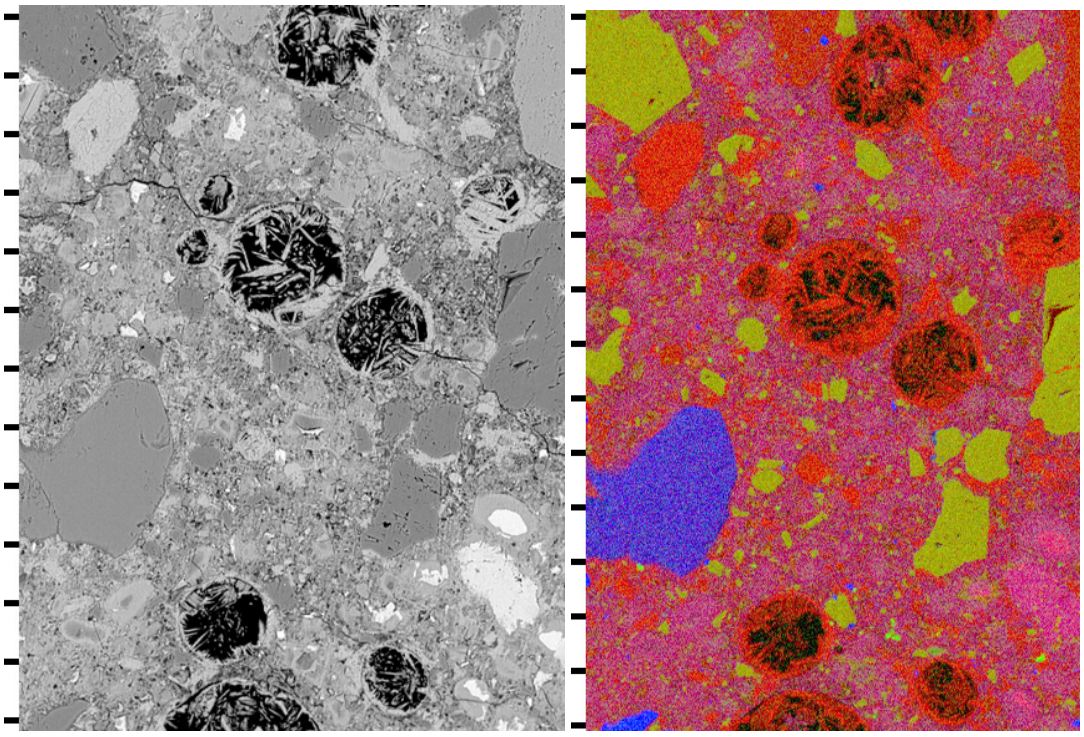

FIGURE 40. BSE IMAGE (LEFT) AND ELEMENTAL MAP (RIGHT) OF CALCIUM HYDROXIDE DEPOSITS IN ENTRAINED AIR VOIDS FROM POLISHED THIN SECTION FROM CORE C, AIRPORT ALPHA. DOLOMITE POWDER FILLER IS ALSO CLEARLY VISIBLE IN THE ELEMENTAL MAP, CA = RED CHANNEL, MG = GREEN CHANNEL, AND SI = BLUE CHANNEL. TICK MARKS EVERY 50 MICROMETERS

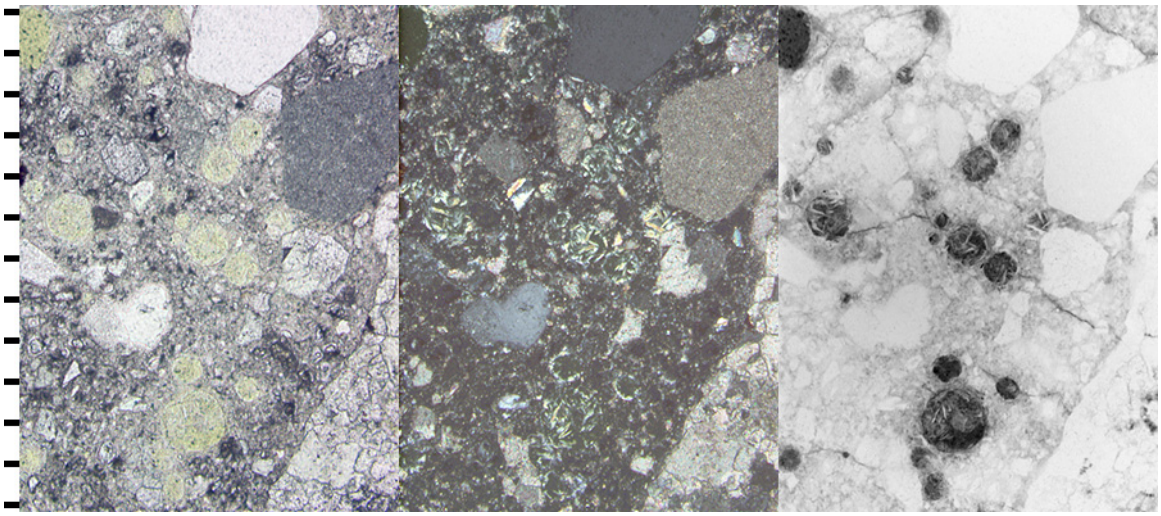

FIGURE 41. PETROGRAPHIC MICROSCOPE IMAGES OF CALCIUM HYDROXIDE DEPOSITS IN ENTRAINED AIR VOIDS FROM POLISHED THIN SECTION FROM CORE C, AIRPORT ALPHA. FROM LEFT TO RIGHT: PLANE POLARIZED LIGHT, CROSSED POLARS, AND EPIFLUORESCENT MODE. TICK MARKS EVERY 100 MICROMETERS

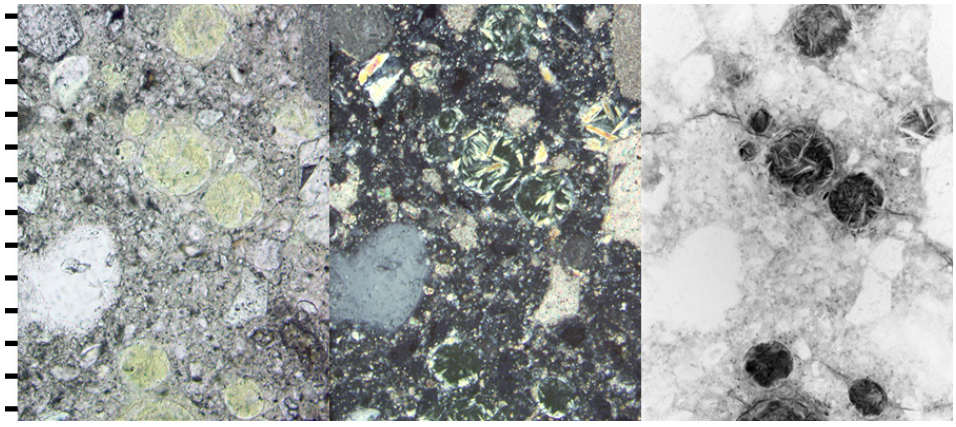

FIGURE 42. CLOSE-UP PETROGRAPHIC MICROSCOPE IMAGES OF CALCIUM HYDROXIDE DEPOSITS IN ENTRAINED AIR VOIDS FROM POLISHED THIN SECTION FROM CORE C, AIRPORT ALPHA. FROM LEFT TO RIGHT: PLANE POLARIZED LIGHT, CROSSED POLARS, AND EPIFLUORESCENT MODE. TICK MARKS EVERY 50 MICROMETERS

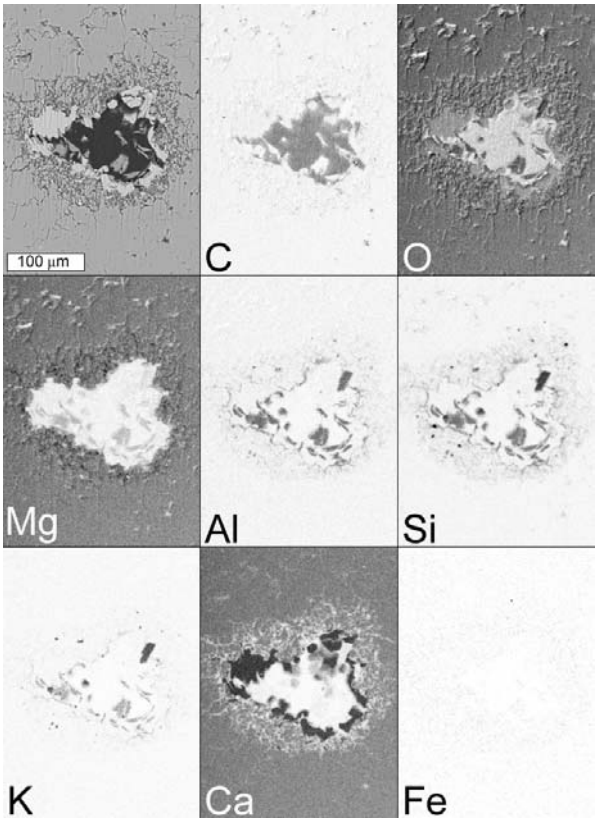

FIGURE 43. BSE IMAGE (UPPER LEFT HAND CORNER) AND ELEMENTAL MAPS SHOWING CALCITE AND POTASSIUM-BEARING CLAY MINERALS IN PORE SPACE WITHIN DOLOMITE COARSE AGGREGATE PARTICLE ON POLISHED THIN SECTION FROM CORE C, AIRPORT ALPHA. IN ELEMENTAL MAPS, DARKER COLORED REGIONS CORRESPOND TO HIGHER X-RAY COUNTS

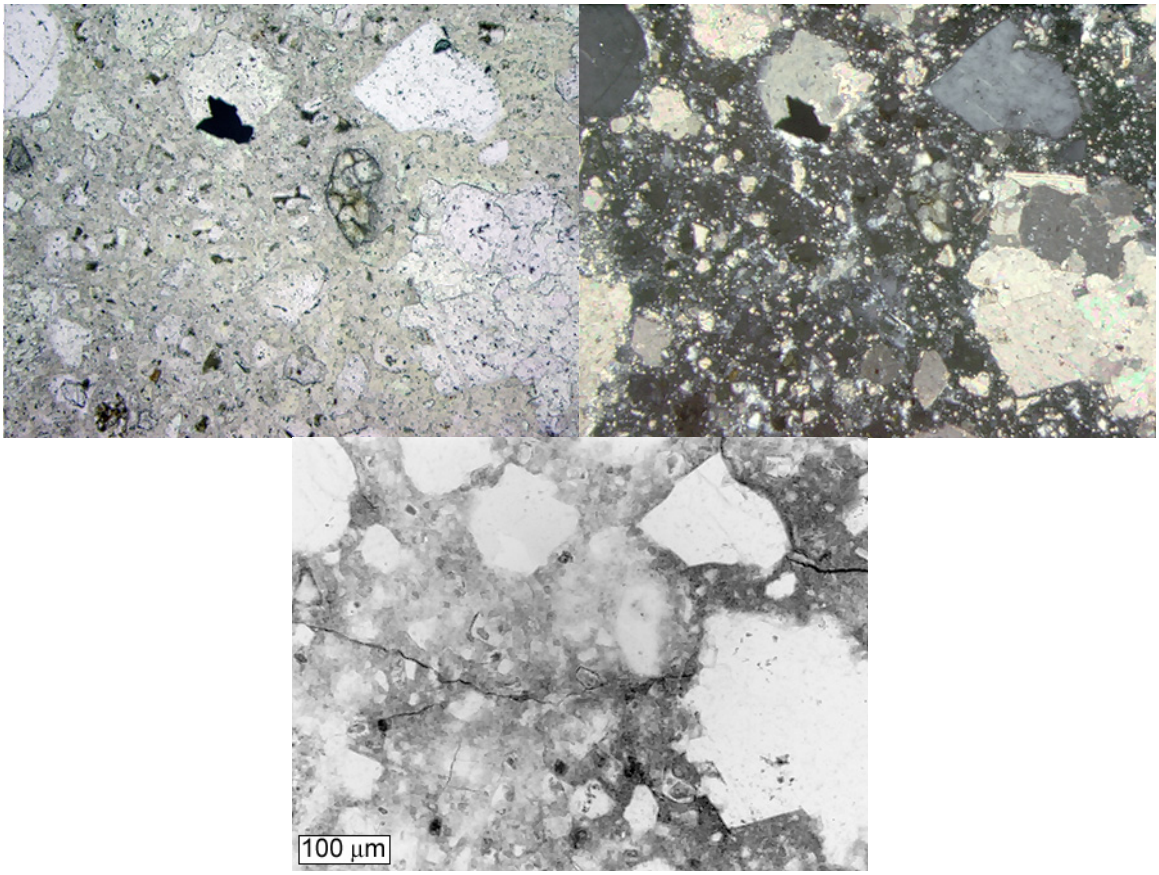

FIGURE 44. PETROGRAPHIC MICROSCOPE IMAGES TO SHOW CEMENT PASTE FRACTION FROM AIRPORT ALPHA. CLOCKWISE FROM UPPER LEFT HAND CORNER: PLANE POLARIZED LIGHT, CROSSED POLARS, AND EPIFLUORESCENT MODE

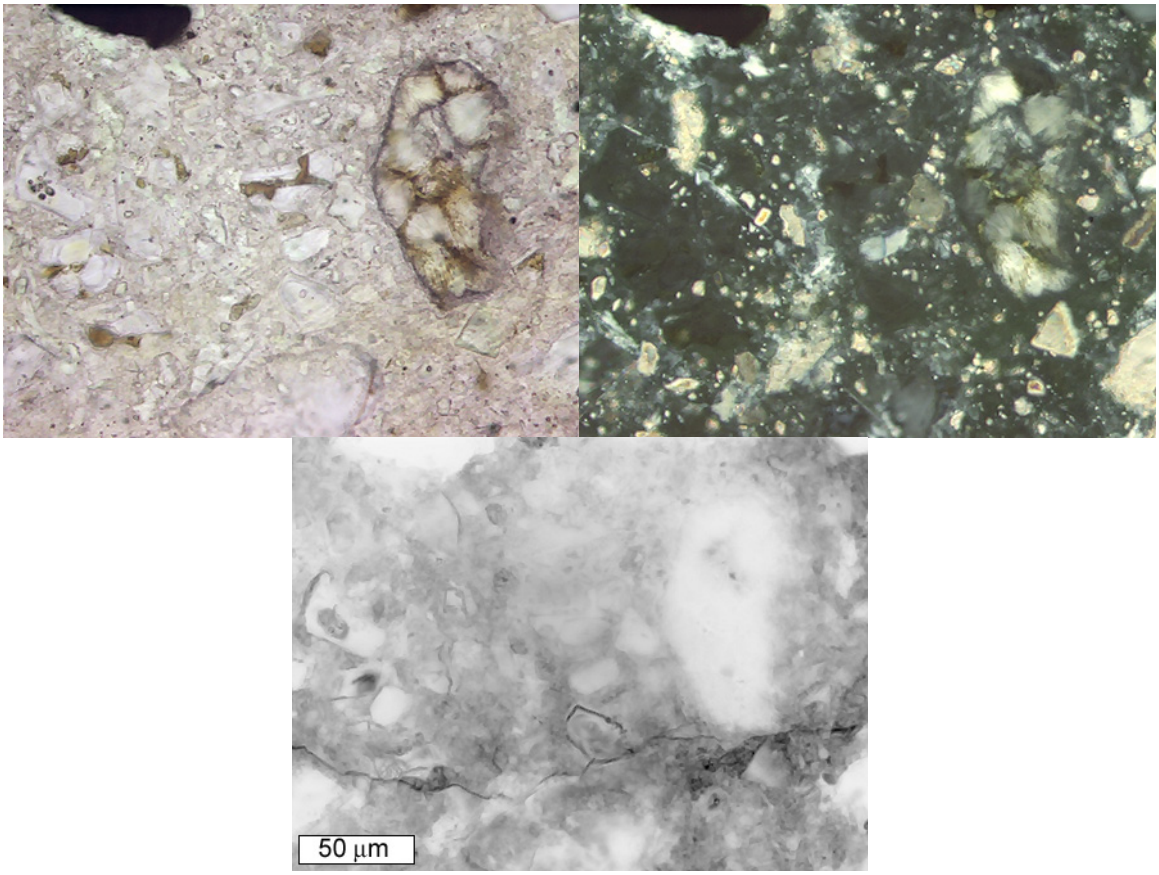

FIGURE 45. CLOSE-UP PETROGRAPHIC MICROSCOPE IMAGES TO SHOW CEMENT GRAINS AND DOLOMITE POWDER FILLER IN CEMENT PASTE FRACTION FROM AIRPORT ALPHA. THE DOLOMITE PARTICLES ARE CLEARLY VISIBLE IN THE CROSSED POLARS IMAGE. CLOCKWISE FROM UPPER LEFT HAND CORNER: PLANE POLARIZED LIGHT, CROSSED POLARS, AND EPIFLUORESCENT MODE

4.3.2. Airport Delta

Description of Cores as Received

Two 4-in diameter cores were received. Both cores represented the entire depth of the concrete with a thickness of approximately 19 in. Both cores appeared to be in good condition.

Stereo-Microscope and Flat-Bed Scanner Observations

All polished slabs were taken from core 44 as shown in figures 46 and 47. The carbonation depth is approximately 1.25 mm. The air-void system parameters of the polished slabs were measured according to ASTM C 457, having a measured spacing factor of 0.115 mm. Figure 48 shows stereo-microscope images of the air-void structure.

The coarse aggregate is a granitic quarried rock, and the fine aggregate is a quartz-rich sand.

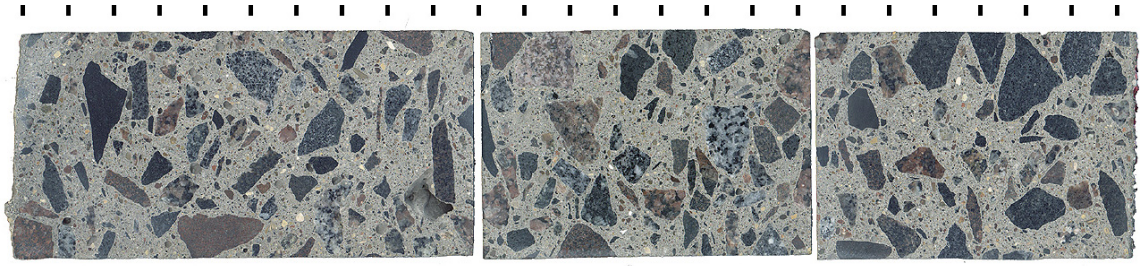

Core 44, away from joint, Airport Delta

FIGURE 46. POLISHED SLABS FROM CORE 44, AIRPORT DELTA. SLABS ORIENTED TO SHOW CROSS-SECTION THROUGH PAVEMENT, PAVEMENT SURFACE AT RIGHT-HAND SIDE, TICK MARKS EVERY 2 CM

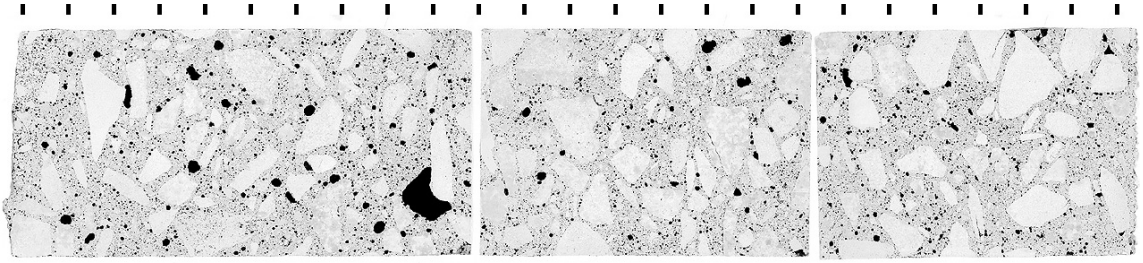

Core 44, away from joint, Airport Delta

FIGURE 47. POLISHED SLABS FROM CORE 44, AIRPORT DELTA AFTER TREATMENT TO ENHANCE VISIBILITY OF AIR VOIDS AND CRACKS. SLABS ORIENTED TO SHOW CROSS-SECTION THROUGH PAVEMENT, PAVEMENT SURFACE AT RIGHT-HAND SIDE, TICK MARKS EVERY 2 CM

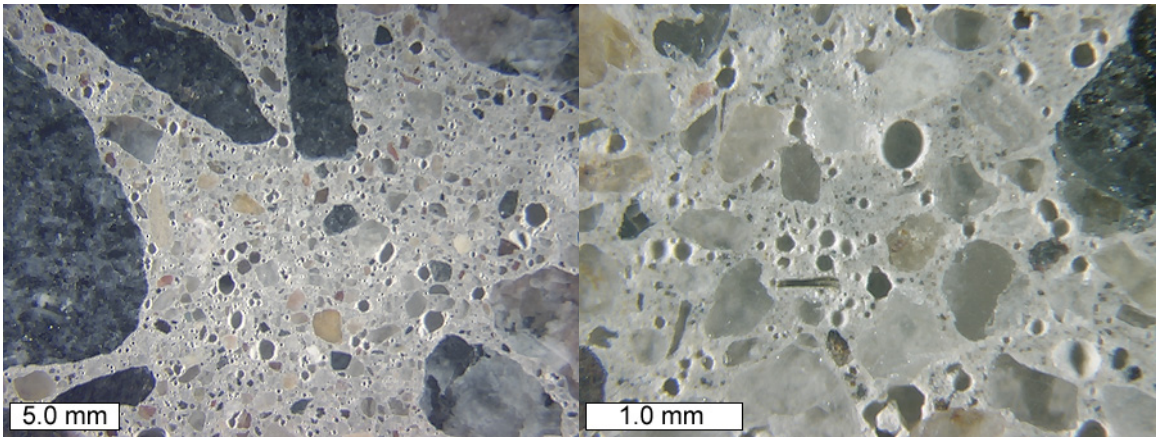

FIGURE 48. STEREO-MICROSCOPE IMAGES TO SHOW AIR VOID STRUCTURE ON POLISHED SLAB FROM TOP THIRD OF CORE 44 AWAY FROM JOINT, AIRPORT DELTA

Petrographic Microscope Observations

Two thin sections were prepared from the top third of core 44. The first thin section from the slab represents a cross section through the pavement surface to a depth of 40 mm. The second thin section from the slab consists of a cross section through the next horizon representing a depth of 40 to 80 mm. Based on the capillary fluorescence intensity of the cement paste, an equivalent average *w/c* value of 0.35 +/- 0.01 was estimated for the Airport Delta thin sections. It is again emphasized that the value of 0.35 is not an absolute measurement of *w/c*, but simply a comparison to the fluorescence intensity to those of laboratory prepared mortar standards made with portland cement cured for 28 days.

Figure 49 shows a cross section through the pavement surface of core 44. Figure 50 shows a petrographic microscope image to illustrate portland cement grains and fly ash in the cement paste.

4.3.3. Airport Echo

Description of Cores as Received

A total of six 4-in diameter cores were received. Only one of the cores, core B, represented the entire depth of the concrete with a thickness of approximately 16 in. The other cores all exhibited fresh fracture surfaces at their bases representing the discontinuity with the remaining depth of the pad. Core B, the only complete core, had a break at a depth of approximately 11 in, the fracture surface at the break appeared fresh and clean. Core D also had a break with a fresh clean fracture surface at a depth of approximately 5 in.

All of the cores exhibited visual signs of alkali silica-reactive fine aggregate particles; an example is shown in figure 51. Both the reactive fine aggregate particles and the surrounding hardened cement paste exhibited discoloration along the aggregate/cement paste interface. No associated cracks were observed in the aggregate or paste. Cores A, B, and C exhibited fine cracks at the pavement surface.

Stereo Microscope and Flat-Bed Scanner Observations

Cores A, B, and C exhibited cracks at the pavement surface. These cracks can be observed in cross section on the polished slabs in figures 52 and 53. The cracks extend to depths of 1 to 2 cm in cores A and B, and to depths of 1 to 4 cm in core C. The depth of carbonation can be observed in phenolphthalein-stained slabs, with carbonation depths of 1 to 2 mm in cores A and C, with carbonation penetrating farther along the depth of the cracks. Reactive fine aggregate particles can best be seen in the sodium cobaltinitrite-stained slab representing the top third of core B (figure 54) where the reactive fine aggregate particles are stained yellow.

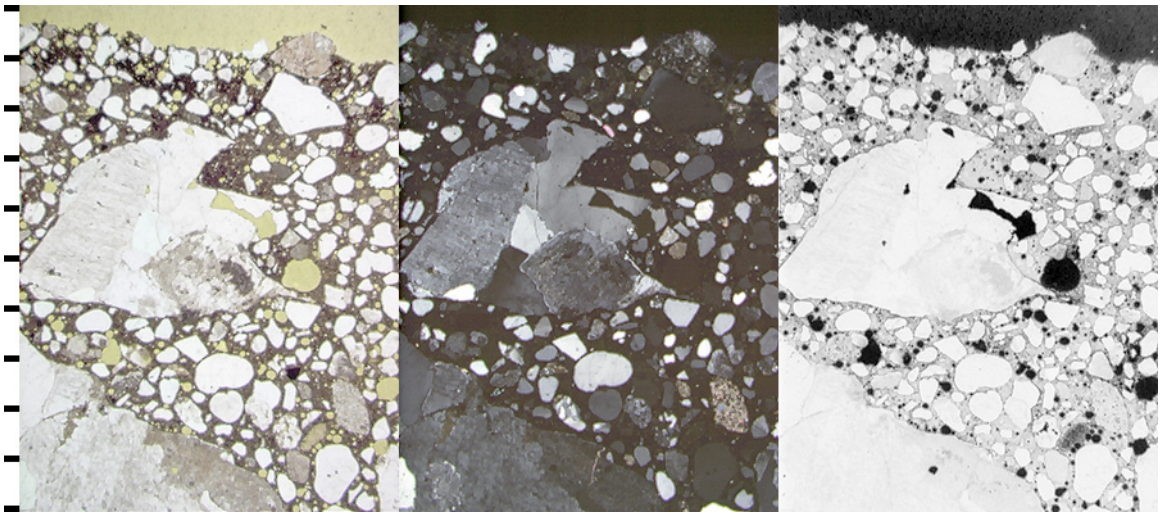

FIGURE 49. PETROGRAPHIC MICROSCOPE IMAGES TO SHOW CROSS SECTION AT PAVEMENT SURFACE FROM CORE 44, AIRPORT DELTA. FROM LEFT TO RIGHT: PLANE POLARIZED LIGHT, CROSSED POLARS, AND EPIFLUORESCENT MODE. TICK MARKS EVERY MM

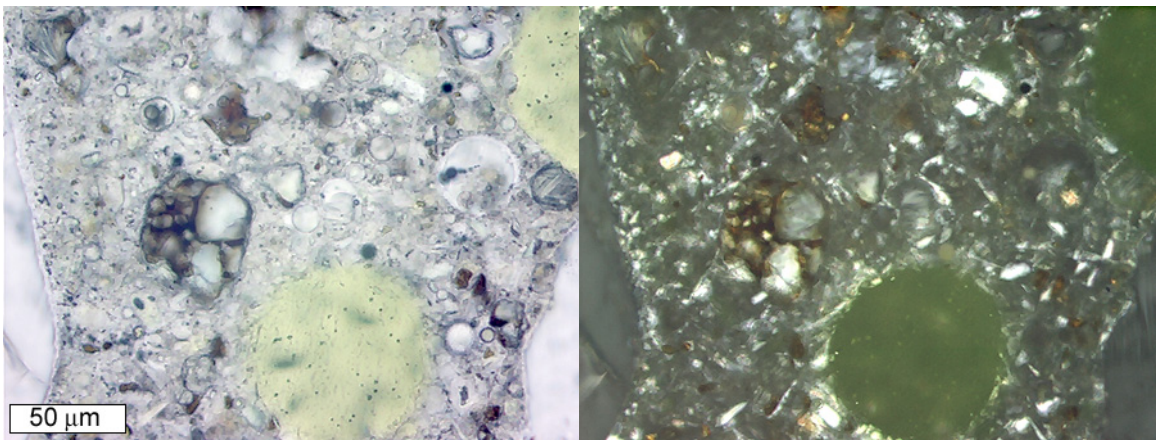

FIGURE 50. CLOSE-UP OF CEMENT PASTE IN THIN SECTION FROM AIRPORT DELTA TO SHOW CEMENT GRAINS AND FLY ASH PARTICLES IN CEMENT PASTE. FROM LEFT TO RIGHT, PLANE POLARIZED AND CROSSED POLARS

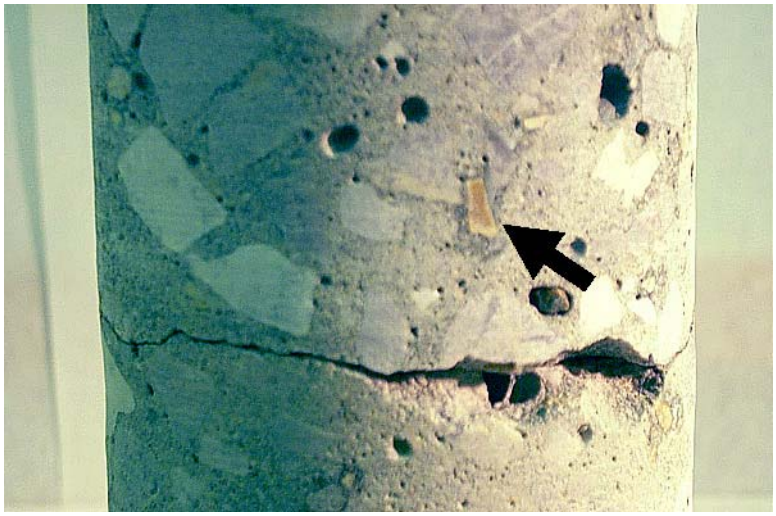

FIGURE 51. CLOSE-UP OF ALKALI-SILICA REACTIVE AGGREGATE (BLACK ARROW) EXPOSED ON EXTERIOR OF CORE D, AIRPORT ECHO

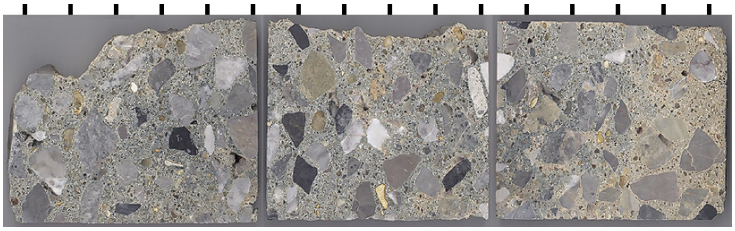

Core A, adjacent to joint, Airport Echo

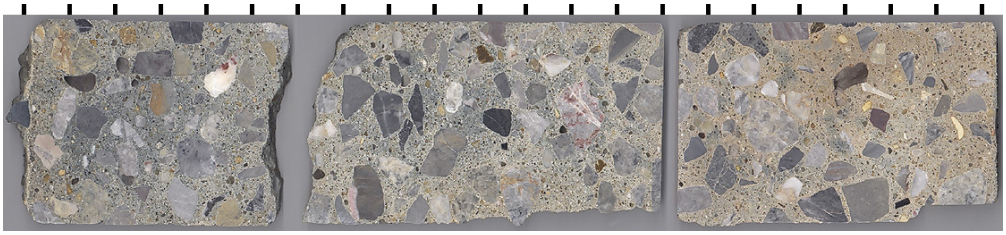

Core B, adjacent to joint, Airport Echo

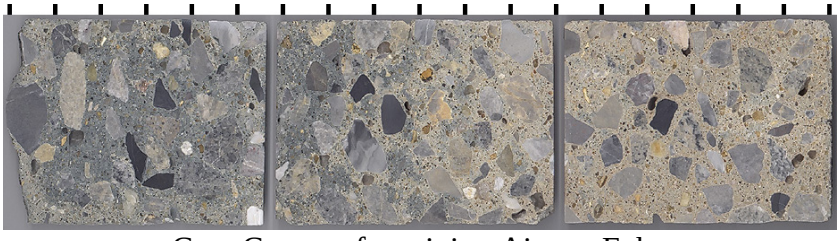

Core C, away from joint, Airport Echo

FIGURE 52. POLISHED SLABS FROM AIRPORT ECHO. PAVEMENT SURFACE AT RIGHT-HAND SIDE; TICK MARKS EVERY 2 CM. ONLY CORE B SAMPLED THE ENTIRE DEPTH. DARK DISCOLORATION OF DUE TO REDUCTION OF IRON IN CEMENT GRAINS BY SULFUR IN GROUND GRANULATED BLAST FURNACE SLAG

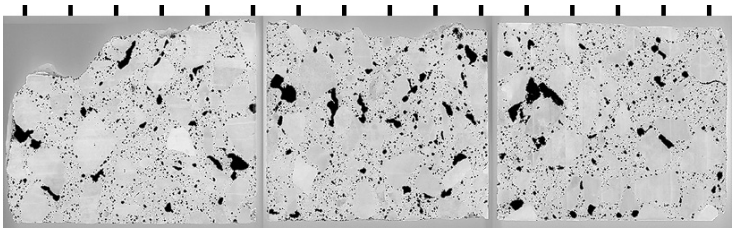

Core A, Airport Echo

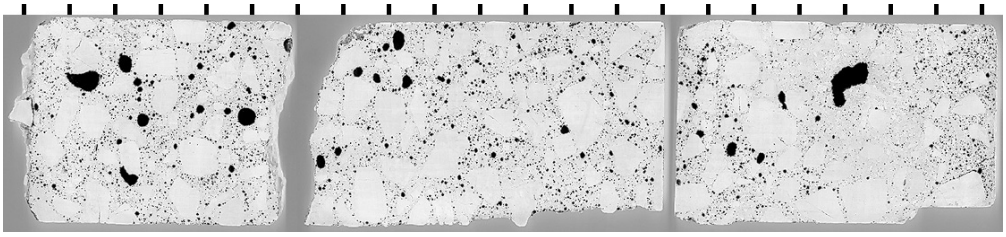

Core B, Airport Echo

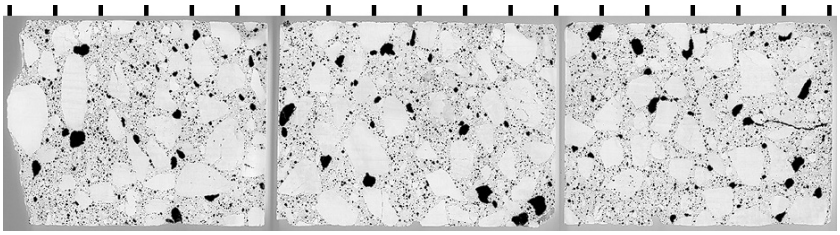

Core C, Airport Echo

FIGURE 53. POLISHED SLABS FROM AIRPORT ECHO AFTER TREATMENT TO ENHANCE VISIBILITY OF AIR VOIDS AND CRACKS. SLABS ORIENTED TO SHOW CROSS-SECTION THROUGH PAVEMENT, PAVEMENT SURFACE AT RIGHT-HAND SIDE; TICK MARKS EVERY 2 CM. ONLY CORE B SAMPLED THE ENTIRE PAVEMENT DEPTH

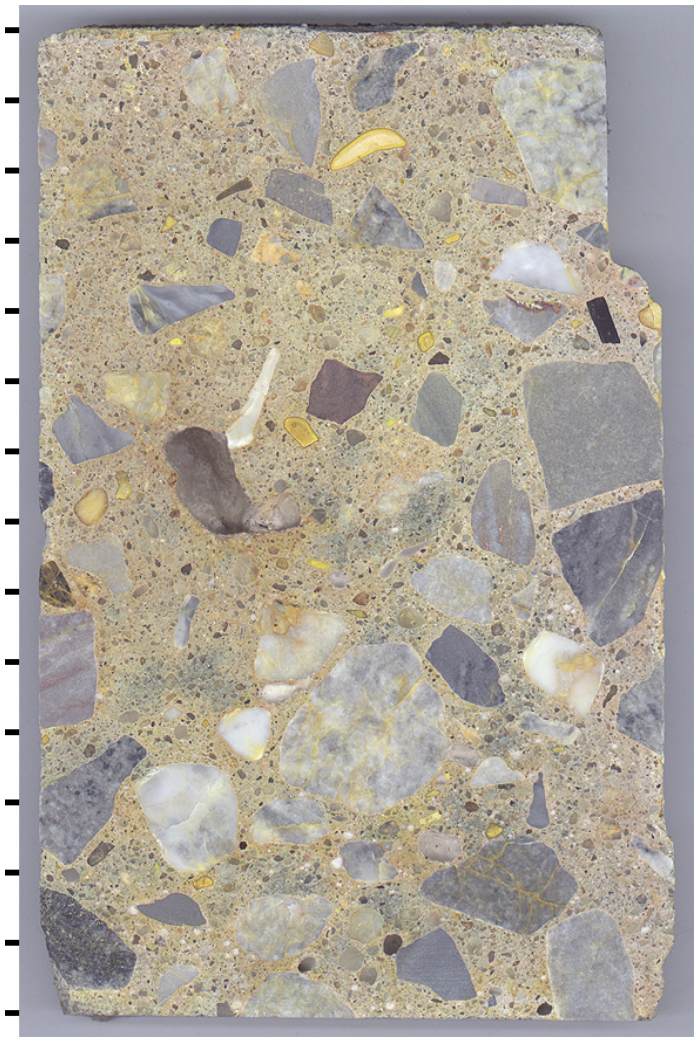

FIGURE 54. CLOSE-UP OF POLISHED SLAB PREPARED FROM TOP THIRD OF CORE B, AIRPORT ECHO, AFTER STAINING WITH SODIUM COBALTINITRITE SOLUTION. TICK MARKS EVERY CM

All of the cores show a trend of dark discolored cement paste with increasing depth. The discoloration becomes pronounced at depths greater than 3 cm for core A, and at depths greater than 15 cm for cores B and C. The dark discoloration of the cement paste is due to reduction of ferric iron (Fe^{3+}) present in the cement to ferrous iron (Fe^{2+}) by reduced sulfur (S^{2-}). Reduced sulfur is present in ground-granulated blast furnace slag (GBFS), which is a constituent of the cementitious material used in this concrete. Closer to the pavement surface, the reduced sulfur is oxidized by oxygen in the atmosphere, so no reduction of iron or discoloration is observed.

The air-void system parameters of the polished slabs were measured according to ASTM C 457. The measured spacing factors were 0.203, 0.214, and 0.161 mm for cores A, B, and C, respectively. Figure 55 shows a stereo-microscope image of the air-void structure typical cores A, B, and C.

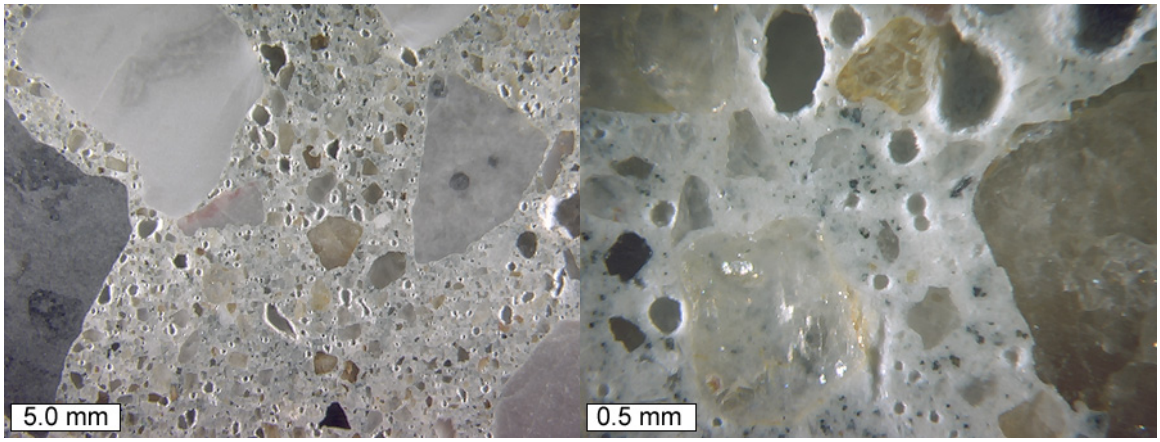

FIGURE 55. STEREO-MICROSCOPE IMAGES TO SHOW AIR VOID STRUCTURE ON POLISHED SLAB FROM MIDDLE THIRD OF CORE A ADJACENT TO JOINT, AIRPORT ECHO

The coarse aggregate is a quarried carbonate rock (limestone) and the fine aggregate is a quartz and feldspar-rich sand.

Petrographic Microscope and SEM Observations

Two thin sections were prepared from the top third of each core. The first thin section from each slab represents a cross section through the pavement surface to a depth of 40 mm. The second thin section from each slab consists of a cross section through the next horizon representing a depth of 40 to 80 mm. Based on measurements of the capillary fluorescence intensity of the cement paste, an average equivalent *w/c* value of 0.34 +/- 0.03 was obtained for the Airport Echo thin sections. It is emphasized that the value of 0.34 is not an absolute measurement of *w/c*, but simply a comparison to the fluorescence intensity of the laboratory prepared mortar standards made with portland cement and cured for 28 days.

Figure 56 shows a cross section through a crack at the pavement surface of core C. The crack morphology is typical of a plastic shrinkage crack. Figure 57 shows a petrographic microscope image of a reactive fine aggregate particle. The epifluorescent mode image on the right hand side of figure 57 shows no cracking associated with the reactive particle. The BSE in figure 58 shows a close-up of the alkali-silica reaction product adjacent to the reactive particle. Other non-reactive fine aggregate particles are incorporated into the reaction product, suggesting that the reaction may have occurred before the concrete had set.

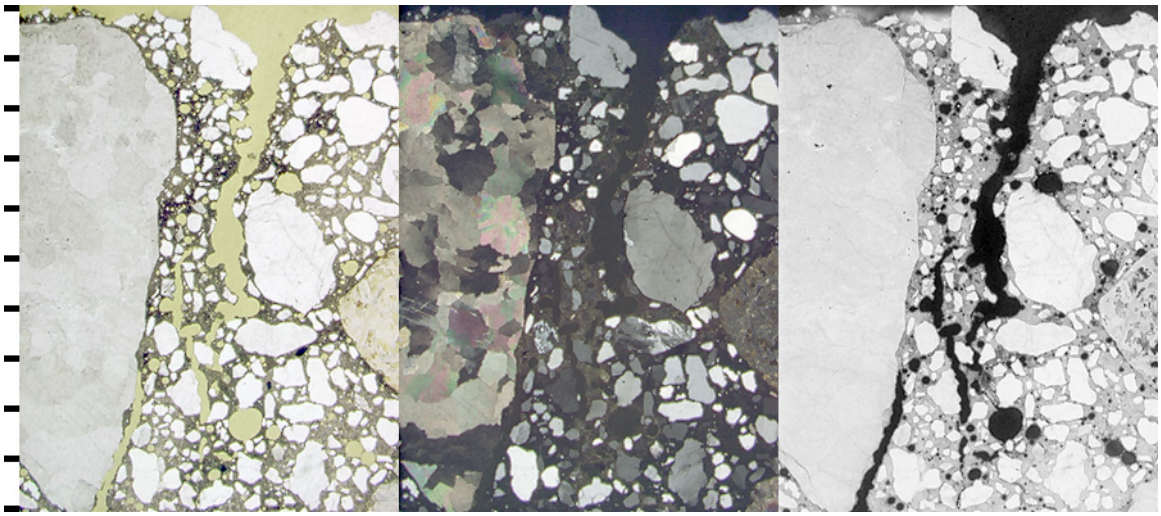

FIGURE 56. PETROGRAPHIC MICROSCOPE IMAGES TO SHOW CROSS-SECTION THROUGH PLASTIC SHRINKAGE CRACK AT PAVEMENT SURFACE FROM CORE C, AIRPORT ECHO. FROM LEFT TO RIGHT: PLANE POLARIZED LIGHT, CROSSED POLARS, AND EPIFLUORESCENT MODE. TICK MARKS EVERY MM

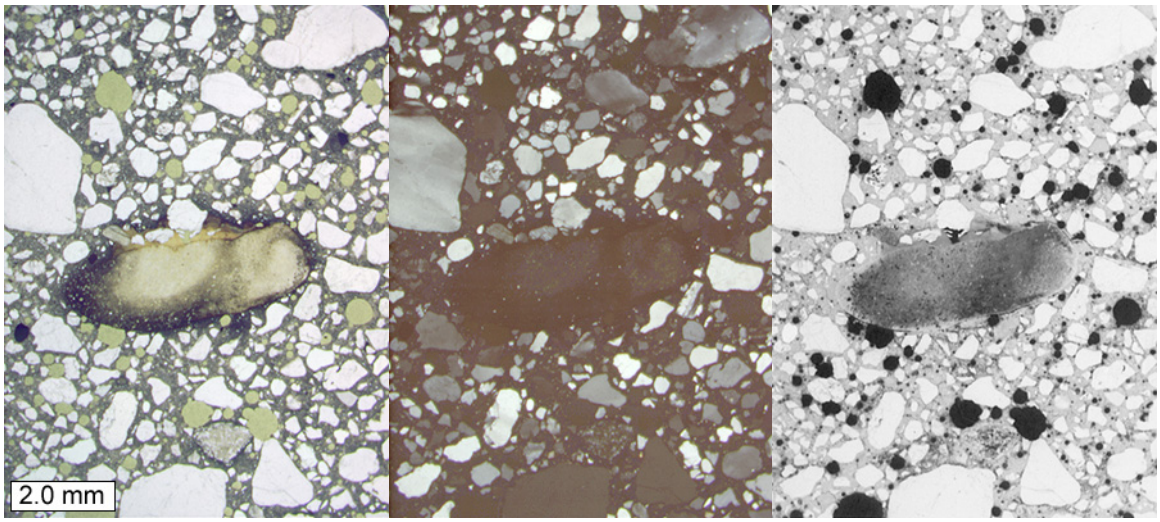

FIGURE 57. PETROGRAPHIC MICROSCOPE IMAGES TO SHOW REACTIVE FINE AGGREGATE PARTICLE IN POLISHED THIN SECTION FROM CORE C, AIRPORT ECHO. FROM LEFT TO RIGHT: PLANE POLARIZED LIGHT, CROSSED POLARS, AND EPIFLUORESCENT MODE

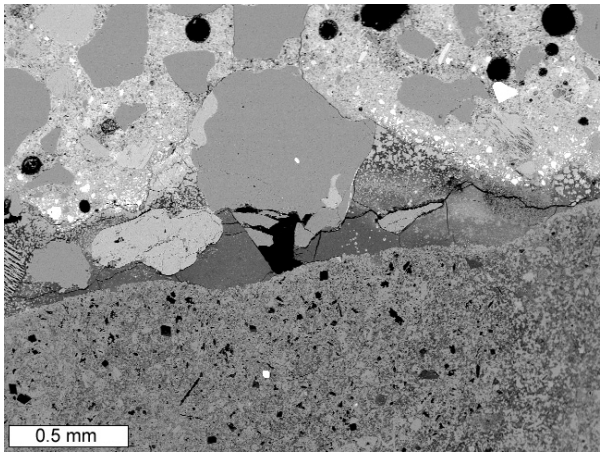

FIGURE 58. CLOSE-UP BSE IMAGE TO SHOW PERIMETER OF REACTIVE FINE AGGREGATE PARTICLE IN POLISHED THIN SECTION FROM CORE C, AIRPORT ECHO. INCORPORATION OF OTHER FINE AGGREGATE PARTICLES INTO GEL REACTION PRODUCT SUGGESTS GEL PRODUCTION OCCURRED BEFORE THE CONCRETE HAD SET

Figure 59 is a petrographic microscope image that illustrates the constituents of the cementitious materials in the concrete. The large cement grain in the lower left hand corner of the images in figure 59 exhibits a red coloration in the interior of the grain due to the ferric iron content of the interstitial phase (C4AF). The dark coloration around the exterior of the large cement grain is due to the reduction of the ferric iron in the interstitial phase by reduced sulfur available from the GBFS. A partially hydrated GBFS fragment is visible in the upper right hand corner of the images in figure 59.

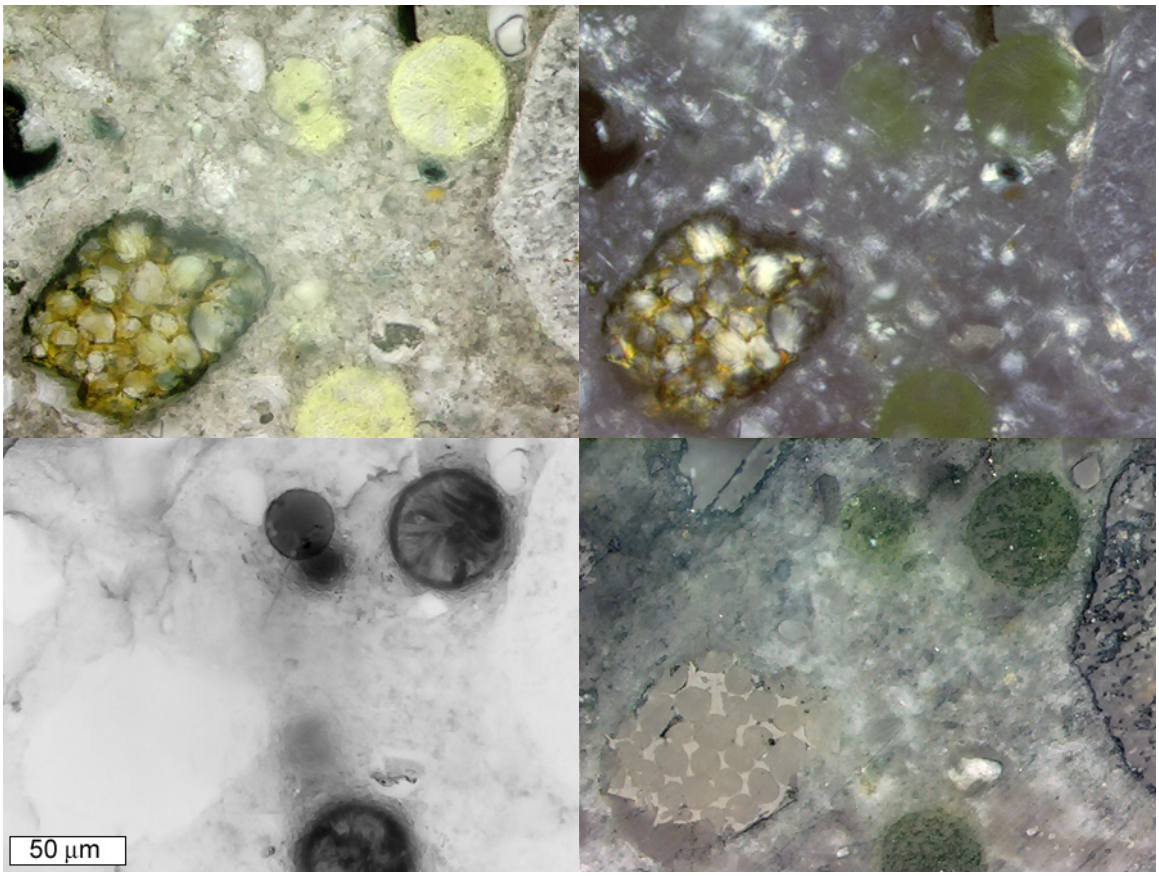

FIGURE 59. CLOSE-UP PETROGRAPHIC MICROSCOPE IMAGES TO SHOW CEMENT GRAINS AND GBFS FRAGMENTS IN CEMENT PASTE FRACTION FROM AIRPORT ECHO SITE. CLOCKWISE FROM UPPER LEFT HAND CORNER: PLANE POLARIZED LIGHT, CROSSED POLARS, REFLECTED LIGHT, AND EPIFLUORESCENT MODE

4.3.4. Airport Foxtrot

Seven 4-in diameter cores were received. All of the cores fully represented the entire depth of the concrete with a thickness of approximately 18 in. Adhering to the base of each core was an asphalt-saturated felt mat of approximately $^{1}/_{16}$-in thickness. Cores D, F, and G each had a single break across each core. The fracture surfaces of the breaks in cores D and F appeared fresh and clean, and were at depths of 6 in and 12 in, respectively. The break on core G was in a plane oriented approximately 45 degrees to the long axis of the core. The fracture surface along the break on core G was interrupted by large interconnected air voids, as shown in figure 60. Core A exhibited a similar network of large interconnected air voids (also shown in figure 60), but the core was intact. In both cores A and G, fine cracks were visible at the pavement surface above the large interconnected air void networks. Core C also exhibited a fine crack at the pavement surface, part of a crack plane running along the entire length of the core.

FIGURE 60. CLOSE-UP IMAGES OF IRREGULAR VOIDS, CORE A ON LEFT, CORE G ON RIGHT

Stereo Microscope and Flat-Bed Scanner Observations

Figures 61 and 62 show overviews of all the polished slabs from cores A, B, C, and F. The large interconnected air void network of Core A is readily observed. The remaining cores—B, C, and F—did not exhibit the same kind of large interconnected air void networks, but core C had a crack plane splitting the entire long axis of the core. The top thirds of cores A and B were stained with phenolphthalein and a carbonation depth of 0.5 to 1 mm was measured with minor additional carbonation noted along the perimeters of the large interconnected air void network of core A. All of the slabs from cores C and F were stained with sodium cobaltinitrite. As shown in figure 63, cracks present in the top third of core C picked up the yellow stain. A large, dark aggregate particle at the bottom of the slab from the middle third of core C also strongly picked up the yellow stain, but this was likely due to weathered potassium-bearing feldspar phenocrysts present in the particle and not due to alkali-silica reactivity. The sodium cobaltinitrite stained slabs from core F did not pick up the yellow stain to the same degree as core C. Figure 64 shows close-up stereo microscope images of yellow-stained regions from the top third of core C.

The air-void parameters of the polished slabs were measured according to ASTM C 457. The measured spacing factors were 0.290, 0.244, 0.167, and 0.269 mm for cores A, B, C, and F respectively, compared to a maximum recommended value of 0.200 mm.

The coarse aggregate is composed of quarried granitic and metamorphic rock, and the fine aggregate is an angular quartz and feldspar-rich sand.

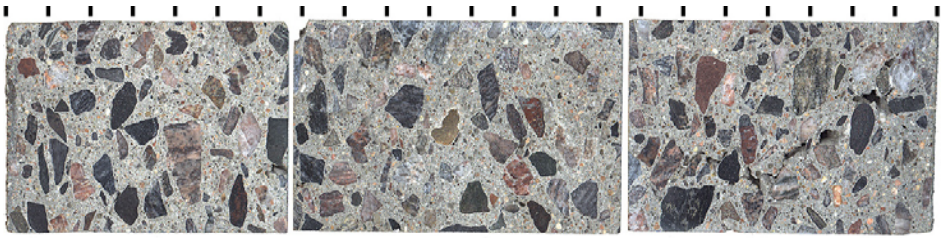

Core A, adjacent to joint, Airport Foxtrot

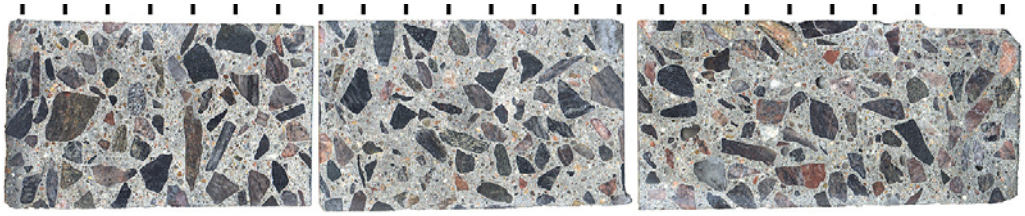

Core B, adjacent to joint, Airport Foxtrot

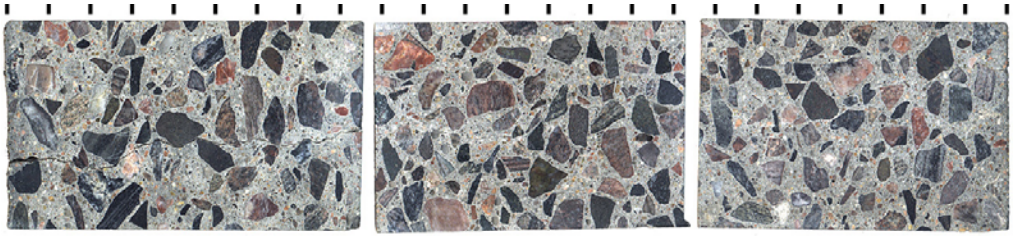

Core C, away from joint, Airport Foxtrot

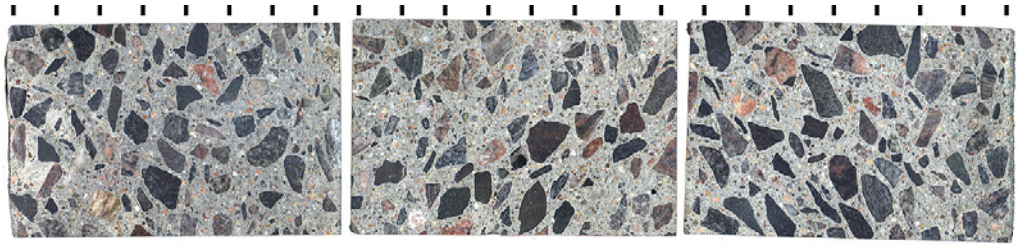

Core F, away from joint, Airport Foxtrot

FIGURE 61. POLISHED SLABS FROM AIRPORT FOXTROT. SLABS ORIENTED TO SHOW CROSS-SECTION THROUGH PAVEMENT, PAVEMENT SURFACE AT RIGHT HAND SIDE, TICK MARKS EVERY 2 CM

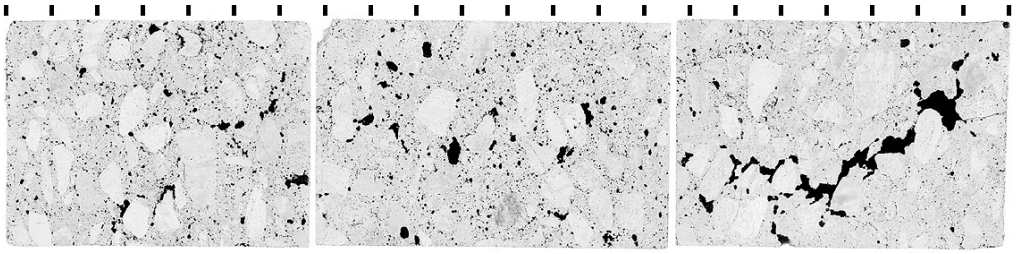

Core A, adjacent to joint, Airport Foxtrot

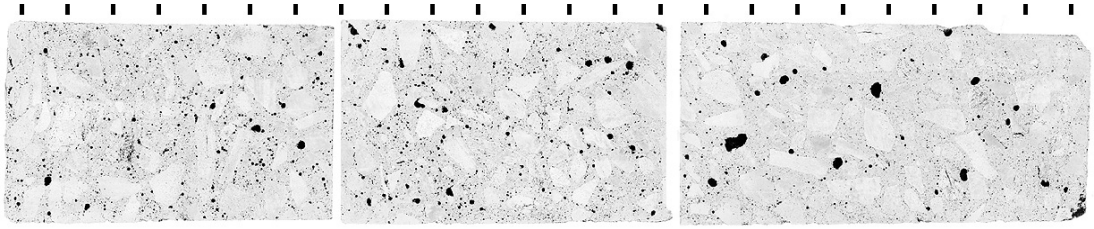

Core B, adjacent to joint, Airport Foxtrot

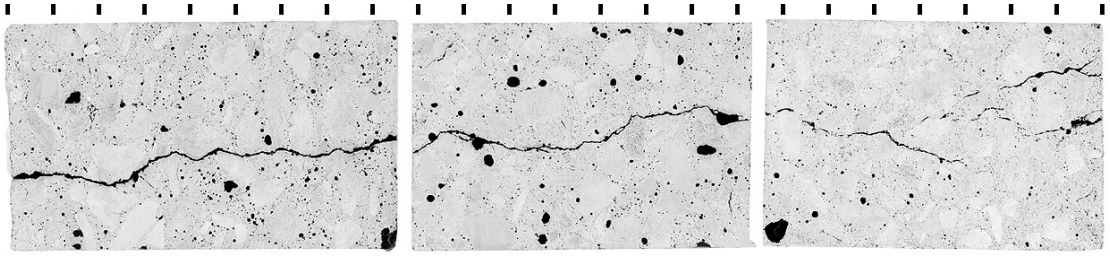

Core C, away from joint, Airport Foxtrot

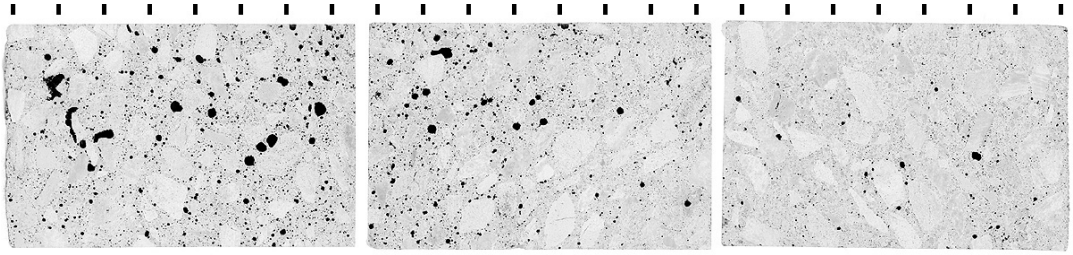

Core F, away from joint, Airport Foxtrot

FIGURE 62. POLISHED SLABS FROM AIRPORT FOXTROT AFTER TREATMENT TO ENHANCE VISIBILITY OF AIR VOIDS AND CRACKS. SLABS ORIENTED TO SHOW CROSS-SECTION THROUGH PAVEMENT, PAVEMENT SURFACE AT RIGHT-HAND SIDE, TICK MARKS EVERY 2 CM

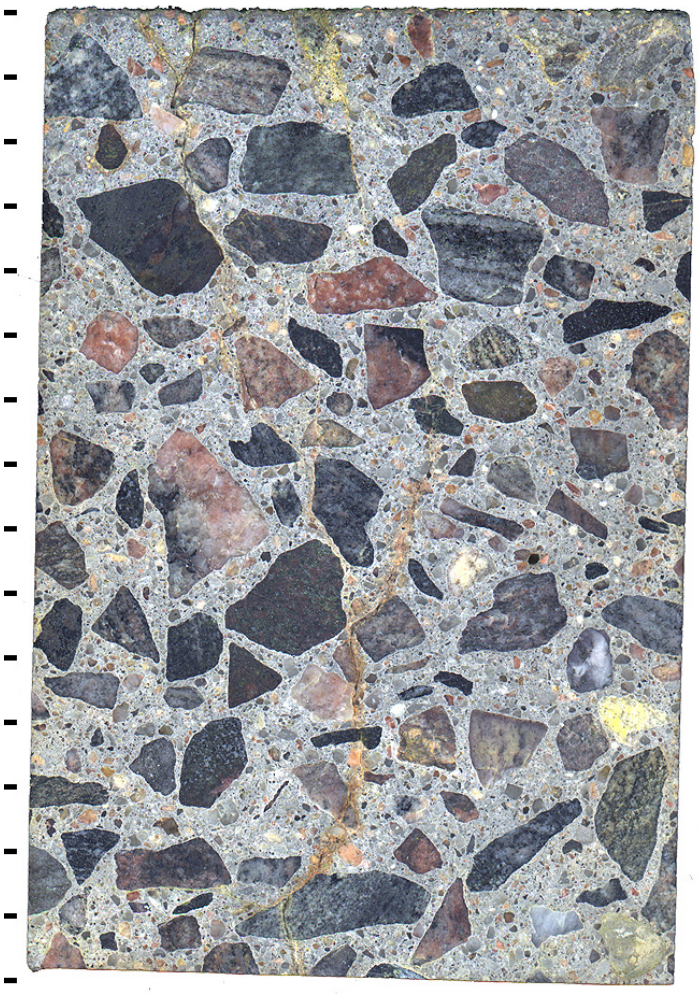

FIGURE 63. CLOSE-UP OF POLISHED SLAB PREPARED FROM TOP THIRD OF CORE C, AIRPORT FOXTROT, AFTER STAINING WITH SODIUM COBALTINITRITE SOLUTION. TIC MARKS EVERY CM

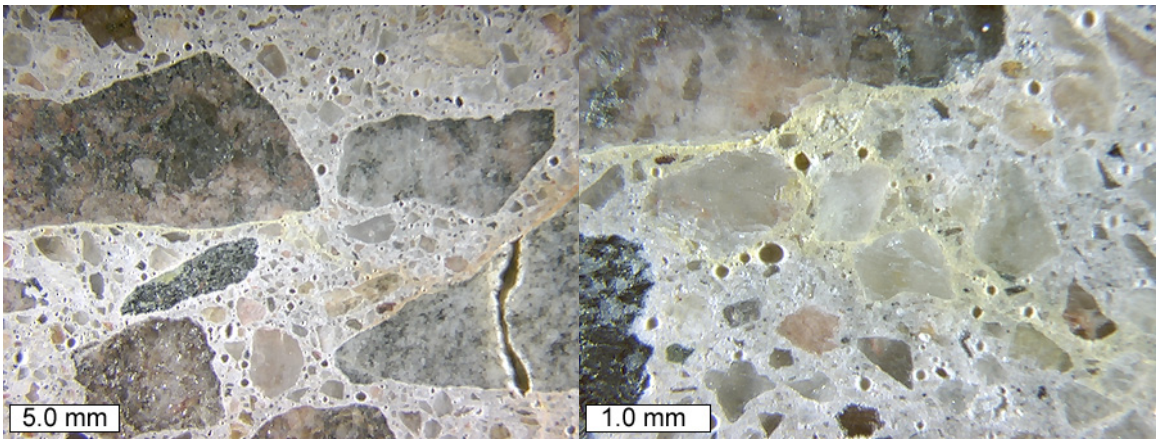

FIGURE 64. STEREO-MICROSCOPE IMAGES TO CRACK THAT PICKED UP YELLOW COLORATION FROM SODIUM COBALTINITRITE STAIN ON THE TOP THIRD OF CORE C AWAY FROM JOINT, AIRPORT FOXTROT

Petrographic Microscope and SEM Observations

Two thin sections were prepared from the top third of each core. The first thin section from each slab represents a cross section through the pavement surface to a depth of 40 mm. The second thin section from each slab consists of a cross section through the next horizon representing a depth of 40 to 80 mm. The second thin section from each slab was used for measurements of the capillary fluorescence intensity of the cement paste. Based on measurements of the capillary fluorescence intensity of the cement paste, an average *w/c* value of 0.33 +/- 0.02 was obtained for the thin sections from Airport Foxtrot. Once again, it is emphasized that the value of 0.33 is not an absolute measurement of *w/c*, but simply a comparison to the fluorescence intensity of the laboratory prepared mortar standards made with portland cement and cured for 28 days.

Figure 65 shows petrographic microscope images of a cross section through a crack at the pavement surface of core C. The crack propagates through the cement paste and through aggregate particles. Figures 66 and 67 compare and contrast epifluorescent mode images of the texture of the cement paste in a region from core B to that of a region of core A near the network of large interconnected air voids. In figure 67, the cement paste of core A has irregularly shaped entrained air voids, and small sub-entrained air sized gaps in the paste.

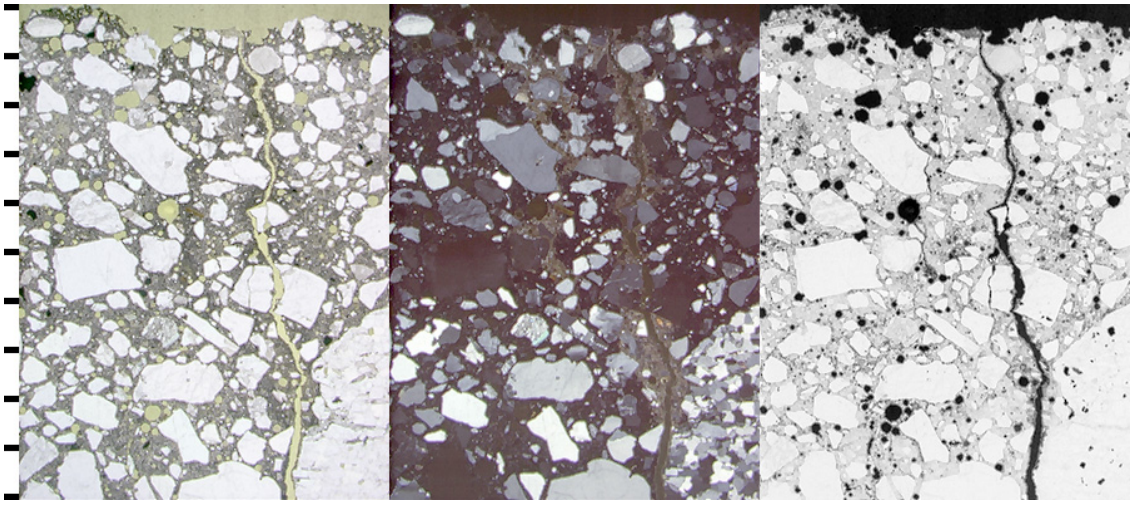

FIGURE 65. PETROGRAPHIC MICROSCOPE IMAGES OF POLISHED THIN SECTION FROM CORE C, AIRPORT FOXTROT, SHOWING CROSS SECTION THROUGH PAVEMENT SURFACE AND CARBONATION ALONG CRACK. FROM LEFT TO RIGHT: PLANE POLARIZED, CROSSED POLARS, AND EPIFLUORESCENT MODE. TICK MARKS EVERY MM

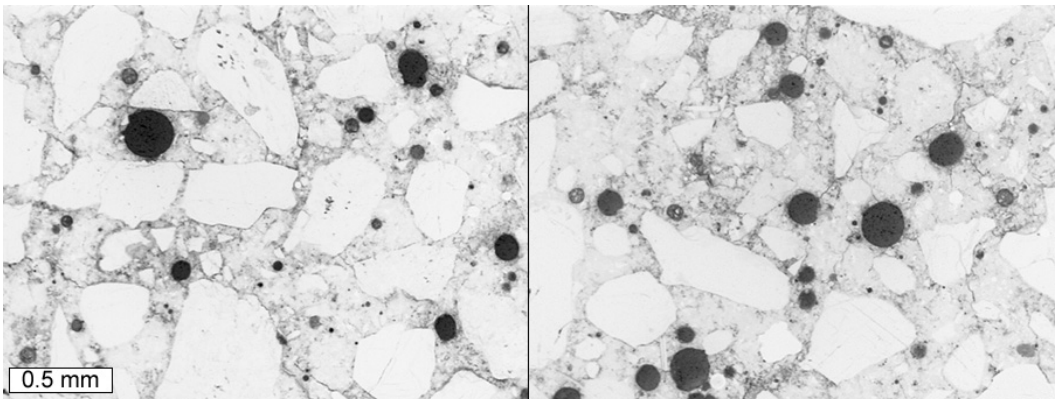

FIGURE 66. EPIFLUORESCENT MODE PETROGRAPHIC MICROSCOPE IMAGES FROM POLISHED THIN SECTION FROM CORE B, AIRPORT FOXTROT. NOTE FAIRLY UNIFORM CEMENT PASTE, AND ROUND ENTRAINED AIR VOIDS

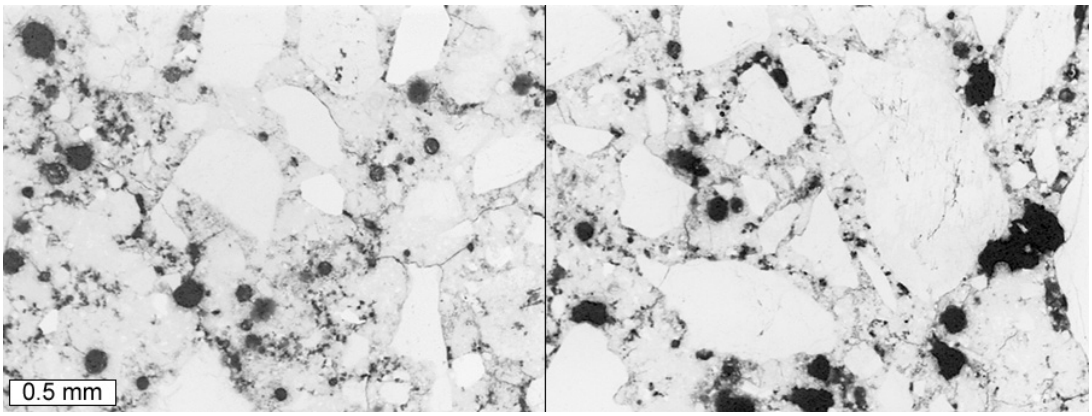

FIGURE 67. EPIFLUORESCENT MODE PETROGRAPHIC MICROSCOPE IMAGES FROM POLISHED THIN SECTION FROM CORE A, AIRPORT FOXTROT. NOTE SLIGHTLY MORE IRREGULARLY SHAPED ENTRAINED AIR VOIDS, AND SUB-ENTRAINED AIR SIZED GAPS IN THE CEMENT PASTE

Figures 68 and 69 show BSE images, elemental maps, and petrographic microscope images of a potassium-bearing alkali-silica reaction deposit along the large crack in core C. X-ray energy dispersive spectrum (EDS) collected from the deposit had large peaks for oxygen, silicon, and calcium, and minor peaks for carbon, sodium, aluminum, and potassium. The small carbon peak is due to carbon coating prior to examination with the SEM. Secondary ettringite deposits were also identified along the large crack in core C. The ettringite deposit transitions into another aluminum and calcium-bearing phase halfway down the crack that contains appreciable amounts of carbon and silicon, minor amounts of sodium and chlorine, and less sulfur as compared to the ettringite phase. It is speculated that the phase may represent a CO_3^{-2} and Si-substituted ettringite. No quantitative EDS chemical composition measurements were made from any of the deposits. Figure 70 is a petrographic microscope image that illustrates the constituents of the cementitious materials in the concrete. Fly ash spheres can clearly be seen in the plane polarized image.

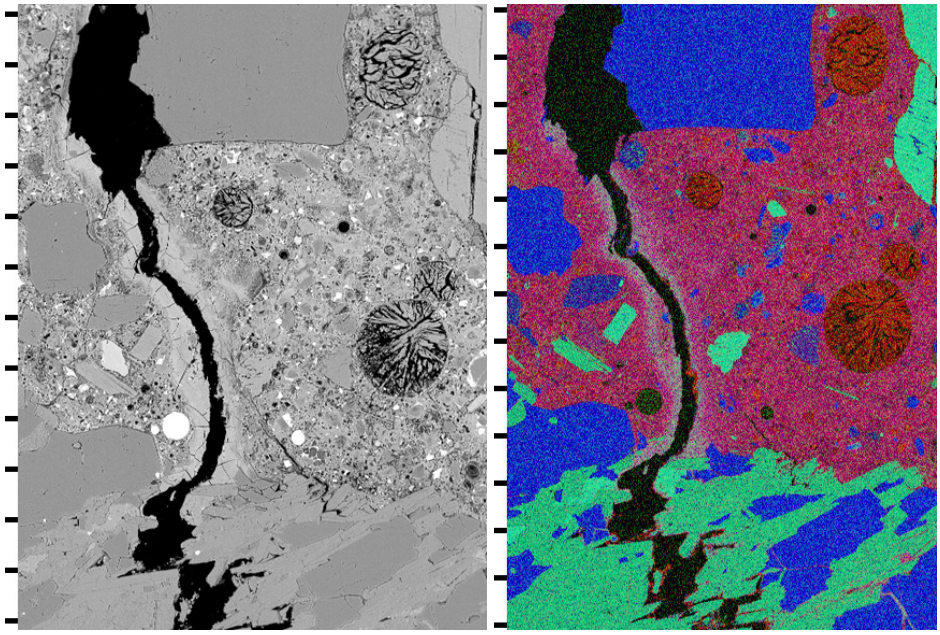

FIGURE 68. BSE IMAGE (LEFT) AND ELEMENTAL MAP (RIGHT) OF CRACK LINED WITH ALKALI SILICA REACTION PRODUCT AND ENTRAINED AIR VOIDS FILLED WITH SECONDARY ETTRINGITE DEPOSITS IN POLISHED THIN SECTION PREPARED FROM CORE C, AIRPORT FOXTROT. IN ELEMENTAL MAP, CA = RED CHANNEL, K = GREEN CHANNEL, AND SI = BLUE CHANNEL. TICK MARKS EVERY 100 MICROMETERS

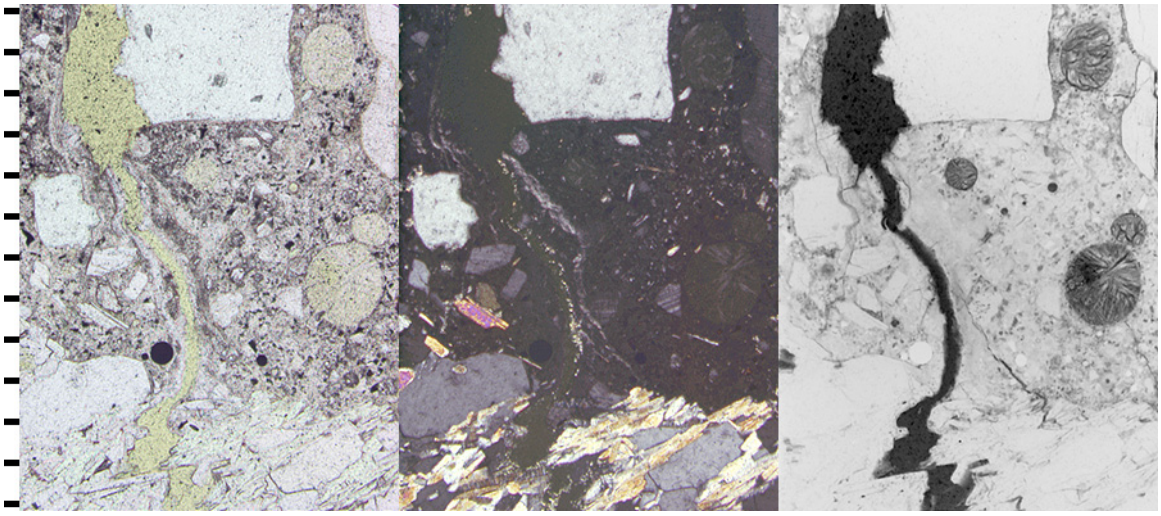

FIGURE 69. PETROGRAPHIC MICROSCOPE IMAGES OF CRACK LINED WITH ALKALI SILICA REACTION PRODUCT, AND ENTRAINED AIR VOIDS FILLED WITH SECONDARY ETTRINGITE DEPOSITS IN POLISHED THIN SECTION PREPARED FROM CORE C, AIRPORT FOXTROT. FROM LEFT TO RIGHT: PLANE POLARIZED, CROSSED POLARS, AND EPIFLUORESCENT MODE. TICK MARKS EVERY 100 MICROMETERS

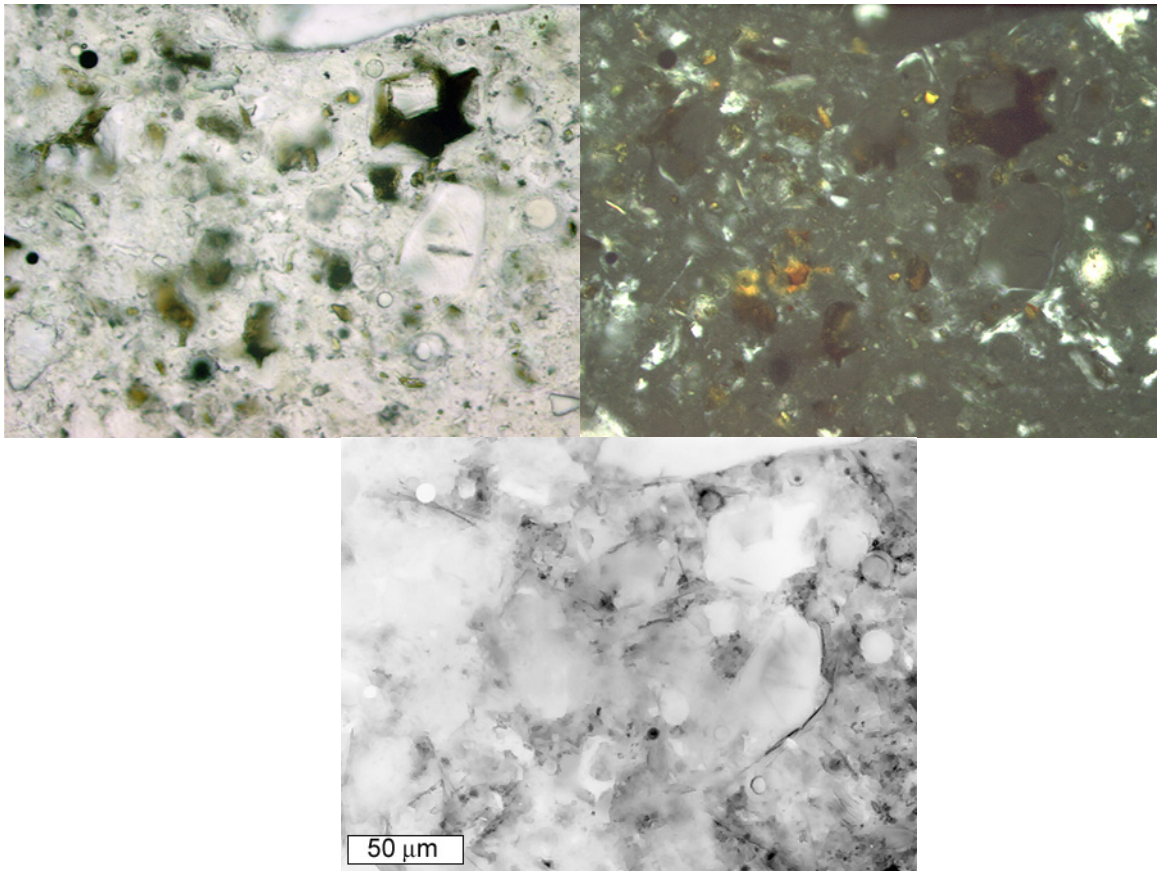

FIGURE 70. CLOSE-UP PETROGRAPHIC MICROSCOPE IMAGES TO SHOW CEMENT GRAINS AND FLY ASH IN CEMENT PASTE FRACTION FROM AIRPORT FOXTROT. CLOCKWISE FROM UPPER LEFT HAND CORNER: PLANE POLARIZED LIGHT, CROSSED POLARS, AND EPIFLUORESCENT MODE

4.3.5. Airport Golf

Description of Cores as Received

Six 4-in diameter cores were received. All of the cores fully represented the entire depth of the concrete with a thickness of approximately 13 in (note that this is 2 in thinner than the design thickness). Figures 71 and 72 show scanned images of polished slabs for cores A, B, C, and D. In some cases, portions of the cement-stabilized recycled concrete aggregate base remained adhered to the core bottom. A 1.25-in diameter, non-coated dowel bar was intersected in core A at a depth of about 5.5 in. The dowel was in good condition. The pavement surface near the joint on core B was covered with an asphalt patch material. A similar patch material may have been applied to the pavement surface of core A, but appears to have been removed. Fine cracks were observed at the pavement surface of both cores A and B running perpendicular to the pavement joint. Core C, taken away from the joint, exhibited a fine crack at the pavement surface, part of a crack plane running almost the full depth of the core.

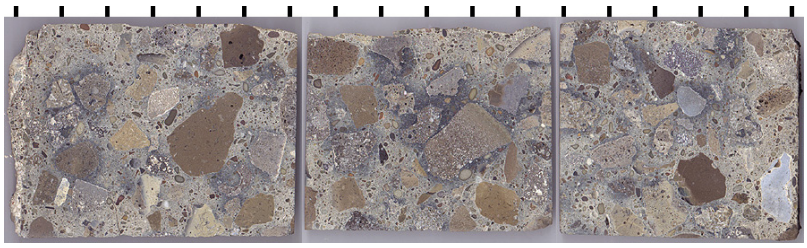

Core A, adjacent to joint, Airport Golf

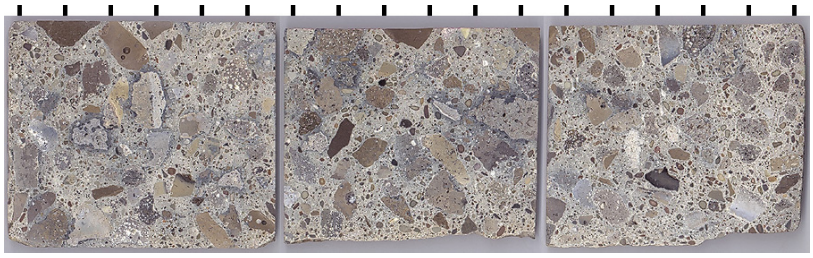

Core B, adjacent to joint, Airport Golf

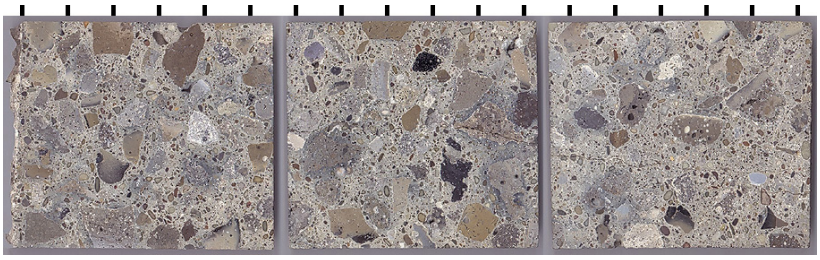

Core C, away from joint, Airport Golf

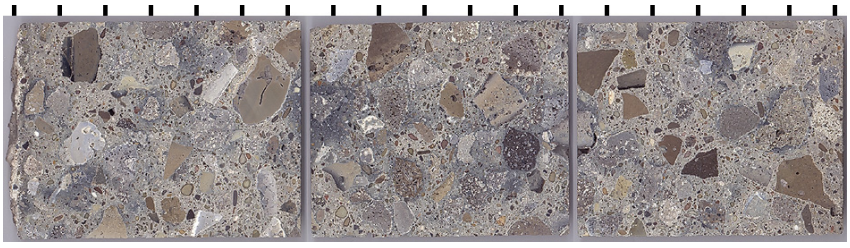

Core D, away from joint, Airport Golf

FIGURE 71. POLISHED SLABS FROM AIRPORT GOLF. SLABS ORIENTED TO SHOW CROSS-SECTION THROUGH PAVEMENT, PAVEMENT SURFACE AT RIGHT-HAND SIDE, TICK MARKS EVERY 2 CM. DARK DISCOLORATION OF CEMENT PASTE DUE TO REDUCTION OF IRON IN CEMENT GRAINS BY SULFUR PRESENT IN AIR-COOLED BLAST FURNACE SLAG COARSE AGGREGATE

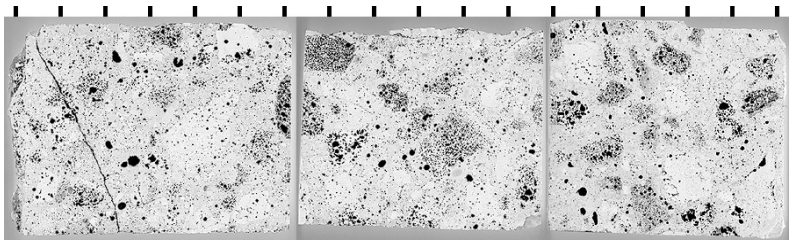

Core A, adjacent to joint, Airport Golf

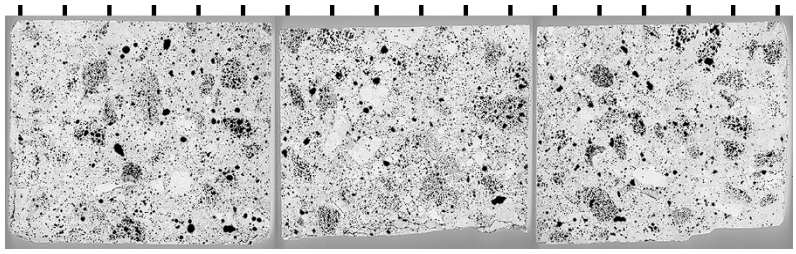

Core B, adjacent to joint, Airport Golf

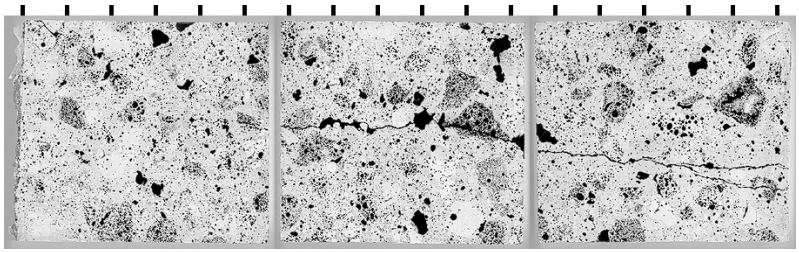

Core C, away from joint, Airport Golf

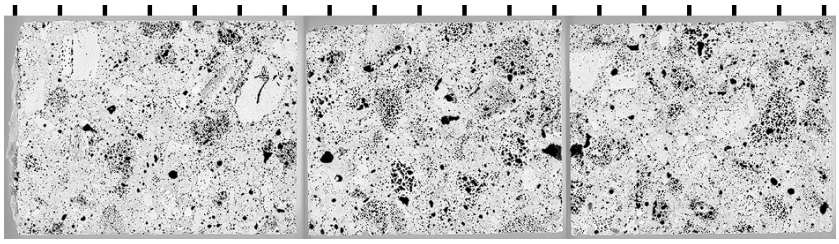

Core D, away from joint, Airport Golf

FIGURE 72. POLISHED SLABS FROM AIRPORT GOLF AFTER TREATMENT TO ENHANCE VISIBILITY OF AIR VOIDS AND CRACKS. SLABS ORIENTED TO SHOW CROSS-SECTION THROUGH PAVEMENT, PAVEMENT SURFACE AT RIGHT-HAND SIDE, TICK MARKS EVERY 2 CM

Stereo Microscope and Flat-Bed Scanner Observations

All of the cores prepared for petrographic examination exhibited dark, discolored cement paste adjacent to the air-cooled blast furnace slag coarse aggregate particles at depths greater than 2 cm. The dark discoloration of the cement paste, shown in figure 73, is due to reduction of ferric iron (Fe^{3+}) in the cement and fly ash to ferrous iron (Fe^{2+}) by reduced sulfur (S^{2-}). Reduced sulfur is present in the blast furnace slag coarse aggregate. At depths less than 2 cm, the reduced sulfur is oxidized by atmospheric oxygen, so no reduction of iron or discoloration is observed.

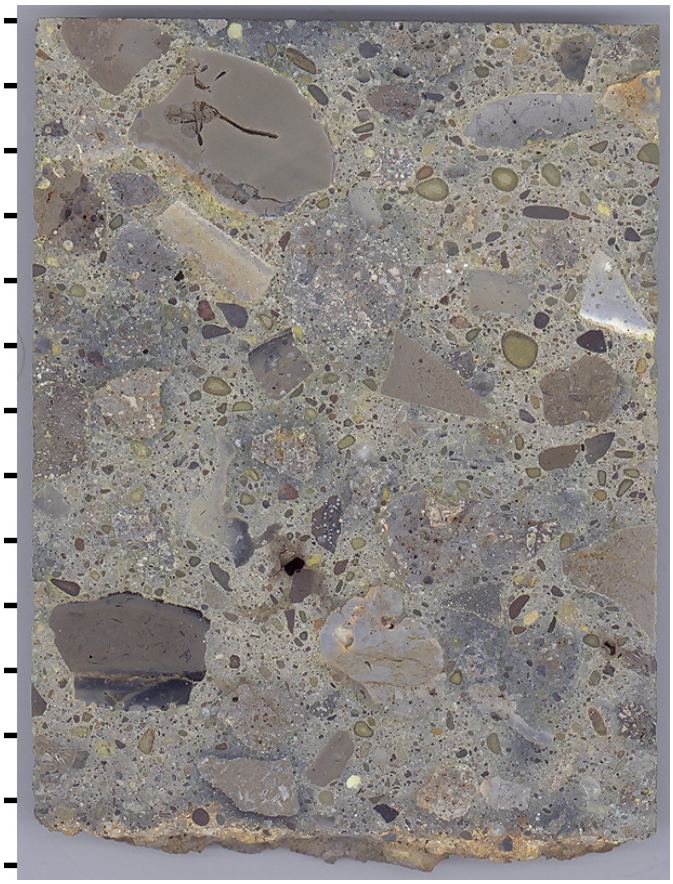

FIGURE 73. CLOSE-UP OF POLISHED SLAB PREPARED FROM BOTTOM THIRD OF CORE D, AIRPORT GOLF AFTER STAINING WITH SODIUM COBALTINITRITE SOLUTION. TICK MARKS EVERY CM

All of the slabs from cores A, B, and C were stained with phenolphthalein to assess carbonation depth, which varied in depth from 0.5 to 2.5 mm with minor additional carbonation along the perimeters of cracks in core C. The crack in core A terminates at a depth of about 2 mm. The fine crack at the surface of core B was not intersected in the polished slabs, but cracks parallel to the joint at greater depths are well defined. Similar cracking parallel to the joint was observed at depth in the polished slab from the middle third of core A. The polished slab from the bottom third of core A also showed a large crack near the base of the core. The large crack exposed in cross section on the polished slabs of core C does not extend to the full depth of the pavement, only to a depth of about 24 cm. The cracks propagate through the cement paste and through aggregate particles. All of the slabs from core D were stained with a solution of sodium cobaltinitrite. The yellow stain was picked up by fine aggregate particles, some with darkened rims were in contact with the cement paste, as shown in figure 73. The reactive fine aggregate particles were not associated with any cracking.

The air-void parameters of the polished slabs were measured according to ASTM C 457; measured existing spacing factors were 0.199, 0.219, 0.187, and 0.181 mm for cores A, B, C and D, respectively. The entrained air voids were frequently filled with secondary mineral deposits.

A solution of barium sulfate and potassium permanganate was used to stain a small region on a polished slab from the middle third of core B. Figure 74 shows the region both before and after staining. The deposits in the entrained air voids picked up the purple stain for sulfate-bearing minerals. Figure 75 shows stereo-microscope images of the air-void structure typical of the concrete sampled at Airport Golf. Note the infilling of some of the smaller voids.

The coarse aggregate is an air-cooled blast furnace slag, and the fine aggregate is a quartz and siltstone-rich sand.

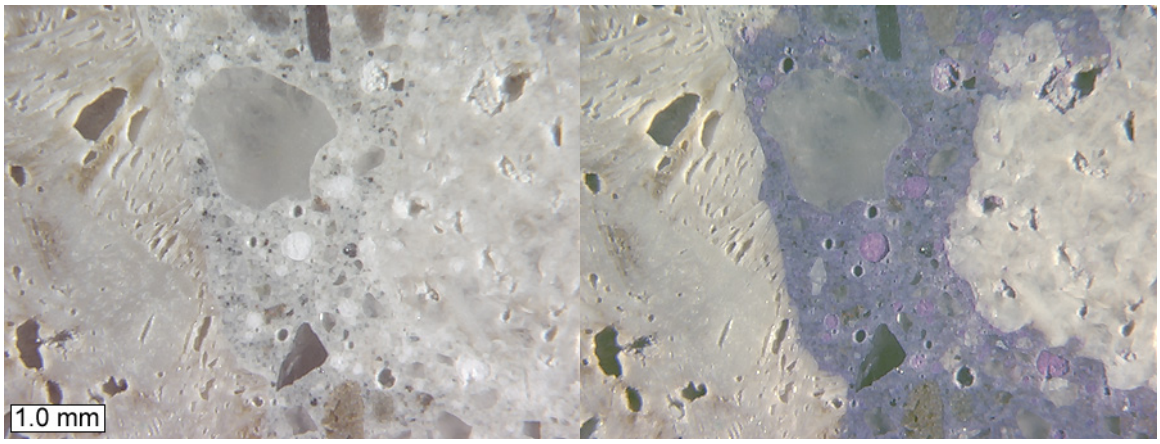

FIGURE 74. STEREO-MICROSCOPE IMAGES OF POLISHED SLAB FROM MIDDLE THIRD OF CORE C SHOWING ETTRINGITE FILLED ENTRAINED AIR VOIDS BOTH BEFORE (LEFT) AND AFTER (RIGHT) STAINING WITH BARIUM CHLORIDE AND POTASSIUM PERMANGANATE SOLUTION

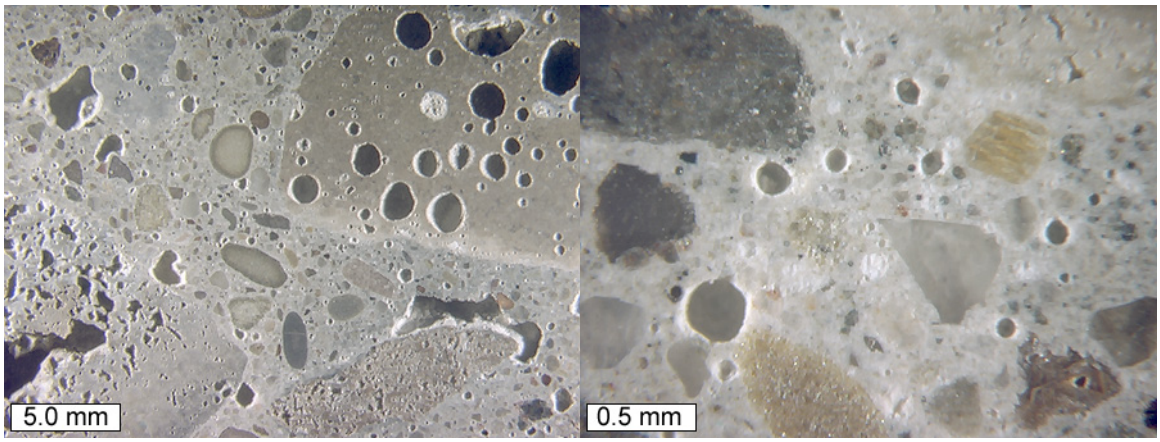

FIGURE 75. STEREO-MICROSCOPE IMAGES TO SHOW AIR-VOID STRUCTURE ON POLISHED SLAB FROM TOP THIRD OF CORE C AWAY FROM JOINT, AIRPORT GOLF

Petrographic Microscope and SEM Observations

Two thin sections were prepared from the top third of each core. The first thin section from each slab represents a cross section through the pavement surface to a depth of 40 mm. The second thin section from each slab consists of a cross section through the next horizon representing a depth of 40 to 80 mm. Based on the capillary fluorescence intensity of the cement paste, an average *w/c* value of 0.30 +/- 0.02 was obtained for the Airport Golf thin sections. The value of 0.30 is not an absolute measurement of *w/c*, but simply a comparison to the fluorescence intensity of the laboratory prepared mortar standards made with portland cement and cured for 28 days.

Figure 76 shows a cross section through cracks at the pavement surface of core C. Carbonation along the crack can be seen in the crossed polars image. Figures 77 and 78 show a BSE image, elemental maps, and petrographic microscope images of ettringite-filled cracks and entrained air voids on a polished thin section from core C. Figures 79 is a petrographic microscope image illustrating the constituents of the cementitious materials in the concrete.

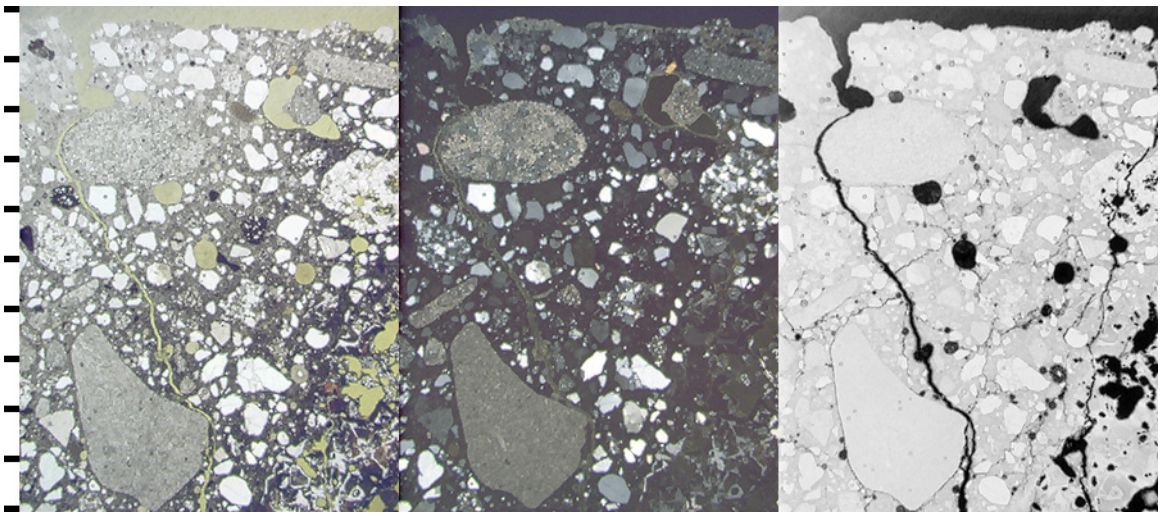

FIGURE 76. PETROGRAPHIC MICROSCOPE IMAGES OF POLISHED THIN SECTION FROM CORE C, AIRPORT GOLF, SHOWING CROSS SECTION THROUGH PAVEMENT SURFACE AND CARBONATION ALONG CRACK. FROM LEFT TO RIGHT: PLANE POLARIZED, CROSSED POLARS, AND EPIFLUORESCENT MODE. TICK MARKS EVERY MM

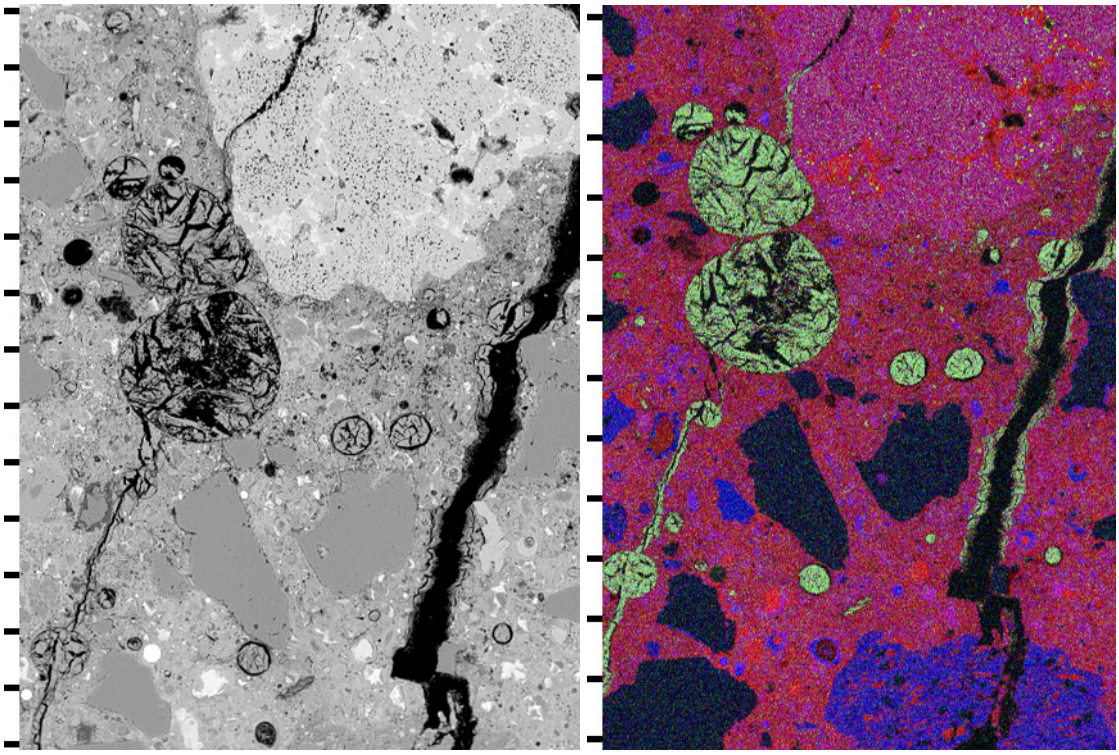

FIGURE 77. BSE IMAGE (LEFT) AND ELEMENTAL MAP (RIGHT) OF CRACK LINED WITH ETTRINGITE DEPOSITS IN POLISHED THIN SECTION PREPARED FROM CORE C, AIRPORT GOLF. IN ELEMENTAL MAP, CA = RED CHANNEL, S = GREEN CHANNEL, AND AL = BLUE CHANNEL. TICK MARKS EVERY 100 MICROMETERS

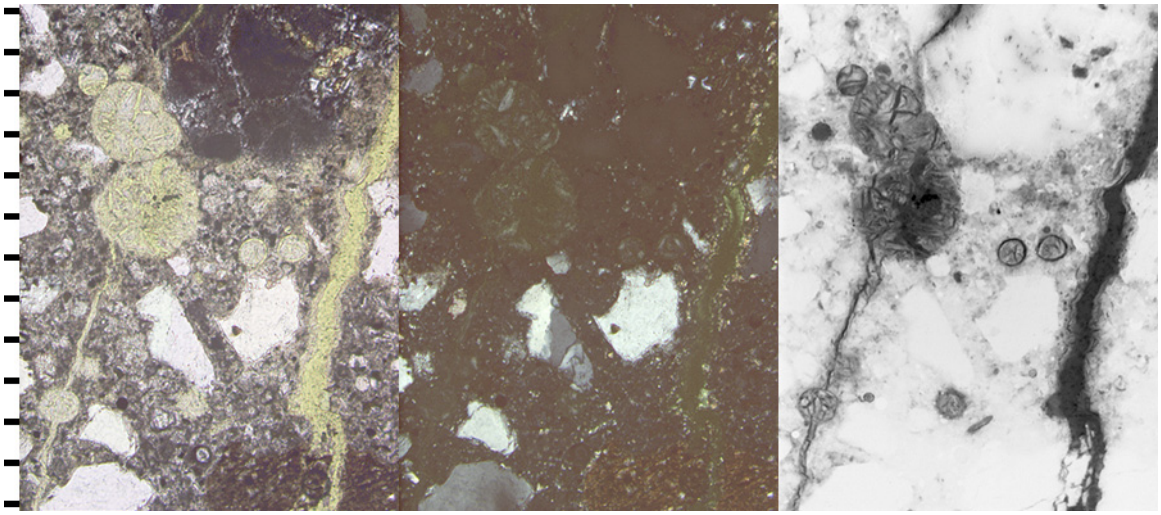

FIGURE 78. PETROGRAPHIC MICROSCOPE IMAGES OF CRACK LINED WITH ETTRINGITE DEPOSIT IN POLISHED THIN SECTION PREPARED FROM CORE C, AIRPORT GOLF. FROM LEFT TO RIGHT: PLANE POLARIZED, CROSSED POLARS, AND EPIFLUORESCENT MODE. TICK MARKS EVERY 100 MICROMETERS

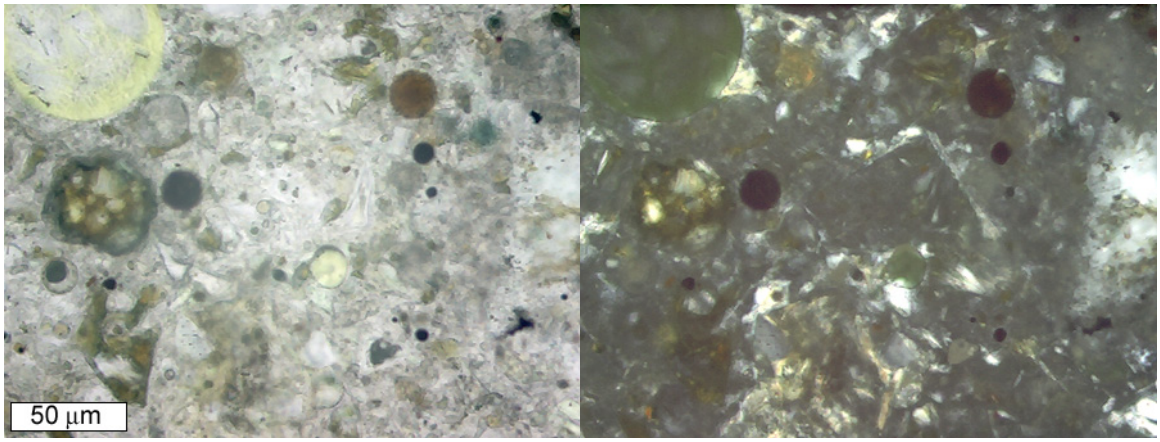

FIGURE 79. CLOSE-UP OF CEMENT PASTE IN THIN SECTION FROM AIRPORT GOLF TO SHOW CEMENT GRAINS AND FLY ASH PARTICLES IN CEMENT PASTE. FROM LEFT TO RIGHT, PLANE POLARIZED AND CROSSED POLARS

4.3.6. Summary of Petrographic Data

Tables 8, 9, and 10 summarize easily tabulated data for the five airports investigated. As can be seen in table 8, all the airports had acceptable total air contents, averaging values within the range of 4.5 to 7.0 percent; however, two cores fell below 4.5 percent and six cores were above 7.0 percent. Most cores had a significant amount of entrapped air and some had clear evidence of poor consolidation characterized by large, interconnected void structures.

Unfortunately, the generally favorable total air contents did not necessarily translate into good air-void systems as measured by the spacing factor. Airport Delta, which was included due to its good performance, had the lowest spacing factor at 0.115 mm. All of the remaining airports had average spacing factors approaching or exceeding the ASTM C 457 maximum recommended limit of 0.200 mm, indicating that not all of the measured air was distributed into a useful air-void system needed to protect the concrete against paste freeze-thaw damage.

Table 9 summarizes the observed cementitious constituents. As would be assumed, relic cement grains were observed in all of the concrete. The presence of GBFS was confirmed in Airport Echo and fly ash in Airports Delta, Foxtrot, and Golf. No supplementary cementitious material was observed in Airport Alpha, but a significant quantity of inert dolomite filler was clearly observed.

Table 10 summarizes the results of the capillary fluorescence measurements. These data clearly show that the hydrated cement pastes at Airports Delta, Echo, Foxtrot, and Golf have less capillary porosity and are denser than the hydrated cement paste at Airport Alpha. Although no conclusions should be drawn regarding the actual *w/c* at time of construction, it is possible that the use of supplementary cementitious materials (fly ash or GBFS) contributed to less capillary porosity.

Detailed analysis of these petrographic results are presented in the next section.

TABLE 8. SUMMARY OF AIR-VOID STATISTICS FROM ALL OF THE AIRPORT SITES

Air-port	Core ID	Air vol %	Paste vol%	Coarse Agg. vol%	Fine Agg. vol%	Second-ary Phase vol%	Spacing Factor (mm)	Paste/ Air Ratio	Air Void Specific Surface (mm^{-1})	Air Void Freq. (voids/mm)	Avg. Chord Length (mm)
Alpha	A	5.0	24.6	44.0	26.3	0.0	0.197	4.9	23.4	293	0.171
	B	5.1	26.6	43.5	24.7	0.0	0.185	5.2	25.4	326	0.157
	C	6.3	26.6	44.1	23.0	0.0	0.197	4.2	21.6	339	0.186
	F	3.4	24.6	53.2	18.6	0.1	0.339	7.3	16.2	138	0.246
Delta	44	7.3	18.6	41.5	32.7	0.0	0.115	2.5	22.1	403	0.181
Echo	A	8.3	28.2	40.7	22.7	0.1	0.203	3.4	16.8	349	0.238
	B	7.6	28.3	38.7	25.3	0.1	0.214	3.7	17.4	331	0.230
	C	6.8	26.3	44.8	22.0	0.1	0.161	3.9	24.0	409	0.167
Foxtrot	A	8.1	26.6	42.5	22.9	0.0	0.290	3.3	11.4	229	0.352
	B	5.3	26.9	44.1	23.7	0.0	0.244	5.0	19.0	254	0.210
	C	5.2	14.8	50.4	29.6	0.0	0.167	2.8	17.0	222	0.236
	F	6.8	27.0	41.2	25.0	0.1	0.269	4.0	14.9	252	0.269
Golf	A	4.4	30.9	43.1	21.3	0.2	0.199	7.0	27.1	301	0.147
	B	7.1	33.7	38.6	19.9	0.6	0.219	4.8	20.9	370	0.192
	C	7.6	27.7	40.9	23.7	0.1	0.187	3.7	19.5	372	0.205
	D	6.5	27.3	44.8	21.5	0.0	0.181	4.2	23.4	378	0.171

TABLE 9. CEMENTITIOUS CONSTITUENTS PRESENT IN AIRPORT DEICER PADS

Airport	Portland Cement	Ground Blast Furnace Cement	Fly Ash	Inert Dolomite Powder Filler
Alpha	yes	no	no	yes
Delta	yes	no	yes	no
Echo	yes	yes	no	no
Foxtrot	yes	no	yes	no
Golf	yes	no	yes	no

TABLE 10. RESULTS OF CAPILLARY FLUORESCENCE MEASUREMENTS FROM THIN SECTIONS PREPARED FROM FIELD SITES AND COMPARED TO MEASUREMENTS FROM THIN SECTIONS PREPARED FROM 28-DAY MOIST CURED MORTAR CYLINDERS OF KNOWN *W/C*.

	0.60 *w/c* standard	**0.50 *w/c* standard**	**0.40 *w/c* standard**	**Airport Alpha**	**Airport Delta**	**Airport Echo**	**Airport Foxtrot**	**Airport Golf**
Average fluorescence intensity measurement per frame (12 frames total)	137	126	106	118	100	89	98	93
	137	124	101	109	101	85	95	89
	130	125	103	94	97	85	95	93
	136	113	102	121	99	87	91	100
	136	135	106	111	99	103	93	91
	134	122	102	115	97	90	92	88
	134	125	114	104	97	107	96	93
	134	130	109	102	99	107	89	85
	135	122	108	91	101	112	88	88
	132	130	113	117	97	102	100	88
	133	130	111	116	97	99	106	87
	136	133	115	98	100	93	99	91
Simple linear regression model	*w/c* = 0.0061 * (*intensity*) - 0.2491				R^2 = 0.82			
Predicted *w/c* values	0.59	0.52	0.40	0.47	0.36	0.29	0.35	0.32
	0.59	0.51	0.37	0.42	0.37	0.27	0.33	0.30
	0.55	0.51	0.38	0.32	0.34	0.27	0.33	0.32
	0.58	0.44	0.37	0.49	0.36	0.28	0.31	0.36
	0.58	0.57	0.40	0.43	0.35	0.38	0.32	0.31
	0.57	0.50	0.37	0.45	0.34	0.30	0.31	0.29
	0.57	0.52	0.45	0.39	0.34	0.40	0.34	0.32
	0.57	0.54	0.42	0.37	0.35	0.40	0.29	0.27
	0.57	0.50	0.41	0.30	0.37	0.43	0.29	0.29
	0.55	0.55	0.44	0.46	0.34	0.38	0.36	0.29
	0.57	0.54	0.43	0.46	0.34	0.36	0.40	0.28
	0.58	0.56	0.46	0.35	0.36	0.32	0.36	0.31
Average	**0.57**	**0.52**	**0.41**	**0.41**	**0.35**	**0.34**	**0.33**	**0.30**
Standard Dev.	0.01	0.04	0.03	0.06	0.01	0.06	0.03	0.02
+/- 95% C.I.	0.01	0.02	0.02	0.04	0.01	0.03	0.02	0.01

5. DATA ANALYSIS

As part of the systematic approach developed by Van Dam et al. (2002) for analysis of concrete pavements exhibiting MRD, the general recommendations for data interpretation were followed. These recommendations are presented in a series of five flowcharts and seven tables, leading the analyst toward diagnosis of the mechanism(s) of distress. The flowcharts assess various characteristics of the concrete, including general concrete properties, the condition of the paste and air, identification of material infilling air voids and cracks, and the condition of the aggregate. The tables list various diagnostic features characteristic of the seven most common types of materials-related distress, including paste freeze-thaw damage and deicer distress. Although some of the distress mechanisms at work in DDFs are unique, the data analysis format is flexible enough to allow recommendations for future work to shed more light on problems identified. Appendix C presents the flowcharts for each of the airports studied. A summary of the data analysis for each airport is presented below.

5.1. AIRPORT ALPHA

The network of large interconnected voids in cores C and G, in combination with the associated localized regions of extremely high *w/c* in the thin section from core C, suggest that poor consolidation and excessive bleed water were present during construction. Cracks at the surface of cores C and G appear to be related to these voids. Only one of the four measurements of spacing factor values exceeded the recommended limit of 0.200 mm, but exceptionally so with a value of 0.399 mm. The fluorescence intensity measurements from the thin sections correlated to an equivalent *w/c* of 0.41 as compared to the mortar standards cured for 28 days. This was the highest *w/c* measured in this study. Further, regions of extremely high *w/c* were not considered typical of the hardened paste as a whole, and were not included in the fluorescence measurements.

It is noted that Airport Alpha was the only site where a supplementary cementitious material was not used. Instead, a significant quantity of inert dolomite filler was observed. Assuming that 5 percent of the cement was replaced with inert filler, the effective cement content would be reduced to 496 lbs/yd^3, raising the design *w/c* to 0.46. And, in the absence of supplementary cementitious materials, higher quantities of calcium hydroxide would be expected in the hydrated cement paste. The abundance of secondary calcium hydroxide deposits suggests leaching of calcium hydroxide in the cement paste and re-deposition in the entrained air voids, a phenomenon made possible by the increased permeability associated with the higher *w/c*.

Using the flowcharts presented in Appendix C to assess the concrete, the major distress mechanism is construction-related, primarily due to poor placement (consolidation). Even with this problem, the concrete compressive strength is good and the split tensile strength is exceptional for the concrete tested that was without consolidation problems. Overall, the air-void system spacing factor was marginal, but in one case it was very poor (core F), emphasizing how concrete variability might contribute to localized freeze-thaw problems. This variability was borne out in the visual assessment of the pavement system, where a paving lane having visible signs of consolidation problems is adjacent to a lane appearing with none. The infilling of the air-void system with secondary calcium hydroxide was unusual, and may be associated with the use of the glycol-based deicer (high moisture availability at or below 32 ^{o}F). The interconnected void system caused by the poor consolidation provides access for water, resulting

in the dissolution of calcium hydroxide from the hydrated cement paste. There was no sign of alkali-aggregate reactivity, aggregate freeze-thaw damage, or sulfate attack.

5.2. AIRPORT DELTA

The concrete from Airport Delta was in good condition. The measured spacing factor value of 0.115 mm was well below the recommended upper limit of 0.200 mm. The fluorescence intensity measurements from the thin sections correlated to an equivalent *w/c* of 0.35 as compared to the mortar standards. While the value of 0.35 does not suggest that such a low *w/c* was actually used, it does indicate that the hydrated cement paste is denser than the 0.40 *w/c* mortar standard. The compressive and split tensile strength data indicated concrete of average quality, but it is noted that this is based on testing of a single core.

The concrete was assessed using the flowcharts presented in Appendix C. There were no problems noted with the concrete.

5.3. AIRPORT ECHO

The surface cracking is likely due to plastic shrinkage cracking that occurred while the concrete was still fresh. Reactive fine aggregate particles, although present, do not appear to be causing any cracking or distress. Strong evidence exists that suggests that the alkali-silica reaction product formed while the concrete was still hydrating. The measured spacing factor values were marginal, being near or just above the recommended limit of 0.200 mm. Overall the air content was relatively high, averaging 7.57 percent for all cores tested, but it was even higher for the bottom third of the cores, averaging 9.57 percent. The fluorescence intensity measurements from the thin sections correlated to an equivalent *w/c* of 0.34 as compared to the mortar standards. While the value of 0.34 does not suggest that such a low *w/c* was actually used, it does indicate that the hydrated cement paste is denser than the 0.40 *w/c* mortar standard. Concrete from Airport Echo had the lowest tested compressive strength, averaging approximately 4000 psi, yet the split tensile strength was average. The strength is not believed to be linked to the observed distress.

Aside from the plastic shrinkage cracks and the poor consolidation toward the bottom of the slab, the concrete appears to be of good quality. The fractured state of the cores as received is related to difficulties experienced during the coring operation.

The concrete was assessed using the flowcharts as presented in Appendix C. The major difficulties were construction-related, with poor placement, mix design, and/or mix proportioning contributing to consolidation problems and poor finishing/curing practices contributing to plastic shrinkage cracking. No evidence of aggregate freeze-thaw damage, deicer damage, or sulfate attack was observed, nor was there physical evidence of paste freeze-thaw damage, even though the air-void system is considered marginal. Alkali-silica reaction product was observed, produced from the fine aggregate, yet no evidence of paste or aggregate cracking or softening was associated with it. It is believed that the reaction occurred while the concrete was very young and it is not deleterious at this time.

5.4. AIRPORT FOXTROT

The network of large interconnected voids in cores A and G are directly related to cracks observed at the pavement surface. Furthermore, the sub-entrained air-sized gaps in the cement paste as observed in the thin section from core A may have developed due to tearing of a stiff and difficult-to-work concrete during placement. The full-depth crack of core C contained deposits of alkali-silica reaction product and ettringite, but these deposits are likely of secondary importance, and not the cause of the large crack, which is most likely due to drying shrinkage. The secondary deposits seemed limited to the proximity to the crack, and were generally not observed in abundance. Three of the four measured spacing factor values exceeded the recommended limit of 0.200 mm. The fluorescence intensity measurements from the thin sections correlated to a *w/c* of 0.33 as compared to the mortar standards. While the value of 0.33 does not suggest that such a low *w/c* was actually used, it does indicate that the hydrated cement paste is denser than the 0.40 w/c mortar standard. The compressive strength results are high, averaging approximately 7500 psi, yet the split tensile strength is very low, averaging approximately 220 psi. This is possibly indicative of a concrete suffering some as yet undetected microstructural weakness, particularly at the paste-aggregate interfaces.

The concrete was assessed using the flowcharts presented in Appendix C. The major difficulties were construction-related, with poor placement, mix design, and/or mix proportioning resulting in consolidation problems. The large network of interconnected void space was directly related to surface cracking. Furthermore, paste-freeze thaw damage might be playing a role as the air-void system is marginal to poor, and is variable from top to bottom in the core. Infilling of the air-system with ettringite, especially near the large macrocrack in core C, is indicative of the movement of moisture through the concrete. Alkali-silica reaction product, as well as an interesting ettringite-like phase, are filling the macrocrack, but it is not believed that ASR is the major contributor in the observed distress as it is isolated to this one location and is not abundant throughout the concrete.

5.5. AIRPORT GOLF

The crack observed at the pavement surface of core A is shallow and likely related to plastic shrinkage. The crack at the pavement surface of core C may have started as a plastic shrinkage crack, but later acted as a starting point for a drying shrinkage crack. Ettringite deposits in the large crack in core C appeared secondary in nature, and are not believed to be the cause of the crack. Reactive fine aggregate particles, although present, did not appear to be associated with cracking or distress. The measured spacing factor values were marginal, being close to the recommended upper limit of 0.200 mm, with one measurement of 0.219 mm exceeding the limit. Ettringite deposits were abundant in the entrained air voids, often completely filling the air voids. Sulfate, from the oxidation of calcium sulfide, a constituent of the slag coarse aggregate, may be contributing to the formation of the secondary ettringite deposits. The fluorescence intensity measurements from the thin sections correlated to a *w/c* of 0.30 as compared to the mortar standards. While the value of 0.30 does not suggest that such a low *w/c* was actually used, it does indicate that the hydrated cement paste is denser than the 0.40 *w/c* mortar standard. The measured compressive strength varied greatly for the two cores, but averaged approximately 5,250 psi. The split tensile strengths were very low, averaging 170 psi. Further, the average thickness of the cores extracted was 13 in, which is 2 in less than the specified 15 in thickness design. The cores were obtained from various locations on the pad, but were not taken in a statistically random fashion as is needed to verify pavement thickness. However, the low tensile

strength and potentially thin slab likely contributed to the presence of the structural cracking observed on this pavement.

The concrete was assessed using the flowcharts in Appendix C. The concrete appeared well consolidated, but evidence of plastic shrinkage cracking suggests poor finishing/curing. The air-void system at the time of construction was adequate, but subsequent infilling of many of the air voids with secondary ettringite has made it marginal. Secondary ettringite is not uncommon in distressed concrete, but this degree of infilling is extremely high and is typical of concrete made with slag coarse aggregate. It is questionable whether secondary ettringite infilling of an air-void system can result in paste freeze-thaw damage, but it does indicate that water is able to move freely within the concrete. Although some fine aggregates appeared to be alkali-silica reactive, no sign of a deleterious reaction were observed. Thus ASR is not considered to be an important contributor to the distress.

5.6. SUMMARY

Table 11 summarizes the generalized distress mechanisms identified in the petrographic analysis, with a subjective rating of the level of significance (high, medium, or low) that each mechanism had on the observed distress. Based on the results of the data analysis, the following conclusions can be drawn from the examination of the concrete from the five DDFs:

- No evidence exists for either a chemical or biological distress mechanism associated directly with the use of glycol-based aircraft deicers. Indirectly, the extensive use of glycol-based deicers at Airport Alpha may have contributed to the infilling of the air-void system with calcium hydroxide, but the relatively high capillary porosity, and poor consolidation likely facilitated this occurrence.

- The most common problems associated with the concrete evaluated can be broadly categorized as poor placement/consolidation and/or finishing curing. In general, the concrete lacked uniformity not only from location to location, but from the top of the core to the bottom. Entrapped air, at times resulting in an interconnected void network, was prevalent in three of the five sites studied. Mixture proportioning has a direct impact on workability, and thus could be contributing to the problems with consolidation. The surface cracking was often associated with plastic shrinkage and/or poor consolidation.

- The air void systems were marginal in many cases, with the spacing factor being at or above the 0.200 mm maximum limit specified in ASTM C 457. Often, the spacing factor was found to be adequate in a portion of the core yet inadequate in another. In only one case (Airport Foxtrot) was a poor air void system thought to be contributing to the observed distress, yet this problem may arise in other locations over time. The environmental conditions present on a DDF are fairly severe due to the presence of moisture under freezing conditions and induced freeze-thaw cycles, so an effective air-void system is thought to be critical to good performance.

TABLE 11. LEVEL OF SIGNIFICANCE OF DISTRESSES OBSERVED AT EACH SITE

Airport	Likely Cause of Distress Based on Evaluation of Cores				
	Construction	**Paste F-T**	**ASR**	**Deicer**	**Sulfate**
Alpha	High	Low	None	Low	None
Delta	None	None	None	None	None
Echo	High	Low	Low	None	None
Foxtrot	High	Moderate	Low	None	None
Golf	Moderate	Moderate	Low	None	Low

- Alkali-silica reactive aggregate particles were observed in cores at three of the sites, but in no case were reactive aggregate linked to the observed distress. In Airports Echo and Golf, reactive fine aggregate particles were observed but with no deleterious effect. In Airport Foxtrot, ASR was localized in the vicinity of a macrocrack likely caused by drying shrinkage.

6. RECOMMENDATIONS FOR MITIGATION AND PREVENTION OF FUTURE DETERIORATION

As described in chapter 5.6, no systemic distress mechanism was identified in the concrete examined that is linked directly to the use of glycol-based aircraft deicers. Poor mix design, ineffective proportioning/batching, and poor placement practices were responsible for the majority of the distress observed. Poor air-void systems also may have contributed to the deterioration in a few cases. For the most part, to prevent the materials-related distress noted in this study, good construction practices must be followed and adequate air-void systems must be produced and verified. In this chapter, some general recommendations are made to avoid future deterioration in newly constructed DDFs.

6.1. MIXTURE DESIGN, PROPORTIONING/BATCHING, AND/OR PLACEMENT

A wealth of knowledge currently exists and is readily available regarding the construction of durable concrete airport pavements (Kohn et al. 2003). Problems often exist not because of lack of knowledge of what needs to be done, but because good practices are not followed. It is well known that difficulties in PCC placement are more acute in airport rather than highway pavement construction because the increased slab thickness requires that mixtures be exceedingly stiff to avoid sloughing of the slip-formed edges. This stiffness can make a poorly designed and/or proportioned mixture difficult to place without encountering consolidation problems (it can also result in the formation of a poor air-void system).

Poor consolidation was observed in cores from three airports, with the formation of interconnected void systems being directly linked to surface cracking at two airports. The prevalence of such poor consolidation suggests that the concrete mixtures were difficult to place, either due to poor mixture design or construction techniques. In the case of Airport Alpha, localized regions of hydrated cement paste having very high *w/c* were observed in the vicinity of this network. This indicates that water was present in these voids while the concrete was plastic, potentially as a result of excessive bleed water. Airport Alpha did not use a supplementary cementitious material, which can help alleviate excess bleed water. Evidence of a difficult-to-place mixture also exists at Airport Foxtrot, where the air-void system appears to be torn due to mix stiffening.

In the late 1990s, the U.S. Air Force recognized that aggregate gradation was a major factor contributing to joint spalling, with poorly proportioned mixtures being more difficult to construct and exhibiting early distress manifestations (Muszynski and LaFrenz 1996; Muszynski, LaFrenz, and Artman 1997). Consequently, specifications for grading aggregates in concrete mixtures for airfield pavements were altered to consider both the coarseness and workability of the gradation. In this system, aggregate is no longer considered to be either fine or coarse, but instead is viewed as a single combined aggregate blend. This approach is supported in the TRB Circular on concrete durability, which states that a lack of mid-sized aggregate (around 9.5 mm size) results in concrete with high shrinkage, high water demand, and poor workability (TRB 1999). Blending of multiple aggregate sources can be used to address this problem (Shilstone 1990), assisting in the production of mixtures that are stiff enough to place without sloughing while maintaining adequate workability to avoid poor consolidation.

To ensure that adequate consolidation has been achieved, a workable test method and specification should be developed. Although an air-void system analysis in accordance with ASTM C 457 could be used, it is much too detailed and difficult to conduct to be of practical use. Instead, such a test method and specification could be based on a test method similar to ASTM C 642, *Standard Test Method for Specific Gravity, Absorption, and Voids in Hardened Concrete*. A workable approach might be to use concrete cores randomly extracted to verify pavement thickness after construction, which are then subdivided into smaller sections and individually tested to determine the volume of permeable pore space (voids) in the top, middle, and bottom of the core. An acceptance criterion could be established such as maximum allowable percent permeable voids or the ratio of percent permeable voids from field concrete compared to well-consolidated concrete made during the mixture design process. This would form a practical basis for judging whether adequate consolidation had been achieved.

6.2. AIR-VOID SYSTEMS

Another potential problem that was observed in this study was the entrained air-void systems, which were marginal to poor in many instances as indicated by the high spacing factors. Figure 80 illustrates the total original air content versus the original spacing factor for every specimen evaluated, including the top, middle, and bottom of each core. This plot illustrates a very important point: that the total air content (which is the parameter typically measured in fresh concrete) has little direct correlation to the spacing factor. It is also evident that nearly 40 percent of the measured spacing factors exceed the maximum recommended value of 0.200 mm, and that all four distressed airports had some concrete that exceeded this limit. Only Airport Delta, which was included as an example of a good performing pavement, had all measured spacing factors well below the limit (note that only a single core from this airport was evaluated). Although little distress can be linked directly to paste freeze-thaw damage at this time, these data suggest that it may be a problem in the future, especially since three of the four airports of interest were under 7 years old at the time the data were collected.

Although it is known that an adequate air-void system in concrete is desirable, ensuring that one is produced is a more intractable problem. Entrained air is created through the addition of either naturally derived or synthetically produced air entraining admixtures, which are basically surfactants that act at the air-water interface to form spherical microscopic bubbles in the fresh cement paste. Many factors contribute to the efficacy of the admixture, including mixture constituents (particularly the properties of the cementitious materials), other admixtures, temperature, and time of mixing. Of less importance is the placement and consolidation, as an acceptable air-void system in well proportioned concrete is not easily removed through normal levels of internal vibration during placement. In modern pavement construction, the air-void system is not directly assessed during construction, but instead measurements are made to determine the total air content of the fresh concrete. As noted previously in figure 80, a direct correlation does not exist between total air and the quality of the air-void system (as assessed by the spacing factor), and thus the current practice is inadequate.

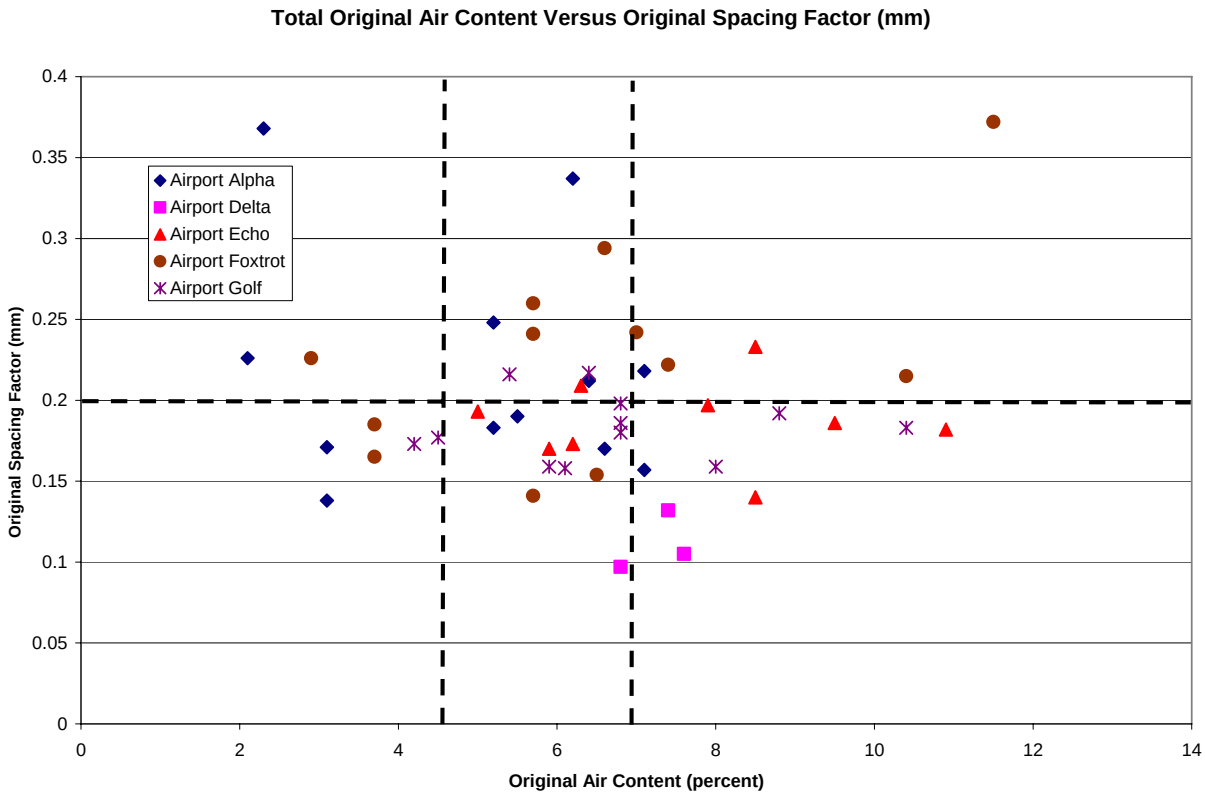

FIGURE 80. TOTAL ORIGINAL AIR CONTENT VERSUS ORIGINAL SPACING FACTOR FOR ALL CONCRETE TESTED USING ASTM C 457

This is of particular relevance to the focus of this study as the DDF environment is believed to be very harsh for concrete due to the availability of moisture and multiple freeze-thaw cycles. An adequate air-void system is thus essential to protect the concrete from paste freeze-thaw damage. Currently, there is no generally accepted method for measuring the characteristics of the air-void system in fresh concrete. Until such a method is developed, the testing of the air-void system in hardened concrete using ASTM C 457 should be considered as part of the mixture design process, especially for new construction of DDFs.

6.3. CURING PRACTICES

In addition to mixture proportioning/consolidation, the occurrence of plastic shrinkage cracking indicates that better curing practices could have been employed. It is known that wide variations exist in the effectiveness of the various curing compounds currently in use and in how they are applied. Ideally, concrete would be wet cured as was done in the past, but this is thought to be unrealistic from a modern construction perspective. Instead, membrane-forming curing compounds are sprayed onto the surface shortly after placement in an attempt to prevent mix water from evaporating. In theory, this makes the mix water available for hydration while preventing evaporation that produces plastic shrinkage cracking. For such membranes to be effective, they must form a continuous waterproof barrier over the entire pavement surface. Poorly formulated curing compounds, excess dilution with water, poor coverage, and/or late application can all result in the formation of plastic shrinkage cracks, particularly on hot, dry, windy days. Again, good practice is known but must be followed to prevent distress.

A recent publication, *Guide for Curing Portland Cement Concrete Pavements, Volume I,* provides excellent guidance on how to cure concrete pavements (Poole 2005). Curing compounds are specified in accordance with AASHTO M 148 (ASTM C 309) and ASTM C 1315, the latter being more stringent. Most often, the curing compound will be applied after time of initial setting at an application rate of approximately 23 yd^2/gal (5 m^2/L). This will generally require that two coats be applied to avoid excessive running into low areas. When a white pigmented curing compound is used, the surface should appear very white after application. Any hint of gray immediately after application means that the compound is under-applied.

7. CONCLUSIONS AND RECOMMENDATIONS

Premature distress, in the form of scaling, spalling, crazing, and map cracking of the slab surface, has been observed on a few concrete airfield pavement dedicated deicing facilities (DDFs) in North America, in some cases occurring as soon as 2 to 3 years after construction. Because the DDFs are specialized facilities that are used strictly for deicing aircraft, there is concern that the heavy applications of glycol-based deicing fluids might somehow be contributing to the development of the premature distress through interactions with the concrete constituent materials, the construction techniques, and the environment.

This project was sponsored by the IPRF in order to determine if there was a relationship between the application of the aircraft deicing fluids and the observed distress. This study included a review of relevant literature, field evaluation of nine DDFs, and field sampling and laboratory evaluation of five DDFs. Significant conclusions and recommendations from this study are provided in the following sections.

7.1. CONCLUSIONS

The following conclusions are drawn from this study:

- No common cause of distress was identified in the concrete evaluated. Further, there is no evidence to suggest that the use of glycol-based aircraft deicers is directly implicated in the chemical or microbial degradation of concrete. Indirectly, the extensive use of glycol-based deicers at Airport Alpha may be contributing to the infilling of the air-void system with calcium hydroxide, but the relatively high capillary porosity, lack of a supplementary cementitious material, and poor consolidation likely facilitated this occurrence.

- The most common problems associated with the concrete evaluated can be broadly categorized as poor placement and consolidation and/or finishing and curing. In general, the concrete lacked uniformity not only from location to location, but from the top of the core to the bottom. Entrapped air, at times resulting in an interconnected void network, was prevalent in three of the five sites studied. Mixture proportioning has a direct impact on workability, and thus could be contributing to the problems with consolidation. Plastic shrinkage and poor consolidation were often associated with surface cracking.

- The air-void systems were marginal in many cases, with spacing factors at or above the 0.200 mm maximum limit specified in ASTM C 457. Often, the spacing factor was found to be adequate in a portion of the core yet inadequate in another. In only one case (Airport Foxtrot) was a poor air-void system thought to be contributing to the observed distress, yet this deficiency may contribute to problems in other locations over time. The environmental conditions present on a DDF are fairly severe due to the presence of moisture under freezing conditions and induced freeze-thaw cycles. It seems plausible that the intensive usage of glycol-based deicers characteristic of DDF operations may contribute to physical paste F-T damage due to increased osmotic pressures, thermal shock, and increased saturation of the concrete, and therefore a good air-void system is thought to be critical to good performance.

- Alkali-silica reactive aggregate particles were observed in three of the sites, but in no case was the occurrence of reactive aggregates linked to the observed distress. In Airports E and G, reactive fine aggregate particles were observed but with no deleterious effect. In Airport

Foxtrot, ASR was localized in the vicinity of a macrocrack likely caused by drying shrinkage. Possible future damage due to ASR cannot be ruled out.

- In general, current construction practices appear adequate to prevent the construction-related problems observed. Although the extremely stiff mixtures associated with slip-form paving of airport pavements can pose difficulties during placement, it is clear from the example set by Airport Delta that such mixtures can be placed with little entrapped air and sufficient entrained air. Better mixture design and proportioning, improved consolidation, and the timely and thorough application of an effective membrane-forming curing compound would prevent much of the distress observed.

- Ensuring that a proper air-void system is entrained in the concrete is a more difficult problem, as common test methods only measure the total air content of the concrete and not the adequacy of the air-void system (e.g., spacing factor, specific surface). A device known as the air void analyzer (AVA) is being investigated to assess actual air-void system parameters (total air, spacing factor, specific surface) of fresh concrete, but work continues to be done to verify its applicability to no- or low-slump concrete and concrete made using synthetic air-entraining admixtures. Until a proven method is available to measure the air-void system characteristics in fresh concrete, ASTM C 457 should be used during the mixture design process to ensure that the air-void system is adequate, particularly for concrete being used in DDFs.

7.2. RECOMMENDATIONS FOR FUTURE WORK

As is true with most research projects, the findings of this study have raised questions that should be addressed in the future. The following recommendations are made for future work:

- Poor consolidation was implicated in much of the deterioration observed on the DDFs studied. Work must be conducted to develop a simple test method and specification to verify that the as-placed concrete has been adequately consolidated. A test method using principles similar to ASTM C 642, *Standard Test Method for Specific Gravity, Absorption, and Voids in Hardened Concrete* must be devised to rapidly measure the interconnected void space within concrete. Randomly extracted concrete cores (such as those used to verify pavement thickness after construction) should be subdivided into smaller sections and individually tested to determine the volume of permeable pore space (voids) in the top, middle, and bottom of the core. An acceptance criterion, such as maximum allowable percent permeable voids or the maximum ratio of percent permeable voids in field concrete compared to well-consolidated laboratory prepared concrete, must be established. Such a test and criteria would form a practical basis for judging whether adequate consolidation had been achieved.

- All but one of the pavements studied was constructed in 1998 or 1999, meaning that the specimens evaluated had only been subjected to six or seven winters prior to extraction and testing. Although there is currently little evidence that paste freeze-thaw damage is causing distress, there is sufficient evidence to support some level of concern regarding future performance. There are on-going discussions regarding the appropriateness of the limit on the spacing factor set in the ASTM C 457 procedure. Some have suggested that it can be raised given the higher strength common in modern pavement concrete. Alternatively, the environment present on DDFs is unique and potentially harsh, and thus the limit may actually be too high. Clearly, more research is needed to determine what limits on the

entrained air-void system need to be set for airport concrete in general, and for concrete used for DDFs specifically. In addition, better test methods for assessing the air-void system parameters in fresh and hardened concrete need to be developed.

- The proper use of supplementary cementitious materials (e.g., fly ahs, ground granulated blast furnace slag) will enhance workability, decrease the amount of calcium hydroxide in the paste, and decrease concrete permeability. Only one of the sites studied, Airport Alpha, did not incorporate supplementary cementitious materials in the mix design, and it was the site with the highest measured capillary porosity and the only site with significant infilling of secondary calcium hydroxide in the air voids. The data collected in this study is insufficient to strongly support the positive effects that supplementary cementitious materials seem to have in preventing the dissolution and redeposition of calcium hydroxide, but additional work should be conducted to evaluate what, if any, benefit supplementary cementitious materials might have in improving the durability of concrete used for DDFs.

8. REFERENCES

American Concrete Institute (ACI) (1992). "Guide to Durable Concrete." *ACI Manual of Concrete Practice—Part 1*. ACI 201.2R-92. American Concrete Institute, Farmington Hills, MI.

American Society for Testing and Materials (ASTM) (1998). *Standard Test Method for Airport Pavement Condition Index Surveys.* ASTM D5340-98. American Society for Testing and Materials, West Conshohocken, PA.

Cheney (2004). *Lime FAQs*. Cheney Lime & Cement Co. Allgood AL. From http://www.cheneylime.com/faqs.htm#18, accessed on 4/29/04.

Cox, D.P. (1978). "The Biodegradation of Polyethylene Glycols." *Advances in Applied Microbiology*, Volume 23. Edited by D. Perlman. Academic Press. NY. pp. 173-194.

Dobie, T. R., "Correlating Water-Soluble Alkalies to Total Alkalies in Cement - Considerations for Preventing Alkali-Silica Popouts on Slabs" in Alkalies in Concrete, ASTM STP 930, V. H. Dodson, Ed.

Housewright, M.E., T.J. Van Dam, L.L. Sutter, and K.R. Peterson (2004). P*reliminary Investigation of the Role of Bacteria in Concrete Degradation.* Final Report. MDOT Research Report RC-1444. Michigan Department of Transportation, Lansing, MI.

Jeknavorian, A.A., and E.F. Barry (1999). "Determination of Durability-Enhancing Admixtures in Concrete by Thermal Desorption and Pyrolysis Gas Chromotography-Mass Spectrometry." *Cement and Concrete Research*,. Vol. 29. pp. 899-907.

Kohn, S., S. Tayabji, P. Okamoto, R. Rollings, R. Detwiller, R. Perera, E. Barenberg, J. Anderson, M. Torres, H. Barzegar, M. Thompson, J. Naughton (2003). *Best Practices for Airport Portland Cement Concrete Pavement Construction (Rigid Airport Pavement)*. Report IPRF-01-G-002-1, Innovative Pavement Research Foundation, Washington, D.C.

Marchand, J., E. J. Sellevold, and M. Pigeon (1994). "The Deicer Salt Scaling Deterioration of Concrete - An Overview." *Durability of Concrete*. V. M. Malhotra, Ed. Third International Conference, Nice, France. ACI SP-145. pp. 1-46.

Mericas, D., and B. Wagoner (2003), "Runway Deicers: A Varied Menu," *Airport Magazine.* http://airportnet.org/depts/publications/airmags/am78796/deice.htm, accessed on May 5, 2004.

Mindess, S., J. F. Young, and D. Darwin (2003). *Concrete*. Second Edition, Prentice-Hall, Inc., Upper Saddle River, NJ. 644 pp.

Minsk, L.D. (1977). *Freeze-Thaw Tests of Liquid Deicing Chemicals on Selected Pavement Materials.* CRREL Report 77-28, U.S. Army Corps of Engineers. p.21.

Muszynski, L. C., and J. L. LaFrenz (1996). *Proportioning Concrete Mixtures with Graded Aggregates: A Handbook for Rigid Airfield Pavements.* Final Report for October 1995. Flight Dynamics Directorate. Wright Laboratory, Tyndall AFB, FL. September.

Muszynski, L. C., J. L. LaFrenz, and D. H. Artman (1997). "Proportioning Concrete Mixtures with Graded Aggregates." *Proceedings: Aircraft/Pavement Technology in the Midst of Change.* American Society of Civil Engineers, Seattle, WA. pp. 205-219.

Pigeon, M. (1994). "Frost Resistance, A Critical Look." *Concrete Technology Past, Present, and Future.* V.M. Mohan Malhotra Symposium. ACI. SP-144. pp. 141-157.

Pigeon, M., and R. Plateau (1995). *Durability of Concrete in Cold Climates*. E & FN Spon. ISBN: 0-419-19260-3. 244 pp.

Poole, Toy S. (2005). *Guide for Curing of Portland Cement Concrete Pavements*. FHWA-RD-02-099. Federal Highway Administration. McLean, VA. pp. 49.

Powers, T. C. (1945). "A Working Hypothesis for Further Studies of Frost Resistance of Concrete." *Journal of the American Concrete Institute*. Vol. 16. No. 4. pp. 245-272.

Powers, T. C. (1949). "The Air Requirement of Frost Resistant Concrete." *Proceedings of the Highway Research Board*. Vol. 29. pp. 184- 211.

Powers, T. C. (1975). "Freezing Effects in Concrete." *Durability of Concrete*. SP-47. American Concrete Institute. Detroit, MI. pp. 1-12.

Ritter, Steve (2001), "Aircraft Deicers," *Chemical and Engineering News*, Volume 79, No. 1, p. 30.

Sabeh, Y., and K.S. Narasiah (1992). "Degradation Rate of Aircraft Deicing Fluid in a Sequential Biological Reactor." *Water Science and Technology*, Vol. 26, Issue 9-11. pp. 2061-2064.

Setzer, M.J. (1990). "Interaction of Water with Hardened Cement Paste." *Advances in Cementitious Materials*. American Ceramic Society Transactions. Vol 16, pp. 415-439.

Shah, S.P., S. Marikunte, W. Yang, and C. Aldea (1996). "Control of Cracking with Shrinkage-Reducing Admixtures." *Transportation Research Record No. 1574.* pp. 25-36.

Shahin, M. Y., and J. A. Walther (1990). *Pavement Maintenance Management for Roads and Streets Using the PAVER System*. Technical Report M-90/05. U.S. Army Engineering and Housing Support Center, Washington, DC.

Shilstone, J. M. Sr. (1990). "Concrete Mixture Optimization." *Concrete International*, American Concrete Institute, Farmington Hills, MI. pp. 33-39.

Transportation Research Board (TRB) (1999). *Durability of Concrete*. Transportation Research Circular. Transportation Research Board, National Academies of Science, Washington, DC.

Van Dam, T.J., L. L. Sutter, K. D. Smith, M. J. Wade, and K. R. Peterson (2002). *Guidelines For Detection, Analysis, And Treatment Of Materials-Related Distress In Concrete Pavements - Volume 2: Guidelines Description and Use.* FHWA-RD-01-164. Federal Highway

Administration. Turner-Fairbank Highway Research Center, McLean, VA. March. pp. 233. http://www.tfhrc.gov/pavement/pccp/pubs/01164/index.htm

Veltman, S., T. Shoenberg, and M.S. Switzenbaum (1998). "Alcohol and Acid Formation During the Anaerobic Decomposition of Propylene Glycol Under Methanogenic Conditions." *Biodegradation*, Vol. 9, No. 2. pp. 113-118.

Willets, A. (1981). "Bacterial Metabolism of Ethylene Glycol." *Biochimica et Biophysics*, Acta. 677. pp. 194-199.

Zitomer, D.H., and G.U. Tonuk (2003). "Propylene Glycol Deicer Biodegradation Kinetics: Anaerobic Complete-Mix Stirred Tank Reactions, Filter, and Fluidized Bed." *Journal of Environmental Engineering*, February. pp. 123-129.